NASA CR-54446
BC/RLD 3015
COPY NO. 22

DEVELOPMENT OF AN ALL-FLUID AMPLIFIER FOR LIQUID ROCKET APPLICATIONS

By J. T. Kasselmann and J. G. Rivard

November 1965

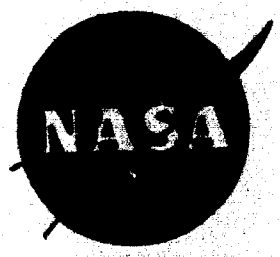

Prepared under Contract No. NAS 3-4198

The Bendix Corporation
Research Laboratories Division
Southfield, Michigan

NATIONAL AERONAUTICS AND SPACE ADMINISTRATION

Requests for copies of this report should be referred to:

National Aeronautics and Space Administration
Office of Scientific and Technical Information
Attention: AFSS-A
Washington, D.C. 20546

FOREWORD

This work was performed by the Research Laboratories Division of the Bendix Corporation for the National Aeronautics and Space Administration under Contract NAS 3-4198. The work was initiated on July 8, 1964 and was conducted under the program management of Mr. John Gregory of the Lewis Research Center, Cleveland, Ohio.

The work described in this report was performed by the Attitude Controls Group of the Energy Conversion and Dynamic Controls Laboratory. Mr. L. B. Taplin is Laboratory Manager and Mr. J. G. Rivard is the Project Engineer. Mr. J. T. Kasselmann was Responsible Engineer, assisted by Mr. J. H. Tarter.

Libraries of contractors and of other qualified requesters may obtain additional copies of this report by submitting NASA Form 492 directly to:

Scientific and Technical Information Facility
P. O. Box 5700
Bethesda, Maryland 20014

TABLE OF CONTENTS

LIST OF ILLUSTRATIONS

LIST OF TABLES

SUMMARY AND CONCLUSIONS

Experimental and analytical studies were conducted to develop a hot gas all-fluid amplifier for controlling the secondary flow for thrust vector control of a liquid rocket engine. The studies resulted in the development of a vortex amplifier, which has been successfully operated with 1500°F hot gas in a simulated application. The amplifier provides total flow modulation as well as output load flow modulation. No moving mechanical parts are required.

A typical conceptual installation of a vortex amplifier on a propulsion nozzle is shown in Figure 1. The development program described in this report resulted in the achievement of flow modulation characteristics shown in Figure 2. The possibility of controlling a hot gas flow for secondary injection by using an all-fluid device has been proven.

The amplifier was designed for a maximum flow rate of 0.5 lb/sec, with a supply pressure of 400 psi. This unit provided a total flow modulation range up to 5 to 1, with load flow modulation from 85 percent of total flow to near zero flow. An overall flow gain (maximum load flow/variable control flow) of 30 to 1 has been achieved with a dynamic frequency response bandpass of 80 cps.

A significant advantage of this amplifier is the realization of similar performance characteristics in operation with gases having different thermodynamic properties. The performance with 1500°F gas supplied from the combustion of hydrogen and oxygen is essentially the same as that obtained with room temperature nitrogen. The gas was supplied from a gas generator which produced a regulated hot gas flow for both supply and control flow.

The elimination of moving parts simplifies the design of seals and minimizes the need for close fabrication tolerances. The compatibility of this device with high temperature gases and its potential long life and high reliability warrant its consideration for future rocket engine control systems. The next logical step is to demonstrate a complete simulated system to realize exact system tradeoff parameters.

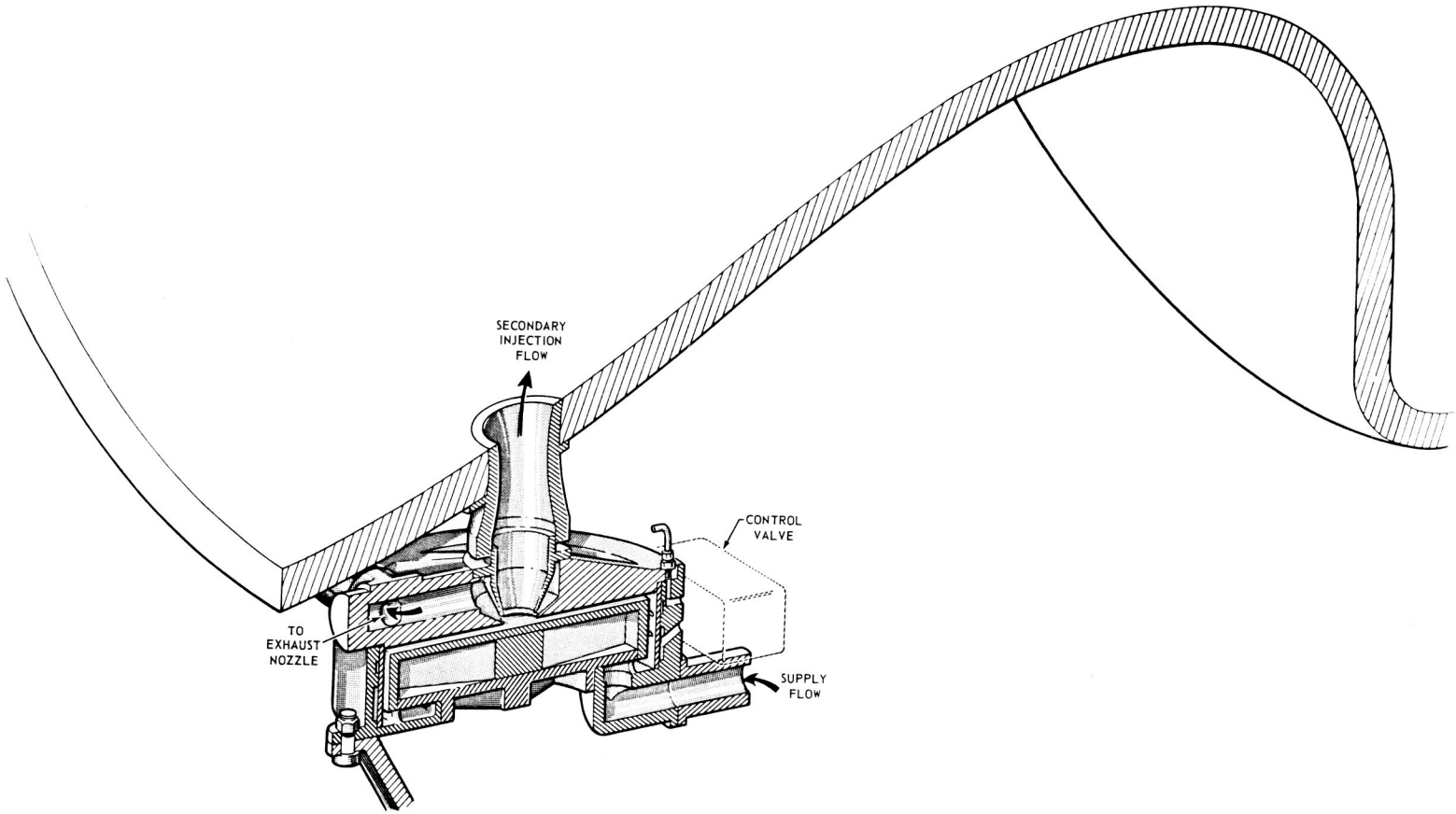

Figure 1 - Fluid State Vortex Amplifier Secondary Injection Thrust Vector Control System

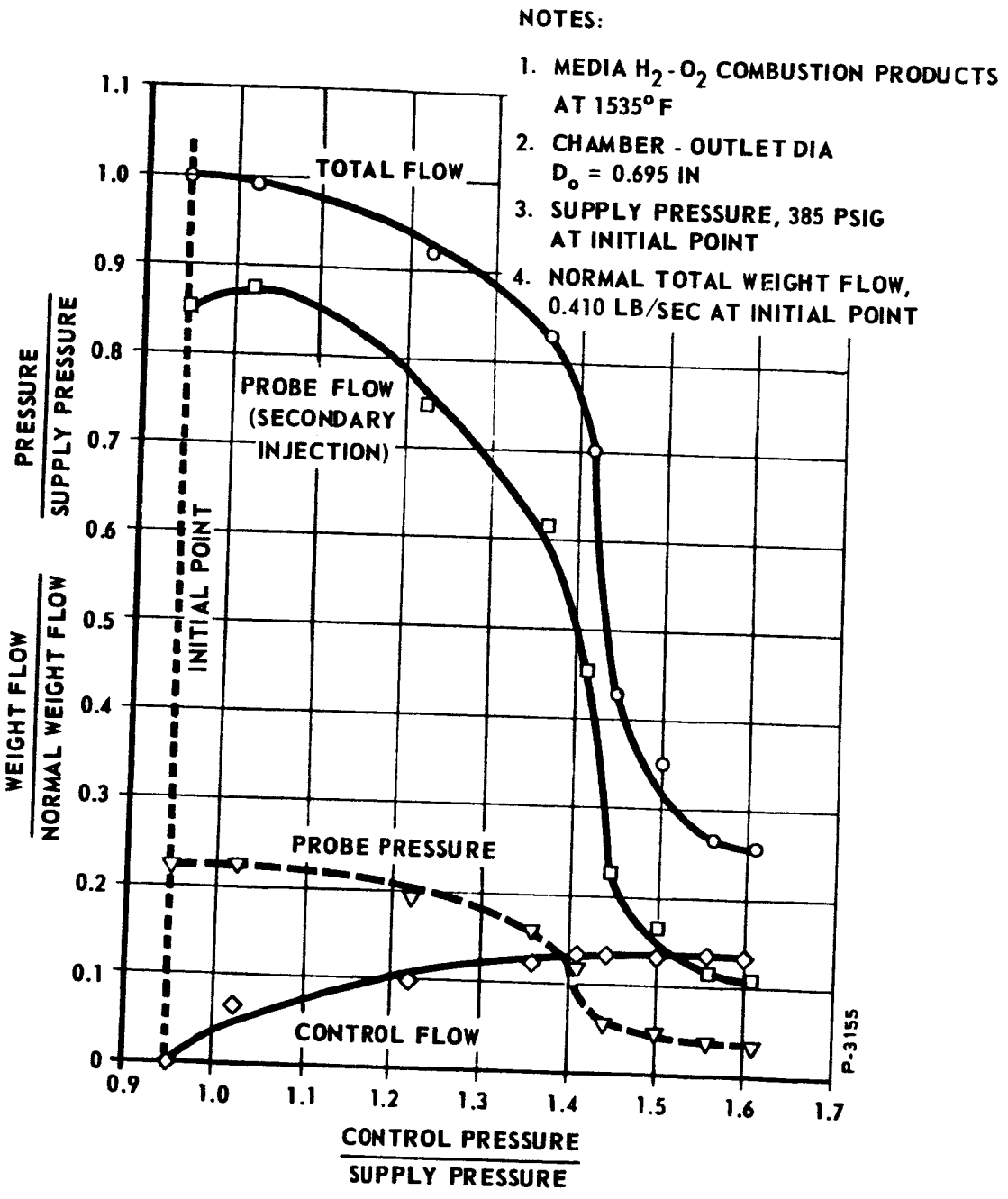

Figure 2 - Typical Hot Static Performance

INTRODUCTION

This report is published in compliance with the requirements of National Aeronautics and Space Administration Contract NAS 3-4198.

Objective

The objective of this program was to demonstrate by analysis, design, and experimentation, the feasibility of a fluid-state amplifier for secondary injection thrust vector control applications. This amplifier must operate with 1500°F hot gas, supplied from the combustion of hydrogen and oxygen. The vortex amplifier principle was selected because this no-moving-part concept provides good throttling characteristics and inherent high reliability. Testing was accomplished using scale models operating with cold gas followed by hot gas test evaluation of a unit designed for a flow rate of 0.5 lb/sec. The program was completed on 30 June 1965.

Basic Vortex Amplifier Technology

The vortex amplifier is a fluid-state active control element requiring no moving mechanical parts. A purely conceptual schematic illustrating gas interaction and the vortex principle is shown in Figure 3. A schematic model of a rudimentary vortex amplifier, along with typical performance characteristics, is shown in Figure 4. The supply flow (P_s) is introduced radially into the cylindrical chamber. The maximum valve flow is determined by an outlet orifice at the center of the chamber. In the absence of control flow, all of the supply flow is radial. When a control flow is introduced into the cylindrical chamber at a point tangent to the outer wall, the momentum rate of the control flow (weight flow times velocity) imparts a rotational flow component to the supply flow as it passes the region of control flow injection. The supply flow thus acquires a tangential velocity component in addition to radial velocity. As the flow proceeds toward the center of the amplifier, the tangential velocity increase is attenuated by the viscous coupling of the fluid;

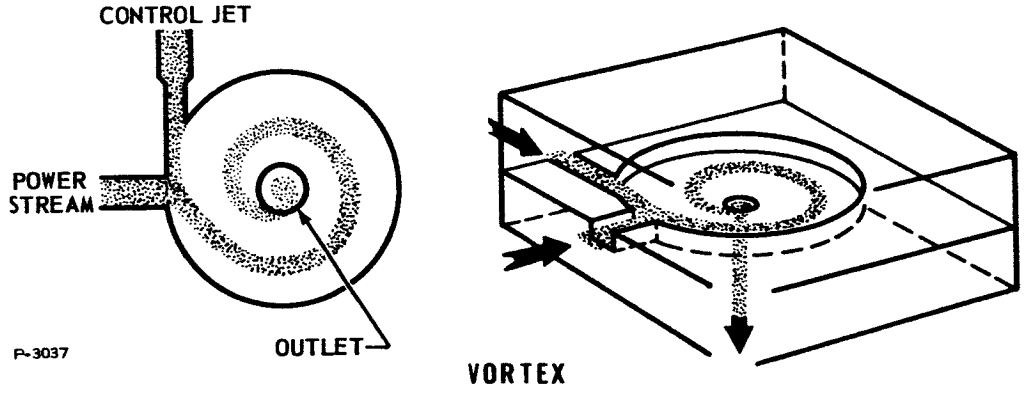

Figure 3 - Schematic of Gas Interaction and the Vortex Principle

however, sufficient velocity buildup can be achieved so that the resulting centrifugal pressure drop provides a mechanism for flow amplification. A small change in control flow results in a relatively large change in total valve flow; typical incremental gains are 100. Near the outlet orifice, the flow field changes from a simple two-dimensional vortex flow into a three-dimensional flow as the fluid leaves the orifice. The maximum tangential and radial velocities occur near the center of the vortex chamber. Basic vortex terminology is defined in Table 1.

A purely analytical approach to the general solution of a physical three-dimensional fluid flow is not practical. The internal losses in the valve due to viscous drag are not predictable by purely analytical means. Simplified analysis based on a number of assumptions has verified simple basic experiments. This analysis can serve as a guide in the initial design of vortex devices and will provide an insight into the basic performance capabilities and limitations of the vortex amplifier. A section on theoretical analysis is included as Appendix D of this report.

The elementary configuration illustrated in Figure 4 has been modified as shown in Figure 5. The supply flow, instead of being admitted to the vortex chamber at one location, is introduced through an annulus formed by the addition of a "button." This configuration forces the supply flow to enter the vortex chamber at the outer wall in a uniform flow sheet. Control flow is introduced into this annulus at right angles to the flow sheet and tangent to the vortex chamber outer wall. Uniform mixing of the two flows is accomplished by the use of several control-flow injection ports. The hot gas vortex amplifier

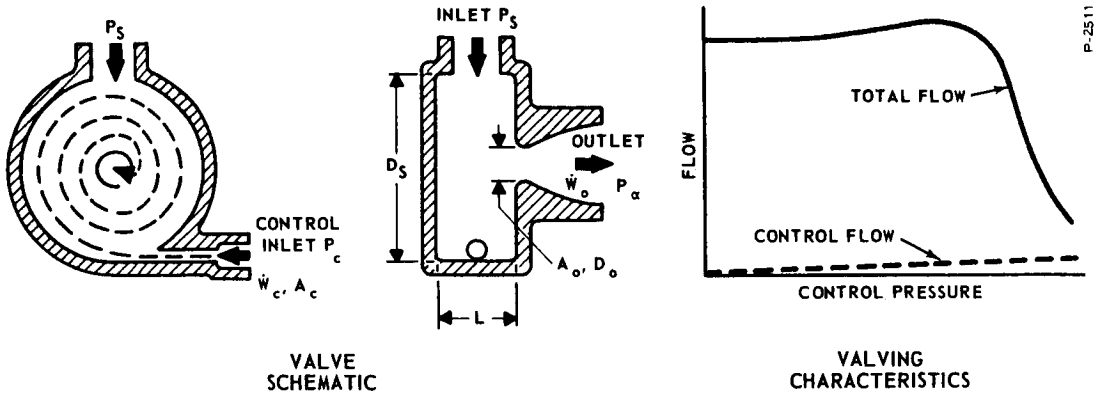

Figure 4 - Schematic Model of a Vortex Valve

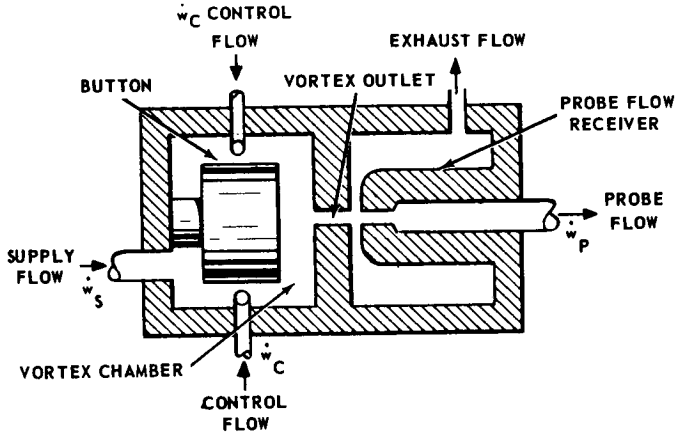

Figure 5 - Vortex Amplifier Configuration Schematic

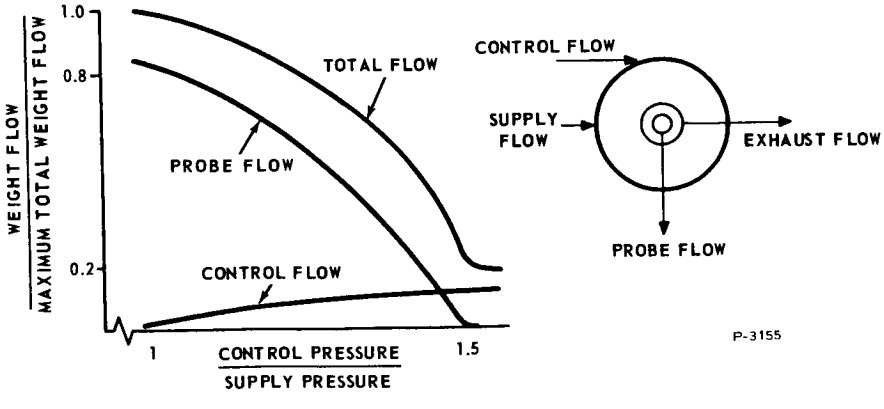

Figure 6 - Typical Non-Dimensional Vortex Amplifier Characteristic Curves

Table 1 - Vortex Amplifier Terminology

Configuration Parameters

Vortex Chamber - Flat cylindrical volume in which the vortex field is induced.

Button - Stationary mechanical element which forms the rear wall at the vortex chamber and guides the supply flow.

Chamber Outlet - Orifice at the center of the vortex chamber which determines the flow capacity of the amplifier.

Probe - Stationary cone-shaped mechanical element located outside of the vortex chamber and concentric with the outlet orifice for the purpose of receiving fluid from the vortex chamber and conveying it to the load.

Performance Parameters

Chamber Turndown - A measure of the ability of the vortex amplifier to throttle the total flow by the addition of control flow.

Gain - The ratio of output or probe flow to the change in control flow.

Recovery - The ratio of probe flow to total flow at minimum control flow.

Probe Turnoff - The minimum value of probe flow at maximum control flow.

Flow Parameters

Supply Flow - Basic flow into the vortex amplifier.

Control Flow - That flow which is introduced at right angles to and impinges upon the supply flow in order to spin the fluid in the vortex chamber.

Total Flow - Sum of supply and control flow.

Probe Flow - That portion of the total flow which enters the probe.

Exhaust Flow - That portion of the total flow which does not enter the probe flow receiver.

Bias Flow - A fixed control flow used for improving gain by providing a minimum swirl to the vortex chamber

developed incorporates this basic vortex amplifier principle. It has a flow modulation range of approximately 5 to 1, as illustrated in Figure 6.* The application of this principle to secondary injection thrust vector control requires that the valve delivering the secondary injection flow modulate from full flow to near zero flow.

*A conventional symbol for a vortex amplifier has been adopted, which consists of three concentric circles. The largest circle represents the vortex chamber outer diameter; the intermediate circle represents the exhaust port; and the inner circle represents the probe flow receiver. Supply flow is represented by an arrow radial to the outer circle and control flow is represented by an arrow tangent to the outer circle. Probe flow is represented by a radial line originating at the inner circle and exhaust flow is represented by a radial line originating at the intermediate circle.

The complete throttling of outlet flow to zero is not possible with a simple vortex amplifier. In order to meet this requirement, a probe flow receiver was added to the basic vortex amplifier configuration. This is shown in Figure 5. With no control flow, the exiting flow from the vortex amplifier enters the probe flow receiver and is carried to the load. With increasing control flow, the exiting flow assumes a hollow cone shape, missing the probe flow receiver, and is diverted to exhaust. The flow to a load is thus inversely proportional to control flow momentum. Typical performance for this device is illustrated in Figure 6. The probe flow approaches zero with maximum control flow. The vortex chamber flow throttling performance is not affected by the addition of the probe flow receiver. The maximum probe flow recovery with zero control flow is set by the spacing between the probe and vortex chamber outlet orifice, and relative diameters. Optimum performance with regard to maximizing gain and flow modulation can be achieved with the probe recovering 80 percent or better of the total flow at the zero vortex swirl condition and near zero flow recovery with maximum vortex swirl.

This technology can be applied to the secondary injection thrust vector control application. A typical system is shown schematically in Figure 7.

The vortex amplifier receives supply flow from a hydrogen-oxygen gas generator. Control flow from the servovalve is used to modulate the supply flow, as described above. The secondary injection flow is obtained from the vortex amplifier as probe flow. In the unswirled condition obtained with zero control flow, most of the entering supply flow is recovered by the probe, as the maximum secondary injection flow. This flow creates a shock in the thrust nozzle which tends to divert the bulk of the flow to the opposite side of the nozzle away from the point of secondary injection. Thrust vectoring is achieved by the combination of this angled mass flow reaction and a pressure field in back of the shock. A minimum of three such systems placed on the thrust nozzle 120 degrees apart would be required for full flight control.

The secondary injection flow can be shut off by applying full control flow to the vortex amplifier from the servovalve. The gas in the vortex chamber is swirled or spun up, which creates a radial pressure gradient in the vortex chamber. This gradient tends to shut down the supply flow, which has the direct effect of reducing the probe or secondary injection flow. This flow is further reduced to practically

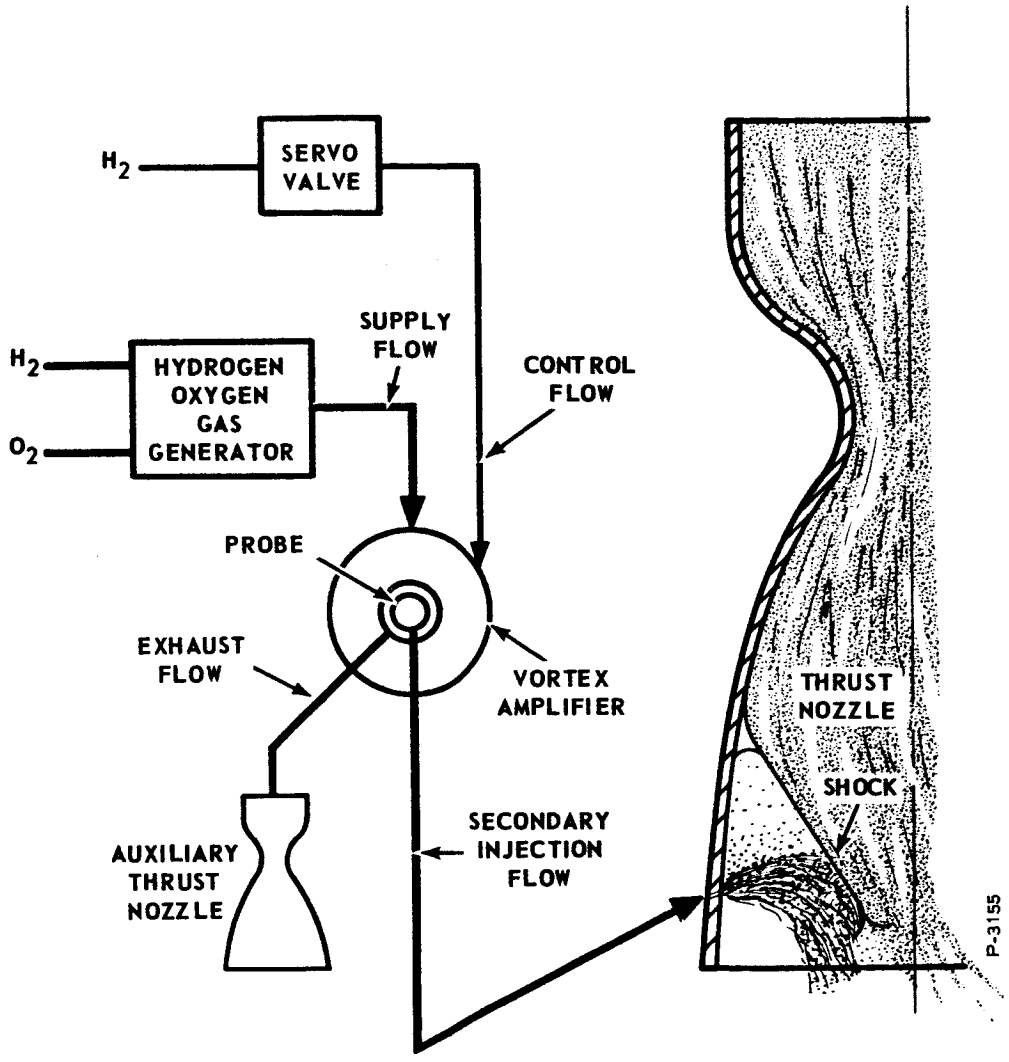

Figure 7 - Typical Secondary Injection Thrust Vector Control System

zero by the fact that the emerging gases from the vortex outlet are spinning and tend to assume the shape of a cone. The probe is axially positioned to allow sufficient space for the coned flow to bypass the probe entrance completely. All gases not entering the probe, exhaust through this space to an auxiliary nozzle, where a portion of the gas energy is recovered as thrust.

In an actual application with a normal load profile, thrust vectoring will be required during a small portion of the powered flight time. In this case, the normal operating mode would be the mode in which the vortex amplifier is completely turned down, allowing no secondary injection flow. The control flow would be maximum and the supply flow

would be nearly shut off. Because of this inherent turndown capability, the vortex amplifier does not waste gas when none is required for thrust vectoring.

Program Description

The primary objective of this program was the realization of design data for an optimized vortex amplifier. The basic amplifier was designed for a flow rate of 0.5 lb/sec, which was considered large enough to provide reliable performance data necessary for extrapolating the design to vortex amplifiers with higher pressures and flow rates. The initial program plan included a two-phase effort, with the second phase involving the test of an amplifier with a 5 lb/sec flow rate. Technical redirection during the course of the program eliminated the 5.0 lb/sec phase in favor of more testing and optimization of performance of the 0.5 lb/sec unit. The 0.5 lb/sec unit will be referred to as the Phase 1 vortex amplifier throughout this report.

The optimization of performance involved studies of the vortex chamber and the probe flow receiver. The optimum chamber configuration is one that maximizes gain and flow modulation. Among the variables investigated were chamber length, diameter ratio, and the number and location of control flow injection points. The specification defines a maximum ratio of vortex chamber diameter to outlet diameter of 6 to 1. An 8 to 1 diameter ratio was investigated in the breadboard phase of the program for possible improvement in flow modulation. Total flow modulation is an important efficiency consideration in the design of a secondary injection thrust vector control system because it sets the minimum quiescent flow when thrust vectoring is not required.

The optimum probe flow receiver is one that maximizes flow recovery and permits smooth continuous flow modulation from maximum to near zero flow with a minimum control flow. The vortex chamber outlet and probe geometry required extensive test evaluation to realize the desired performance. The program included breadboard vortex amplifier cold gas testing, using hardware easily modified for parameter studies, and provided an economical method of evaluating design configurations before incorporation in the Phase 1 vortex amplifier. Desired performance is described in Appendix A.

The nature of this test program made it necessary to devote considerable time to the test installation. A hydrogen-oxygen gas generator with throttling capability was designed and built, based on the already proven vortex combustion chamber concept. The test installation, described in detail in Appendix E, included special pressure regulation valves and required several circuits for providing the control flow to the vortex amplifier. The test installation was equipped for evaluating static and dynamic performance.

VORTEX AMPLIFIER DESIGN

A breadboard vortex amplifier test program was started immediately at the onset of the program to obtain test experience on the vortex amplifier configuration. The subprogram provided a solid experimental base from which the Phase 1 vortex amplifier was designed. The breadboard program was active for approximately two-thirds of the project and provided an economical means of evaluating modifications and new configurations.

Two breadboard vortex amplifiers were built. Several test series were run, evaluating the performance of different configurations at different operating conditions. Both breadboard vortex amplifiers were sized with a capacity of one-tenth the flow of the Phase 1 vortex amplifier. Nitrogen at a supply pressure of 200 psig and ambinet temperature was used as the testing media. Significant dimensions are as follows:

D_o = 0.226 in. (Chamber Outlet Diameter)

D = 1.250 in. (Chamber Diameter)

A complete description of the hardware, tests and results are contained in Appendix B. The Phase 1 vortex amplifier was designed with the information obtained in Test Series No. 1 of Breadboard vortex amplifier No. 1. Later, breadboard tests aided in the development of the Phase 1 vortex amplifier from its initial to its final design.

A layout drawing of the Phase 1 vortex amplifier is shown in Figure 8. Figures 9 and 10 show assembled and disassembled views of the amplifier. The supply flow enters the vortex amplifier around the "button" in a thin annular sheet moving axially toward the vortex chamber. The tangential control and bias control ports are located at the edge of the "button," and the flow from these ports imparts a tangential swirl to the supply flow as it enters the vortex chamber. The gas then moves toward the center of the chamber and exits through the outlet orifice. The final total flow includes the supply flow and control flow. It is measured with an in-line orifice at the exit of the gas generator. A portion of the total flow is recovered in the probe flow receiver, and is measured by the pressure drop across a load orifice. The remaining flow exhausts through the annular area between the chamber orifice and the probe into an exhaust manifold.

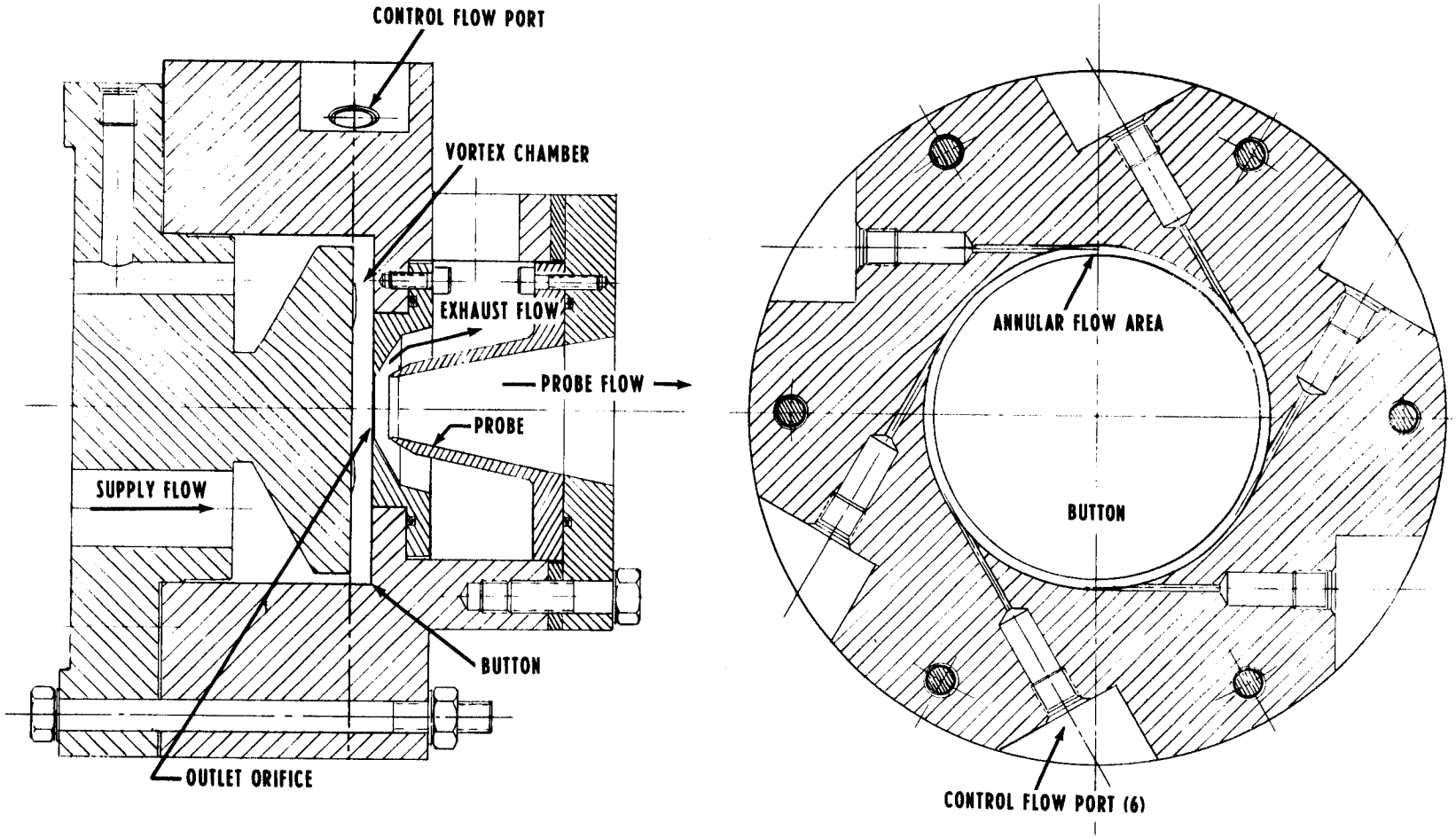

Figure 8 - Phase 1 Vortex Amplifier Layout

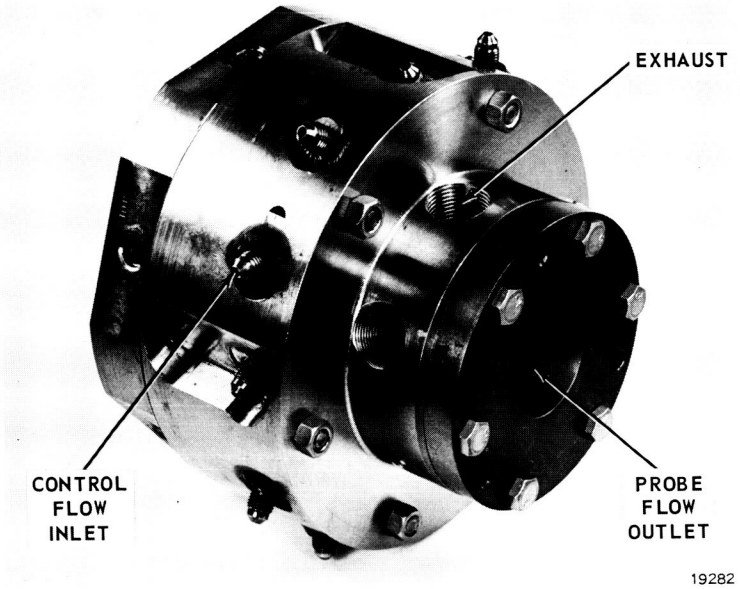

Figure 9 - Phase 1 Vortex Amplifier (Final Design)

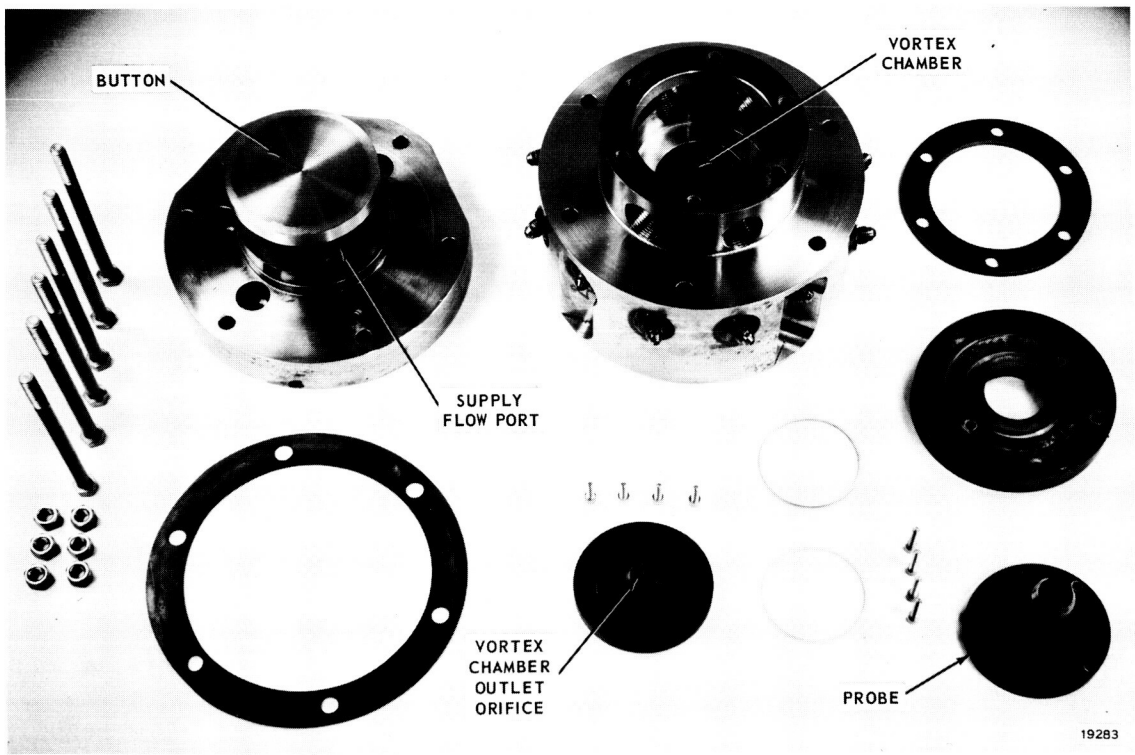

Figure 10 - Phase 1 Vortex Amplifier - Disassembled (Final Design)

Design Analysis

The Phase 1 vortex amplifier was designed for a total flow of 0.5 lb/sec at a supply pressure of 400 psig. The vortex chamber outlet orifice size sets the capacity of the vortex amplifier. This is calculated as follows:

$$A_o = \frac{\dot{w}_t \sqrt{T}}{C_{do} C_2 P_s f_1 \left(\frac{P_p}{P_s}\right)} \qquad (1)$$

where:

A_o = outlet orifice area

$\dot{w}_t$ = (total flow rate) 0.5 lb/sec

T = (gas temperature) 1500°F = 1960°R

C_2 = (constant) 0.185 °R/sec

P_s = (supply pressure) 400 psig

P_p = (probe pressure) 100 psig (max)

f_1 = sonic flow function - (Reference 1)

$f_1 \left(\frac{P_p}{P_s}\right)$ = 1 (Sonic Flow)

C_{do} = 0.763 (This value of discharge coefficient derived from test)

From equation (1), the following dimensions are established:

A_o = 0.379 in^2 (Vortex Chamber Orifice Area)

D_o = 0.695 in. (Vortex Chamber Orifice Diameter)

The chamber diameter was limited to six times the chamber outlet diameter to restrict the envelope size.

$$D_{(cham)} = 6 D_o \qquad (2)$$

A chamber diameter of 4.0 inches was selected.

The button diameter was sized to provide an annular flow area around the button equal to 4 times the area of the vortex chamber outlet orifice. This flow area does not appreciably restrict the supply flow, but does confine the flow sufficiently to provide good mixing with control and bias flow for optimum vortex swirl. This is a sensitive parameter which has not been fully evaluated. Larger annular areas tend to produce degraded performance. This is attributed to the annular sheet being too thick for efficient mixing with control flow. An annular area that is too small represents a restriction in flow in series with the vortex chamber outlet orifice.

The "button" diameter is calculated from:

$$D^2_{(but)} = D^2_{(cham)} - \frac{16\, A_o}{\pi} \qquad (3)$$

resulting in a $D_{(but)} = 3.76$ inches (Button Diameter). This button diameter establishes an annular flow sheet 0.120 inch thick.

The chamber length is calculated using the following considerations. The limiting case or the minimum chamber length is that length which provides a greater flow restriction or smaller flow area than the vortex chamber outlet area.

$$A_o = \frac{\pi}{4} D_o^2 \quad \text{(Vortex Chamber Flow Area)} \qquad (4)$$

$$A_{(cyl)} = \pi D_o \ell \quad \text{(Cylindrical Flow Area inside vortex chamber bounded by } D_o \text{ and chamber length, } \ell) \qquad (5)$$

Letting $A_o = A_{(cyl)}$ and substituting, results in $\ell = \frac{D_o}{4}$.

The minimum chamber length is one-fourth the chamber diameter. Test experience has shown that chamber lengths in excess of $D_o/2$ tend to produce an instability when the vortex amplifier is in the partially modulated condition; the vortex chamber can exhibit an undesirable negative resistance characteristic. A design with stable performance and relatively unrestricted flow can be achieved by using a chamber length equal to $D_o/3$. The resulting length used was 0.232 inch.

Two important ratios must be established during the design of the control ports. These are:

$$(a)\ \frac{P_c}{P_s} = 1.5 \quad \text{(Maximum control/supply pressure ratio)} \tag{6}$$

$$(b)\ \frac{\dot{w}_t}{\dot{w}_c} = 9 \quad \text{(Flow Gain, unbiased)} \tag{7}$$

Ratio (a) establishes the pressure drop across the control ports and ratio (b) defines the control weight flow. The orifice weight flow equation is solved for a single control orifice:

$$A_c = \frac{\dot{w}_c \sqrt{T}}{12\, C_{dc}\, C_2\, P_c\, f_1 \left(\frac{P_s}{P_c}\right)} \tag{8}$$

Substituting (6) and (7) into (8) results in:

$$A_c = \frac{\dot{w}_t \sqrt{T}}{162\, C_{dc}\, C_2\, P_s\, f_1\, (0.667)} \tag{9}$$

where:

A_c = area of one control port

$\dot{w}_t$ = 0.5 lb/sec

T = 1500°F = 1960°R

C_2 = 0.185 $\sqrt{°R}$/sec

P_s = 400 psig

$f_1\,(0.667)$ = 0.961 (k = 1.35)

C_{dc} = 0.84 (This value of discharge coefficient derived from cold gas tests.)

Substituting and calculating the area of each control port.

$$A_c = \frac{0.5 \sqrt{1960}}{162 \times 0.84 \times 0.185 \times 415 \times 0.961}$$

$$A_c = 0.00222 \text{ in}^2$$

$$D_c = 0.054 \text{ in (12 ports)}$$

Twelve control ports are used. These ports are located in a plane perpendicular to the center line of the vortex amplifier and tangent to the chamber outer diameter. Axially, they are positioned at the chamber end of the button inside the annular flow region. The flow restriction over the button is negligible with an annular space of 0.120 inch.

The maximum total flow issues from the vortex chamber orifice in a free jet. Under the maximum flow conditions, control flow is zero and the vortex chamber acts as a simple orifice restriction. As control flow is introduced in increasing amounts, the total flow is reduced and the gas exiting from the vortex chamber orifice assumes a hollow cone shape. The probe flow receiver has a dual requirement in that it must be of sufficient diameter and properly positioned relative to the vortex chamber exit to recover a minimum of 80 percent of the total flow (no swirl) condition. Also under minimum flow (maximum swirl) condition, the total flow must be sufficiently coned to completely miss the probe, with all flow diverted to exhaust. This results in a probe flow modulation from 80 percent of maximum total flow to near zero. The two requirements are mutually conflicting and the best diameter and spacing cannot be theoretically analyzed at this time. They were experimentally resolved during the scale model test program. The following relationships were found to be near optimum:

$$\frac{D_p}{D_o} = 1.1 \tag{10}$$

$$\frac{D_o}{x} = 2.08 \tag{11}$$

where

$$D_p = 1.1 \times 0.695$$

$$D_p = 0.765 \text{ in. (Probe Diameter)}$$

$$x = \frac{0.695}{2.08}$$

$$x = 0.333 \text{ in.}$$ (Probe spacing measured from inside the vortex chamber to the probe face.)

The probe position was made adjustable using replaceable shims. The following table is a summary of significant vortex amplifier dimensions. (see Figure 8 for locations of various parts).

Table 2 - Phase 1 Vortex Amplifier Significant Design Parameters (Final Design)

(a) Vortex Chamber Outlet Diameter	D_o = 0.695 in.
(b) Chamber Diameter	$D_{(cham)}$ = 4.00 in.
(c) Button Diameter	$D_{(but)}$ = 3.76 in.
(d) Chamber length	ℓ = 0.232 in.
(e) Control Port Diameter (12 Ports)	D_c = 0.054 in.
(f) Probe Diameter	D_p = 0.765 in.
(g) Probe Spacing	x = 0.333 in.

These are all final dimensions realized after extensive testing.

Materials Selection

The vortex amplifier, all major test system components, and the manifolding are fabricated from 303 stainless steel. The flow measuring orifices are fabricated from a molybdenum alloy (Mo-0.5 Ti). This material has excellent high temperature properties with good resistance to erosion. The valve and seat of the supply pressure regulator, and the vortex chamber orifice insert and probe of the vortex amplifier are also fabricated from this alloy. All internal screws are fabricated from Haynes Alloy No. 25. Raybestos-Manhattan gasket material (Grade A56) is used throughout as a sealing material. Special metal seals were used under the chamber orifice insert and probe. Copper seals were used in the total and probe flow orifice assemblies. A rubber "O"-Ring seal was found to function successfully on the main parting line between the vortex chamber and button. This is convenient for this type of testing, where many tests are performed, and considerable disassembly is required.

EXPERIMENTAL RESULTS

The design analysis previously described was supported by a test program to continuously evaluate the performance of the Phase 1 vortex amplifier under various conditions. The static performance tests and hysteresis tests to be described were conducted with the final design amplifier, with dimensions as shown previously in Table 2. Baseline testing, which is briefly described, was conducted with an initial design amplifier with built-in flexibility for the purpose of adjusting important parameters.

Test Procedure

Initial testing was accomplished on a cold gas scale model to establish design parameters for the amplifier. This unit is shown in Figure 11. Nitrogen gas was used for all cold gas testing. Its thermodynamic properties are considerably different from the hot gas; however, experience indicated that performance correlation between the two gases would be very close.

All testing with hot gas on the amplifier was accomplished after evaluation of geometry changes in the cold gas test units. A second cold gas test amplifier was fabricated after building the hot gas hardware. It was designed, based on insight gained from testing the initial unit. It proved to be more versatile in evaluating wide range changes in configuration. The unit is shown in Figure 12. Test results using the cold gas hardware are summarized in Appendix B.

The significant performance results obtained with the final design amplifier, shown in Figures 9 and 10, are described in the following sections.

Static Performance

The best static performance realized from the Phase 1 vortex amplifier is shown in Figures 13 and 14, for both hot gas and cold gas test on the same unit. The significant performance parameters realized from these tests are summarized in Table 3.

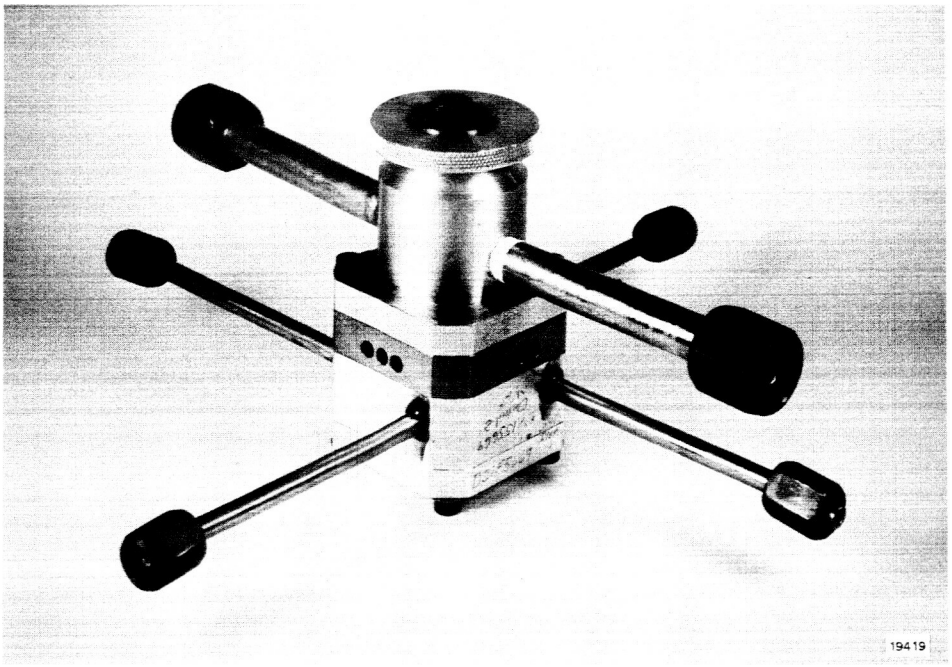

Figure 11 - First Cold Gas Scale Model Vortex Amplifier
(Breadboard No. 1)

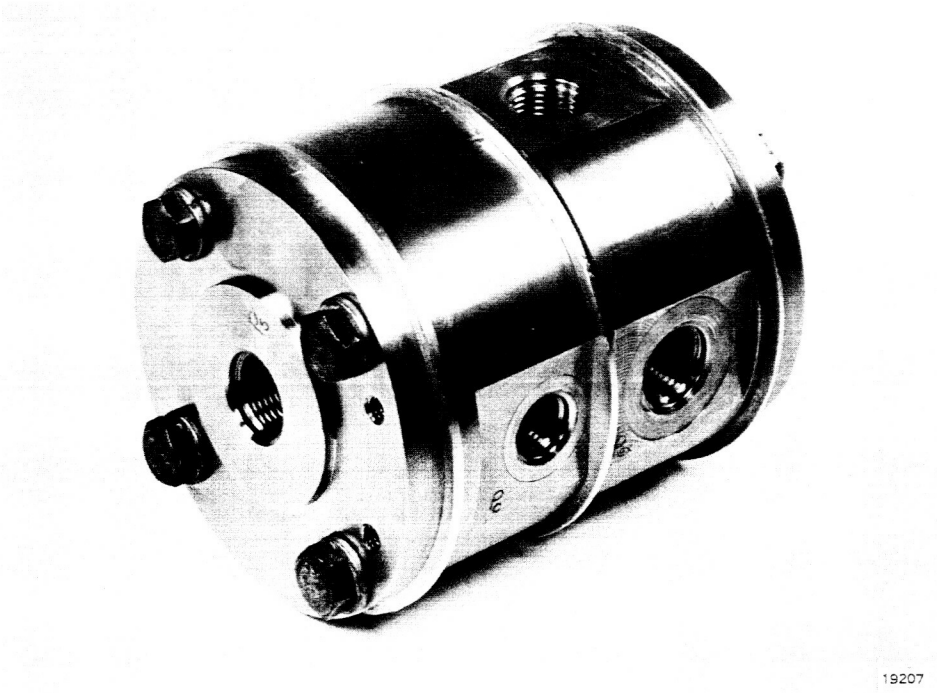

Figure 12 - Second Cold Gas Scale Model Vortex Amplifier
(Breadboard No. 2)

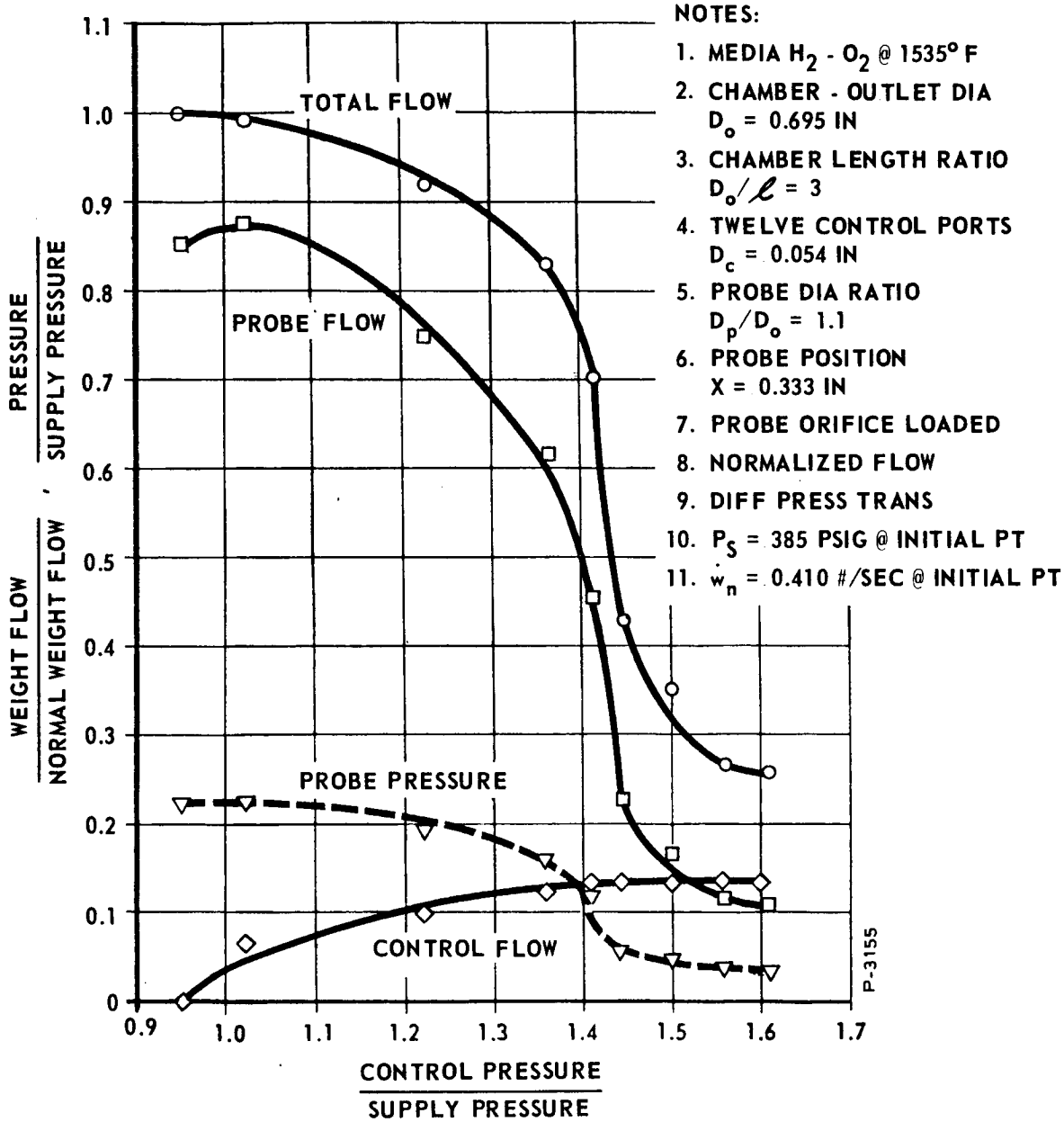

Figure 13 - Hot Static Performance - Test No. 46

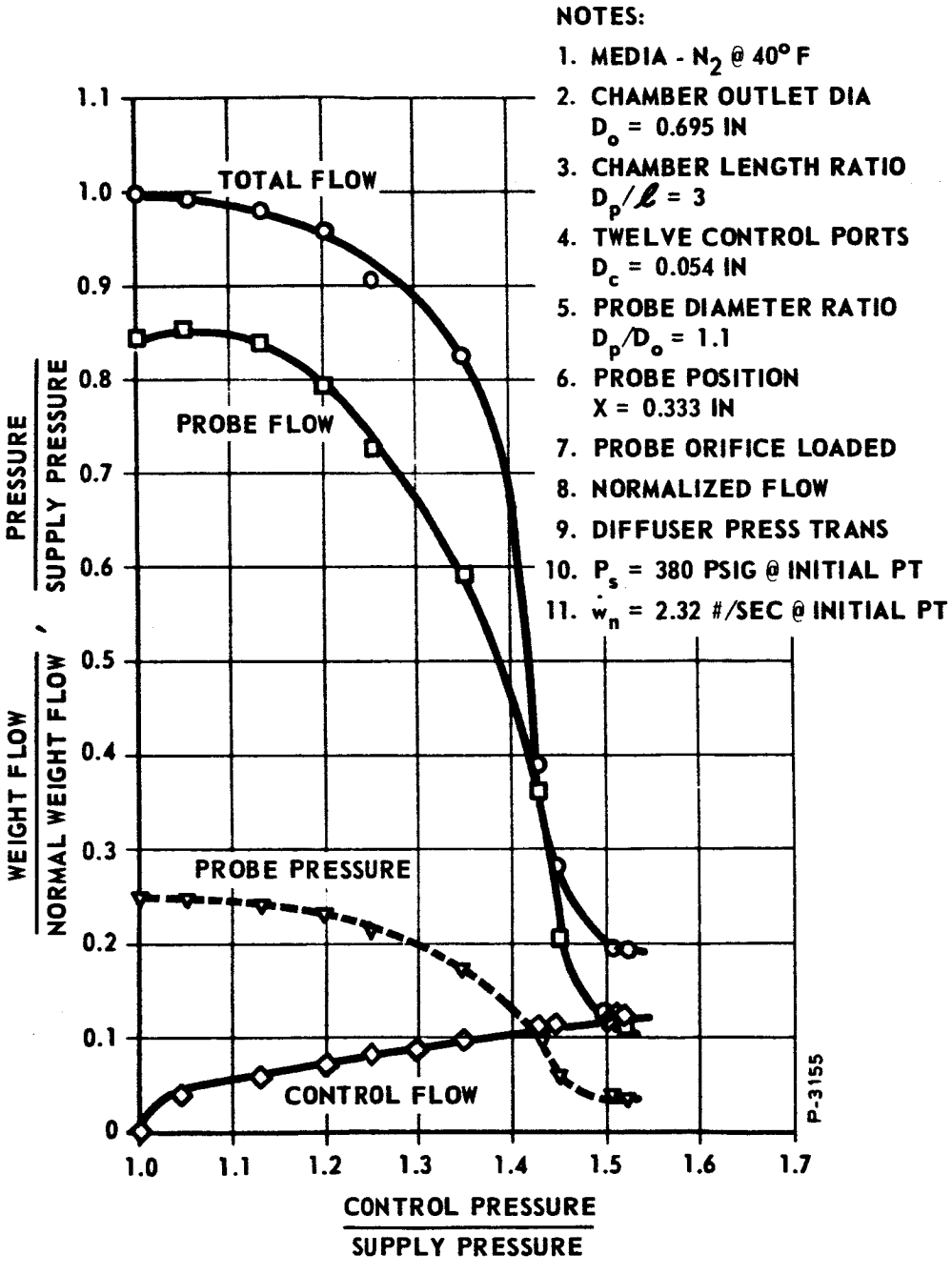

Figure 14 - Cold Static Performance - Test No. 45

Table 3 - Phase 1 Vortex Amplifier Static Performance Characteristics

	Hot Test (Figure 12)	Cold Test (Figure 13)
Initial Probe Flow Recovery	87%	85%
Initial Probe Pressure Recovery	22%	25%
Gain (Unbiased, $\dot{w}_{pi}/\Delta\dot{w}_c$)	6.3	7.2
Total Flow Modulation	3.8:1	5.1:1
Probe Flow Modulation	8.0:1	8.2:1
Final Probe Pressure	4.5 psig	4.0 psig
Control/Supply Pressure Ratio	1.60	1.52

P-3155

The pressure recovery in the probe flow receiver is 85 percent, with a load pressure equal to approximately 25 percent of supply pressure. The goal of decreasing probe flow to zero was not met in this series of tests. It was achieved in the cold gas scale model unit, and there is no reason to believe that it cannot be achieved with this larger unit. There is still one substantial difference in geometry which could affect this significantly. The annular clearance over the button in the Phase 1 vortex amplifier is equal to 4 times the vortex chamber outlet area. The cold gas scale model had a clearance equal to 3 times the vortex chamber outlet area. The total flow modulation is less when operating with hot gas than that for cold gas. This could also be affected significantly by the above difference. The cold gas scale model had a total flow modulation of better than 8 to 1. This geometric effect will be evaluated in the near future for potential improvement in the performance of the Phase 1 vortex amplifier.

The ratio of control pressure to supply pressure is significant, especially in the final system application. Decreasing this ratio reduces the demand for a wide range pressure source. The initial goal was a maximum control pressure equal to one and one-half times supply pressure. This was achieved with the cold gas test. The hot gas test pressure ratio was 1.6. This again is believed to be related to the efficiency in total flow modulation of the vortex chamber. Future efforts will be devoted to reducing this pressure ratio.

One of the most significant parameters is the flow gain of the amplifier or ratio of the maximum flow received at the load to the control flow required at receiver shutoff. This unit shows a flow gain of 6.3 to 1. In a final system application, this is very significant. The original target goal for gain was 100 to 1. High incremental gain can be provided in a single vortex amplifier; however, in order to achieve total flow gains of this magnitude, staging of two units will be necessary.

The flow gain of a single vortex amplifier can be improved by biasing the unit with a percentage of the control flow. It can be seen from the performance curves of Figures 13 and 14 that a control flow equal to approximately 70 percent of the total control flow is required to achieve a significant change in total flow. This suggests the possibility of setting up a lower control flow limit and only operating in the high gain regions of performance. This improves the apparent total flow gain.

The performance assuming the use of bias flow can be evaluated using basic amplifier test data because the same control ports could be used for introducing bias and variable control flow. It is simply a matter of selecting the best operating point. In this case, a bias point corresponding to a ratio of control pressure to supply pressure equal to 1.25 was selected. The resulting performance is shown in Figures 15 and 16 for hot and cold operation. The total flow at the bias point was referenced to unity and all other flows are similarly referenced. Significant performance parameters derived from the bias data plots are shown in Table 4.

The use of bias flow to improve gain is easily accomplished and is very effective. The flow gain is improved for the hot test from 6.3 to 32. Achieving a higher flow gain now becomes a matter of staging more than one vortex amplifier. This is discussed in this report, in a section devoted to staging, on page 42.

Hysteresis

In any device operating with fluids which have viscosity, it is important to evaluate the hysteresis. Figure 17 shows the results of a hysteresis test on the Phase 1 vortex amplifier. The test was started at a control/supply pressure ratio of one and proceeded to full flow modulation (solid line) and returned to the starting point (dashed line).

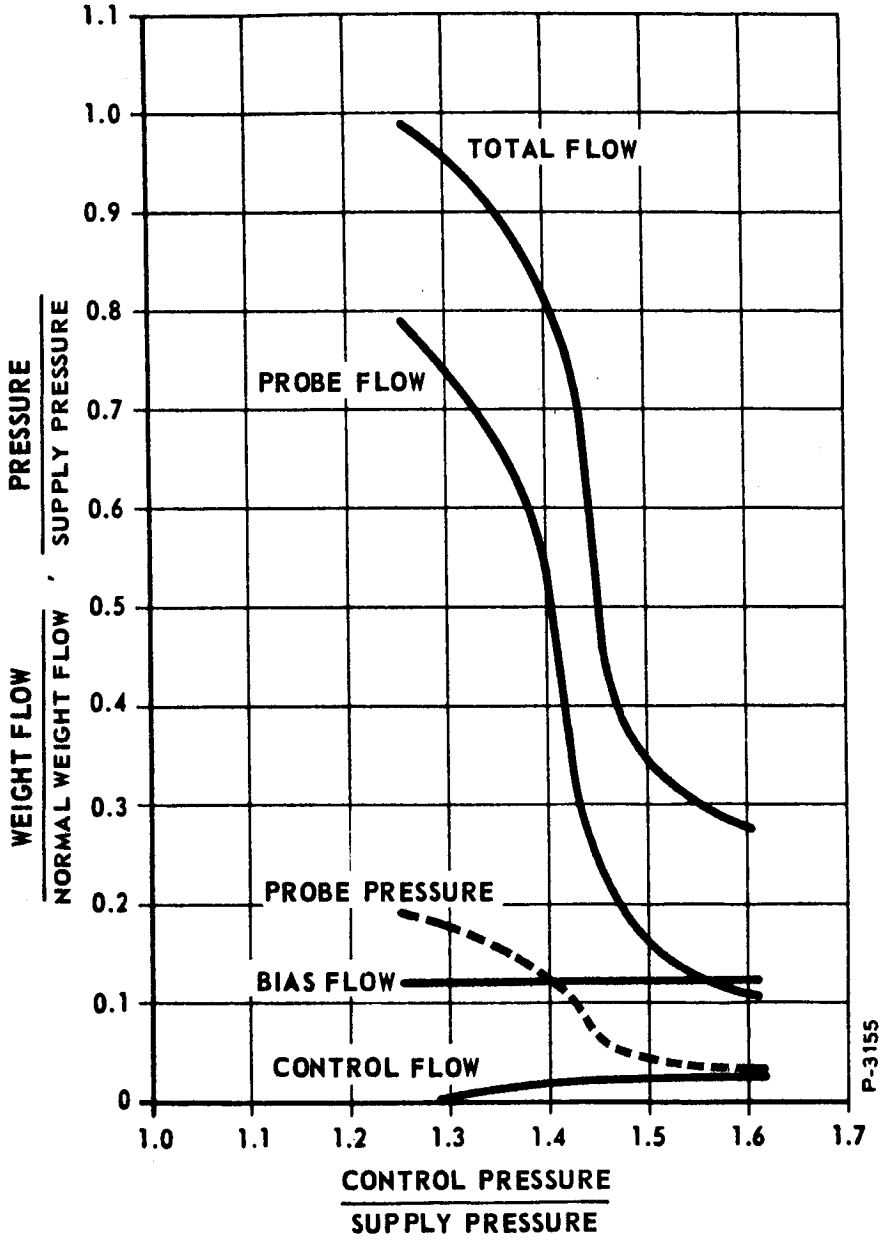

Figure 15 - Hot Bias Performance - Test No. 45

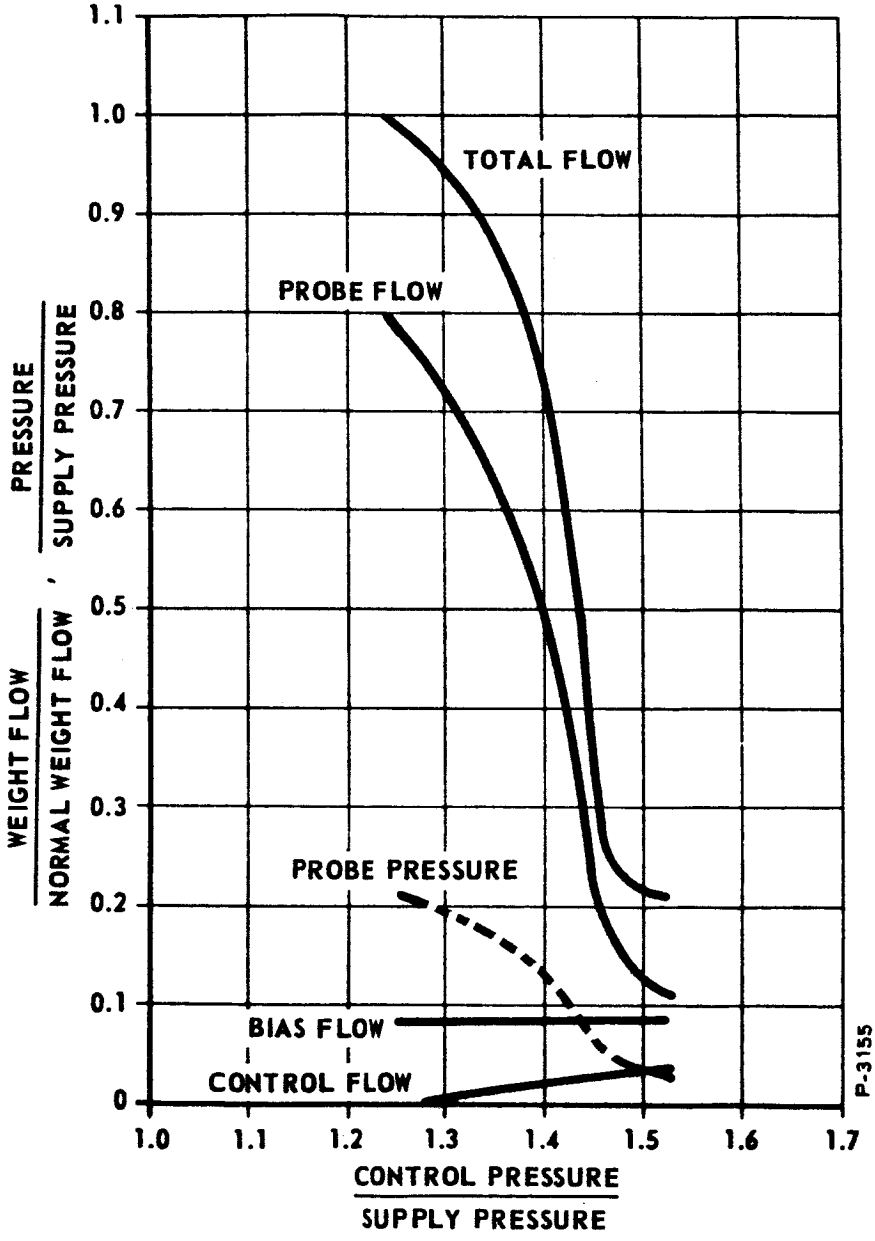

Figure 16 - Cold Bias Performance - Test No. 46

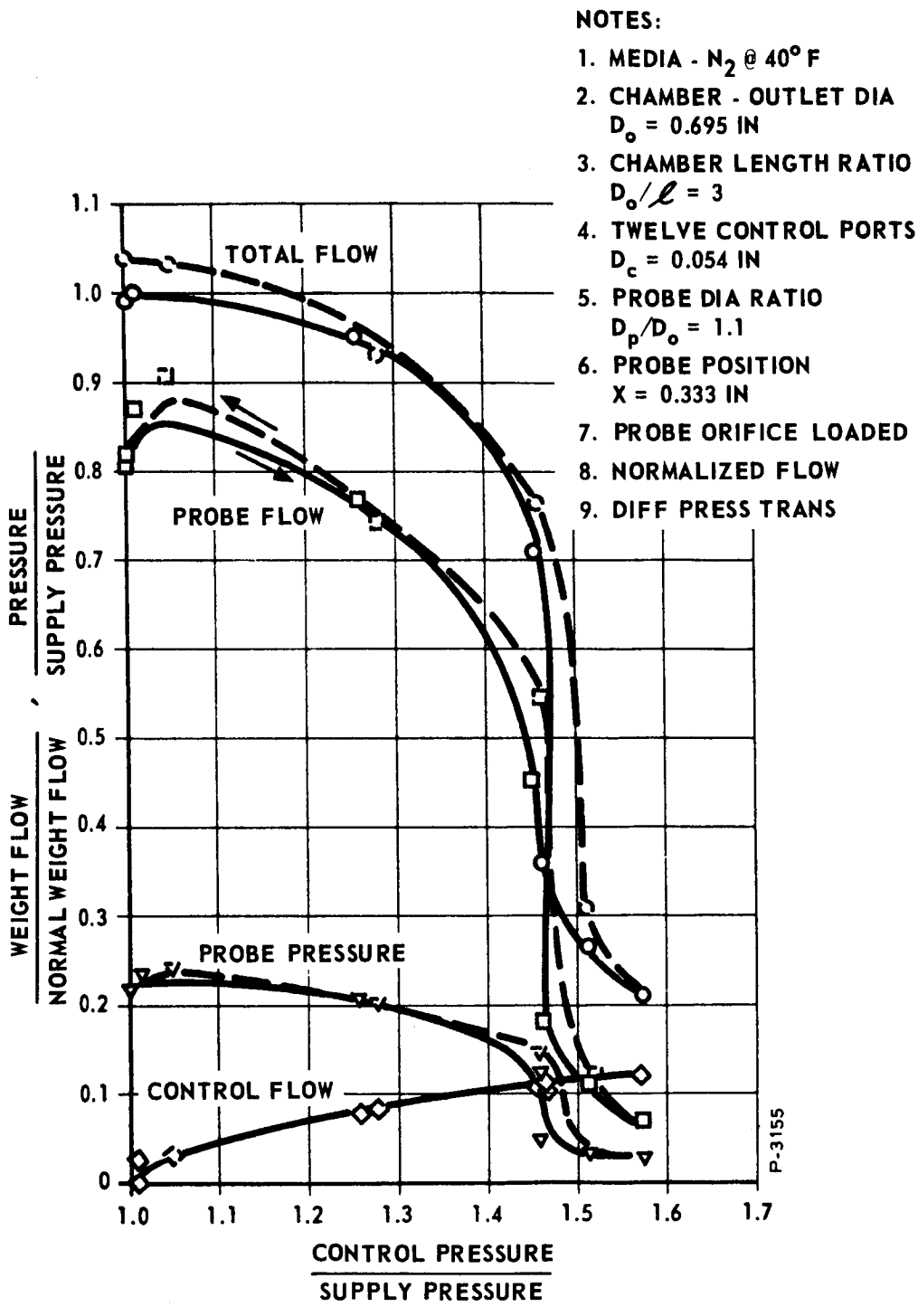

Figure 17 - Hysteresis Performance - Test No. 43

Table 4 - Phase 1 Vortex Amplifier Static Bias Performance Characteristics

	Hot Test Bias (Figure 14)	Cold Test Bias (Figure 15)
Gain (Biased, $\dot{w}_{pb}/\Delta\dot{w}_c$)	32.0	22.8
Bias Probe Flow Recovery	80%	80%
Bias Probe Pressure Recovery	20%	22%
Total Flow Modulation	3.6:1	4.8:1
Probe Flow Modulation	7.3:1	7.3:1
Bias Point (P_c/P_s)	1.25	1.25

P-3155

It is noted that the flow values on the return to maximum flow exceed the initial curve values. The difference is attributed to normal limits of instrumentation and regulator accuracy. The results are preliminary in nature and apply specifically to the configuration tested.

Baseline Testing

The series of hot firings on the Phase 1 vortex amplifier started with the baseline test shown in Figure 18. Significant performance for this test is summarized as follows:

Flow Modulation	3.7:1
Gain	6.3:1 (Unbiased)
Probe Flow Recovery	79%
Gas Temperature	1470°F

Design parameters for this initial unit are shown in Table 5. Concurrent testing on the scale model cold gas units resulted in several changes in the amplifier design. The button length was decreased from 1.125 inches in length to 0.40 inch. The annular area over the button was decreased

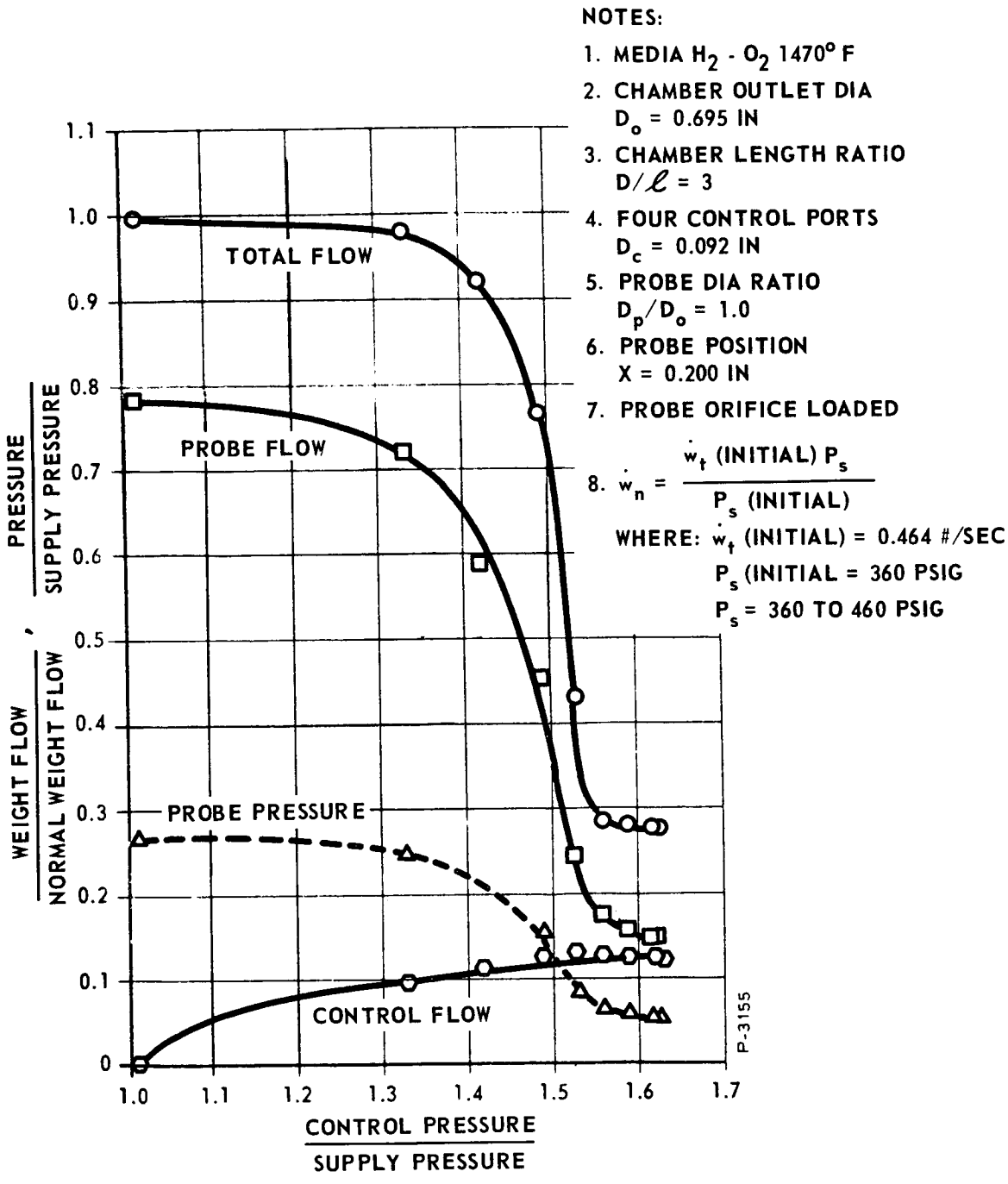

Figure 18 - Baseline Hot Performance - Test No. 27

to four times the area of the vortex chamber outlet. The control ports were relocated to inject at the front edge of the button at the point where the flow enters the vortex chamber. The probe flow receiver entrance was changed from a blunt edge to a sharp edge. The effect of 4 versus 12 control ports was evaluated. Comparison of the values of the various design parameters in Table 5 with Table 2 indicates the changes made to improve performance.

Table 5 - Phase 1 Vortex Amplifier Significant Design Parameters (Initial Design)

(a)	Vortex Chamber Outlet Diameter	D_o = 0.695 in.
(b)	Chamber Diameter	$D_{(cham)}$ = 4.00 in.
(c)	Button Diameter	$D_{(but)}$ = 3.57 in.
(d)	Chamber Length	ℓ = 0.174 in.
(e)	Control Port Diameter (4 Ports)	D_c = 0.092 in.
(f)	Probe Diameter	D_p = 0.695 in.
(g)	Probe Spacing	x = 0.170 in.

VORTEX AMPLIFIER DYNAMIC PERFORMANCE

The vortex amplifier dynamic performance was evaluated using variable frequency sinusoidal and transient inputs. All testing was accomplished using a control flow input equal to 10 percent of maximum control flow. A schematic of the system tested is shown in Figure 19. The vortex amplifier was biased into its high gain operating region using a manual control valve supplying the four control injectors. A separate control injection point was supplied from an electropneumatic hot gas servovalve. The test installation is shown in Figure 20. Supply flow is admitted through a fixed orifice which replaced the hot gas supply pressure regulator. This component was removed because its dynamic response characteristics would contribute to the total response. The probe flow receiver is loaded with a fixed orifice the same as used for the static tests. The probe pressure which is indicative of chamber flow is used as the dynamic output. The exhaust was unrestricted.

Testing was accomplished with sinusoidal frequencies of 5, 10, 20, 50 and 80 cps. Results are shown in Figures 21 through 25. Response to a transient square wave is shown in Figure 26. The operating point was set statically, with the servovalve at half stroke as follows:

P_g	= 840 psig	(Gas Generator Pressure)
P_s	= 315 psig	(Supply Pressure)
P_c	= 320 psig	(Static Control Pressure)
P_p	= 52 psig	(Static Probe Pressure)
$\dot{w}_t$	= 0.400 lb/sec	(Total Flow)
$\dot{w}_c$	= 0.0117 lb/sec	(Static Control Flow)
$\dot{w}_p$	= 0.248 lb/sec	(Probe Flow)

The dynamic control and output pressure amplitudes at a frequency of 5 cps were as follows:

P_{cd}	= 260 to 440 psig	(Dynamic Control Pressure)
P_{pd}	= 43 to 63 psig	(Dynamic Probe Pressure)

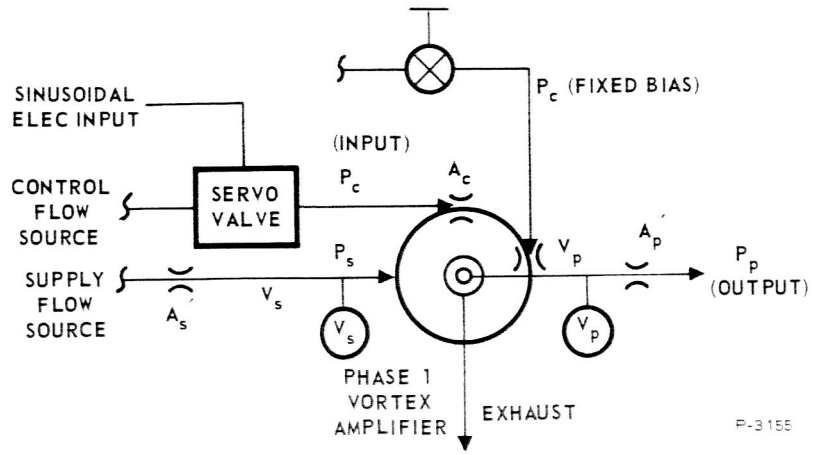

Figure 19 - Dynamic Test Schematic

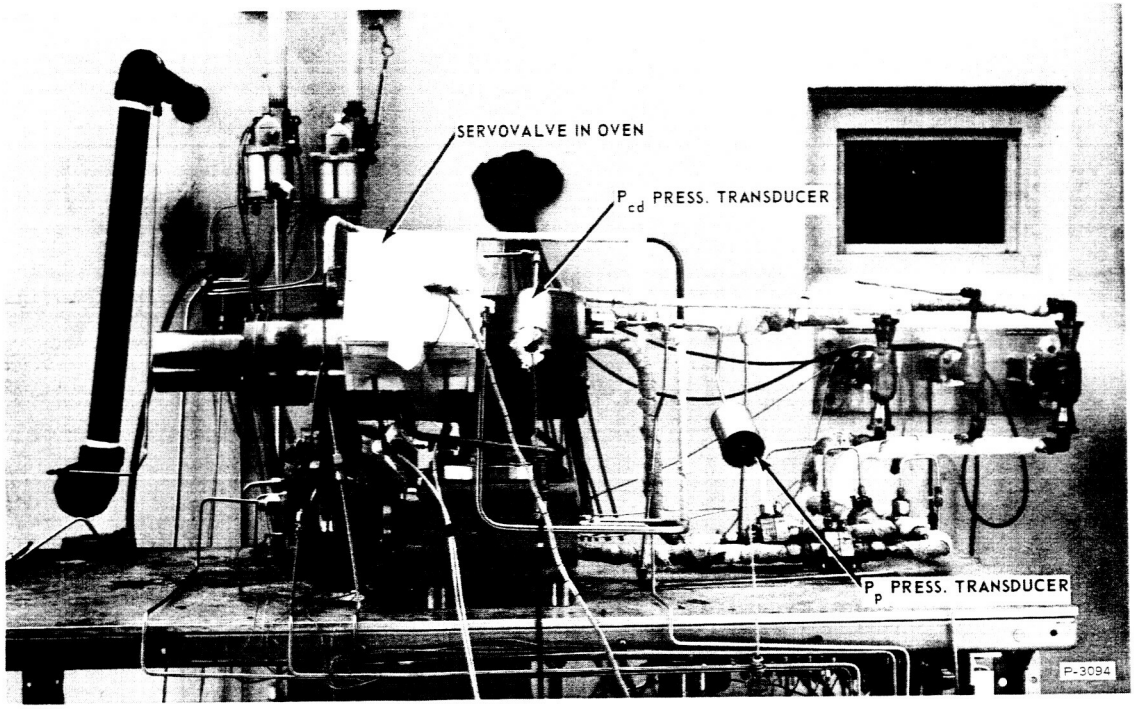

Figure 20 - Dynamic Test Setup

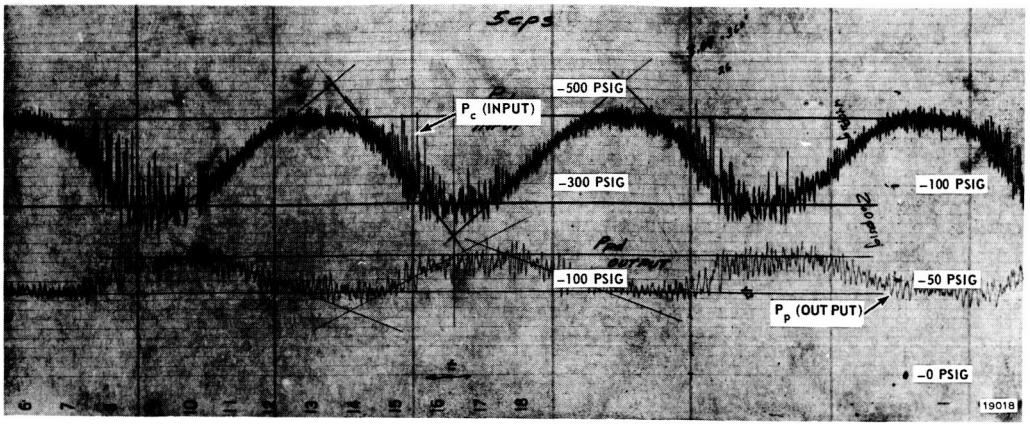

Figure 21 - Frequency Response Data at 5 cps

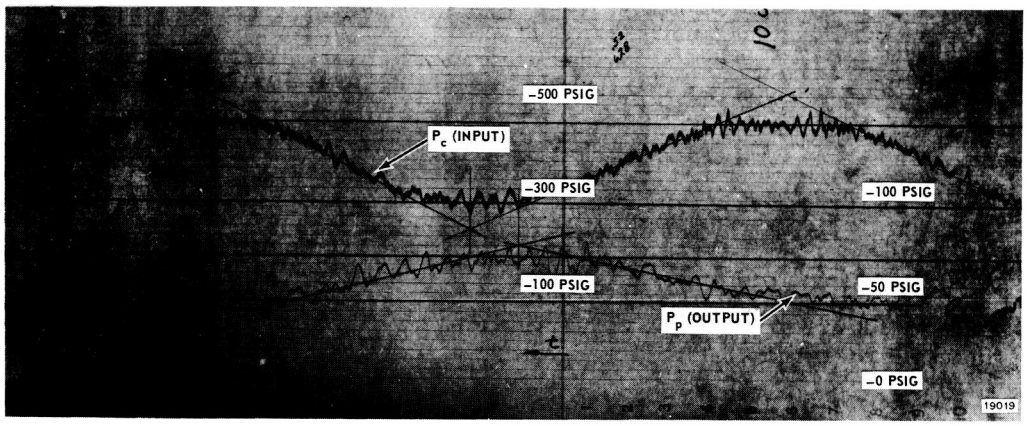

Figure 22 - Frequency Response Data at 10 cps

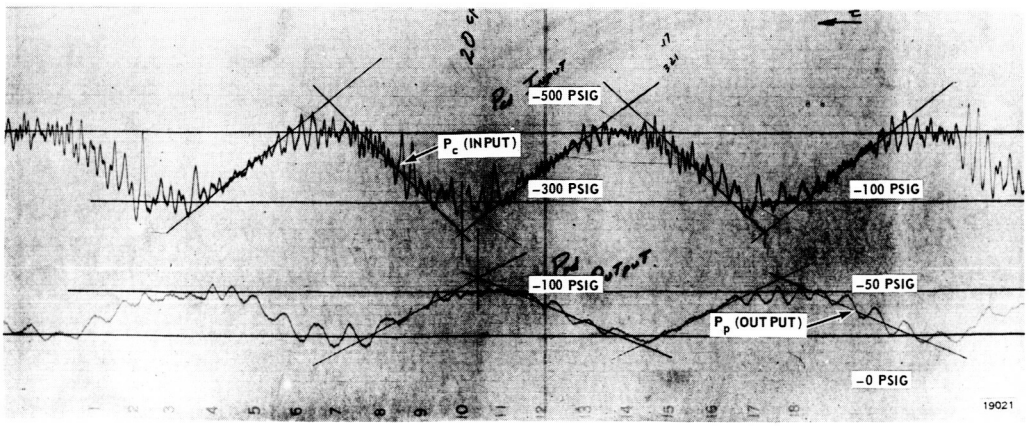

Figure 23 - Frequency Response Data at 20 cps

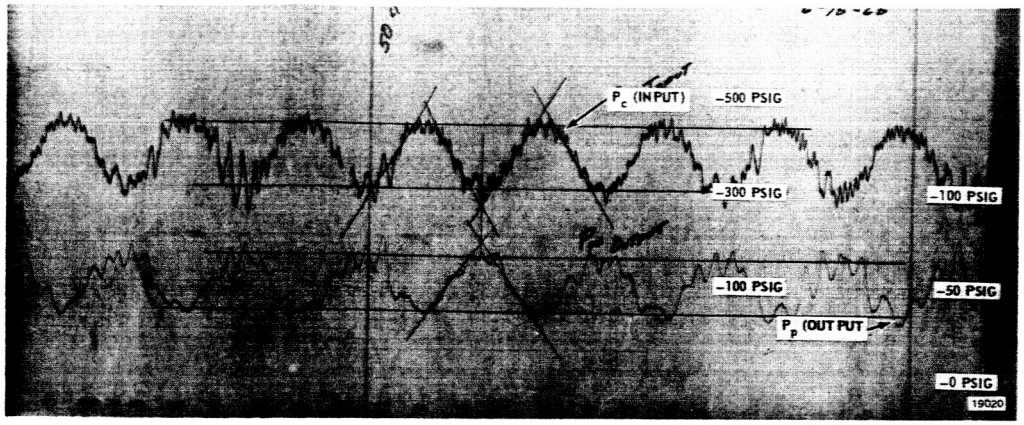

Figure 24 - Frequency Response Data at 50 cps

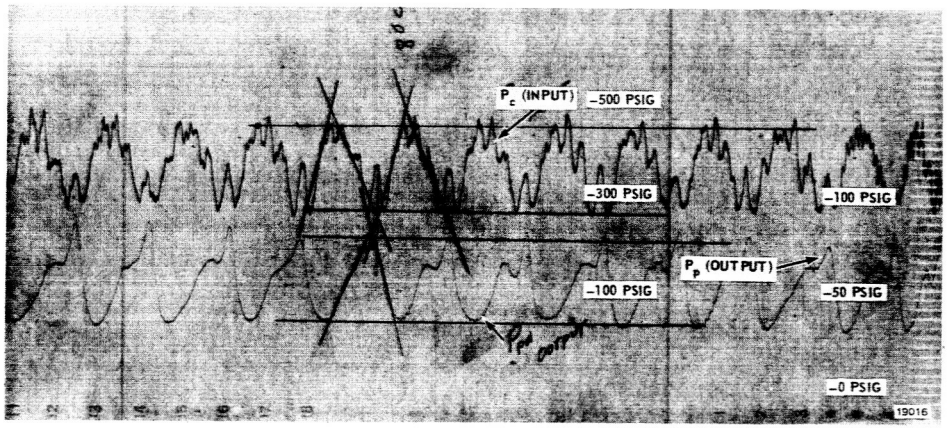

Figure 25 - Frequency Response Data at 80 cps

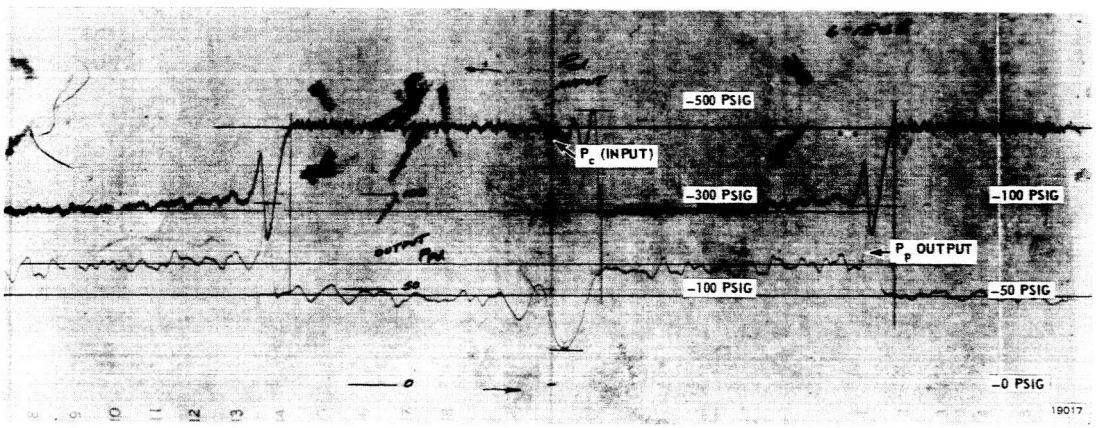

Figure 26 - Square Wave Response

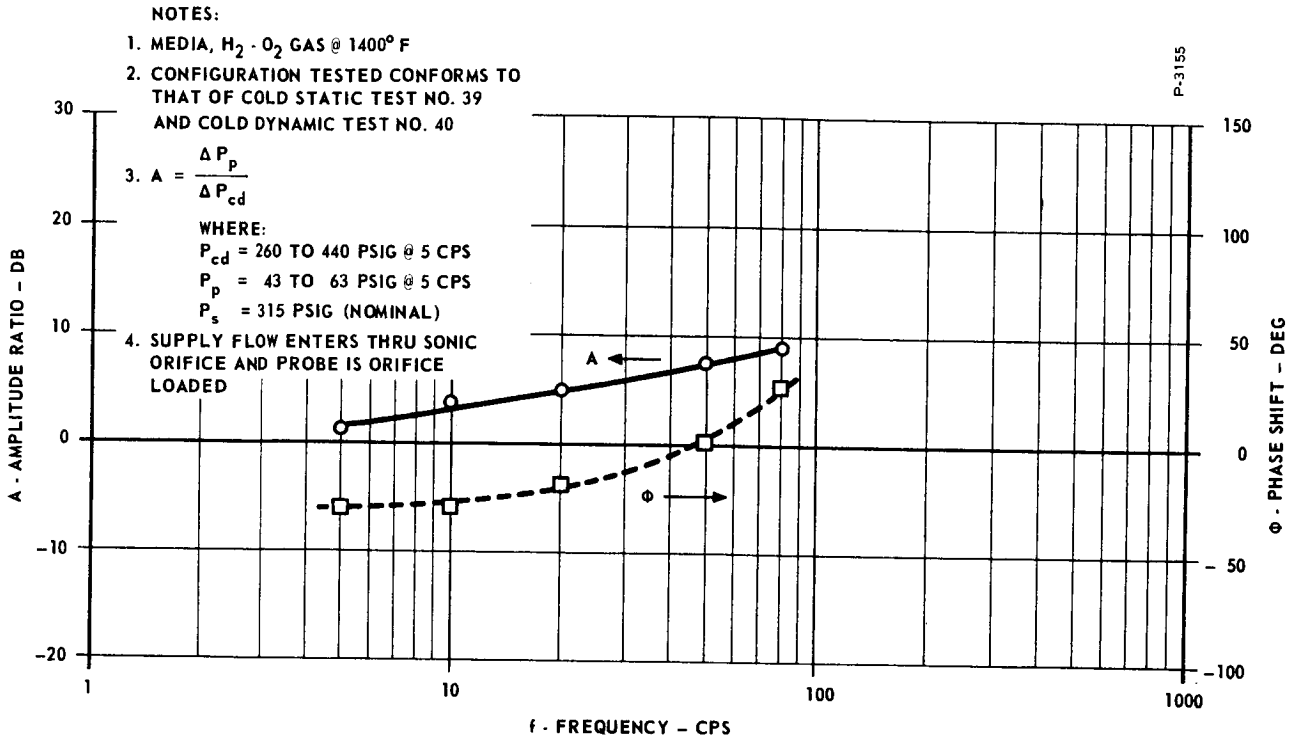

Figure 27 - Hot Dynamic Performance

Figure 27 is a Bode plot of the frequency response obtained for the total system. The zero decibel point was computed from the square wave output/input amplitude relationship. Negative phase shifts are indicative of phase lead, where the output amplitude peaks in time before the input amplitude. At 5 cps, the lowest test frequency, there is an amplitude ratio (A) of +1 db and 30 degrees phase lead. At sufficiently low frequencies, the amplitude ratio would be zero and the phase shift would be zero. As the frequency increased, the amplitude ratio increased and the phase lead decreased until, at 50 cps, the phase lead was equal to zero. This lead characteristic may be useful for systems where this concept will be applied. The effect is definitely phase lead compensation.

This phenomenon can be explained by analyzing the complete system, including supply dynamics. The supply pressure in this case was not held constant while sinusoidally varying the control pressure, and the dynamics of the variation of control pressure in combination with the inherent impedance characteristics of the vortex amplifier produce the phase lead. In a typical secondary injection thrust vector

control application, the supply pressure would probably be obtained from the rocket engine combustion chamber and would be held nearly constant. It is therefore desirable to determine the dynamic response of the vortex amplifier with a constant supply pressure.

An analysis of the total system is contained in Appendix C. This was done for the cold gas system test; however, the transfer functions are applicable with proper substitution of constants. The basic block diagram is shown in Figure 28.

The transfer function between probe pressure and control pressure with a varying supply pressure is:

$$\frac{P_p}{P_s} = \frac{-(K_1 - K_2K_3)}{(1 + T_1 s)(1 + T_2 s)} \left[1 + \left(\frac{K_1 T_2}{K_1 - K_2K_3} \right) s \right] \qquad (12)$$

where:

$K_1 = \frac{P_{pc}}{P_c} = 0.15$ psi/psi (Small increment gain resulting control pressure to control pressure-dependent probe pressure.)

$K_2 = \frac{P_s}{P_c} = 0.40$ psi/psi (Small increment gain relating control pressure to supply pressure.)

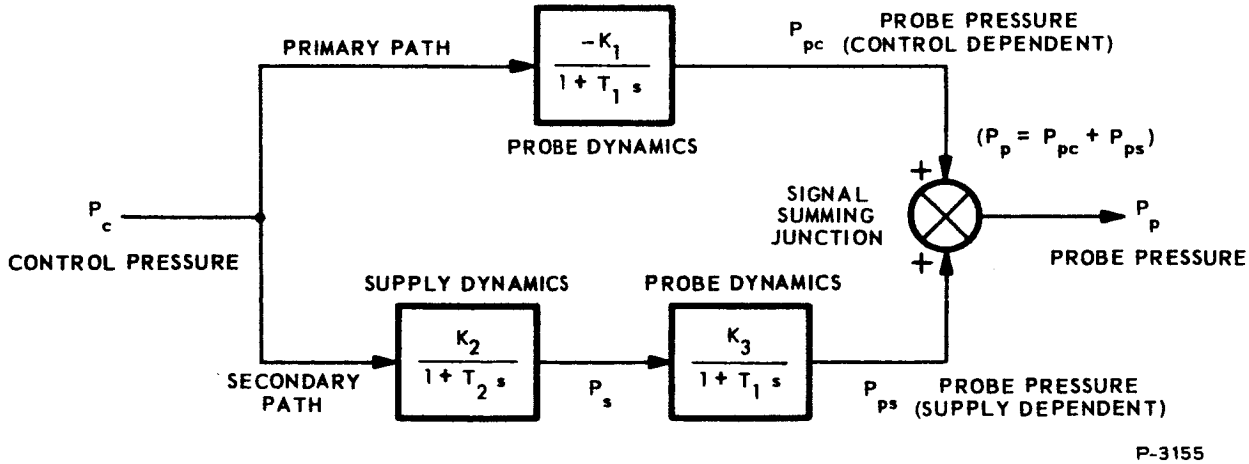

Figure 28 - Block Diagram of Basic System

$$K_3 = \frac{P_{ps}}{P_s} = 0.25 \text{ psi/psi}$$

(Small increment gain relating supply pressure to supply pressure-dependent probe pressure.)

These values of gain are taken from Appendix C. It can be shown that there is little change in these gains between cold and hot gas testing. The time constants are computed as follows:

$$T_1 = \frac{V_p}{kQ_p} \tag{13}$$

where

T_1 = time constant between P_c and P_{pc}

k = 1.36 (Ratio of specific heats for $H_2 - O_2$ hot gas.)

V_p = 24 in^3 (Actual measurement, probe volume made purposely large to facilitate probe pressure measurement, also to simulate SITVC application.)

$$Q_p = \frac{\dot{w}_p R T}{P_p}$$

$\dot{w}_p$ = 0.248 lb/sec

P_p = 67 psia

R = 5190 in/°R

T = 1860°R @ 50 cps

Substituting into above equation:

$$Q_p = 35{,}700 \text{ in}^3/\text{sec}$$

$$T_1 = \frac{24}{1.36 \times 35{,}700}$$

$$T_1 = 4.95 \times 10^{-4} \text{ sec (Probe Response Time Constant)}$$

This time constant has an equivalent frequency of:

$$f_1 = \frac{1}{2\pi T_1} = \frac{1}{2\pi \times 4.95 \times 10^{-4}}$$

f_1 = 321 cps (Probe response and potential response of Phase 1 vortex amplifier)

Compute T_2:

$$T_2 = \frac{V_{se}}{k Q_s} \tag{14}$$

where

T_2 = time constant between P_s and P_{ps}

V_s = 52 in^3 (actually measured)

V_{se} = 26 in^3 (effective volume reduced because of volume separation)

$$Q_s = \frac{\dot{w}_s R T}{P_s}$$

$$\dot{w}_s = \dot{w}_t - \dot{w}_c$$

$$= 0.400 - 0.0117$$

$\dot{w}_s$ = 0.388 pound/sec

P_s = 330 psia

$$Q_s = \frac{0.388 \times 5190 \times 1860}{330}$$

Q_s = 11,320 in^3/sec

$$T_2 = \frac{26}{1.36 \times 11320}$$

T_2 = 16.86×10^{-4} sec (Supply Response Time Constant)

This time constant has an equivalent frequency of:

$$f_2 = \frac{1}{2\pi T_2} = \frac{1}{2\pi \times 16.86 \times 10^{-4}}$$

$$f_2 = 94.5 \text{ cps (Supply Response)}$$

Substitute gains and time constants into equation (12):

$$\frac{P_p}{P_c} = \frac{-0.05\ (1 + 0.00506\ s)}{(1 + 0.000495\ s)\ (1 + 0.001686\ s)} \qquad (15)$$

Equation (15) is the analytically derived transfer function relating probe pressure to control pressure. It is plotted in Figure 29. It is seen that the curves are similar, indicating a fairly accurate analytical model. Since the analysis was successful in simulating the actual performance with varying supply pressure, it is only necessary to eliminate the varying supply pressure from the analysis to predict the performance for a constant supply pressure. This is done by allowing $T_1 = 0$ in equation (12) and the effects of a varying supply pressure are isolated.

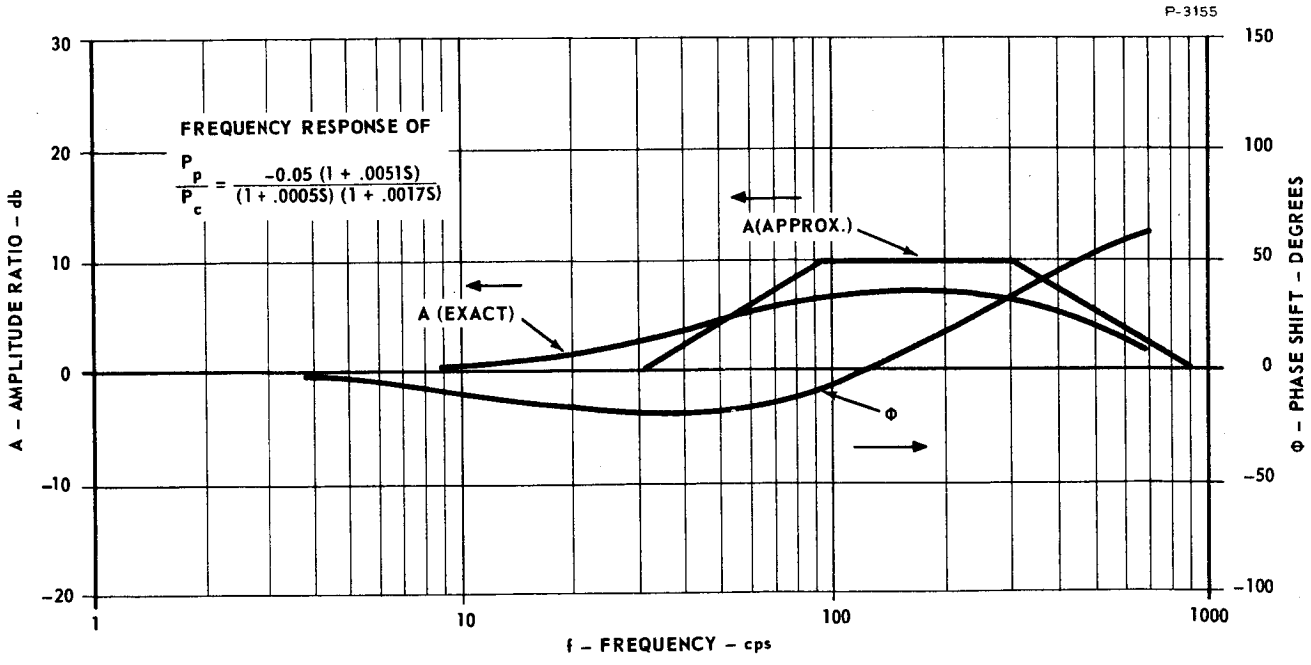

Figure 29 - Theoretical Dynamic Performance - Varying Supply Pressure

$$\frac{P_p}{P_c} = \frac{-(K_1 - K_2 K_3)}{(1 + T_2 s)} \left[1 + \left(\frac{K_1 T_2}{K_1 - K_2 K_3}\right) s\right] \qquad (16)$$

Substituting constants

$$\frac{P_p}{P_c} = \frac{-0.05\ (1 + 0.00506\ s)}{(1 + 0.001686\ s)}$$

Subtracting these dynamics from the test performance shown in Figure 28 results in the performance shown in Figure 30, which is for the basic vortex amplifier with supply pressure assumed constant. This performance is very good and for applications to rocket engine thrust vector control, will provide considerably better dynamic performance than concepts presently being used.

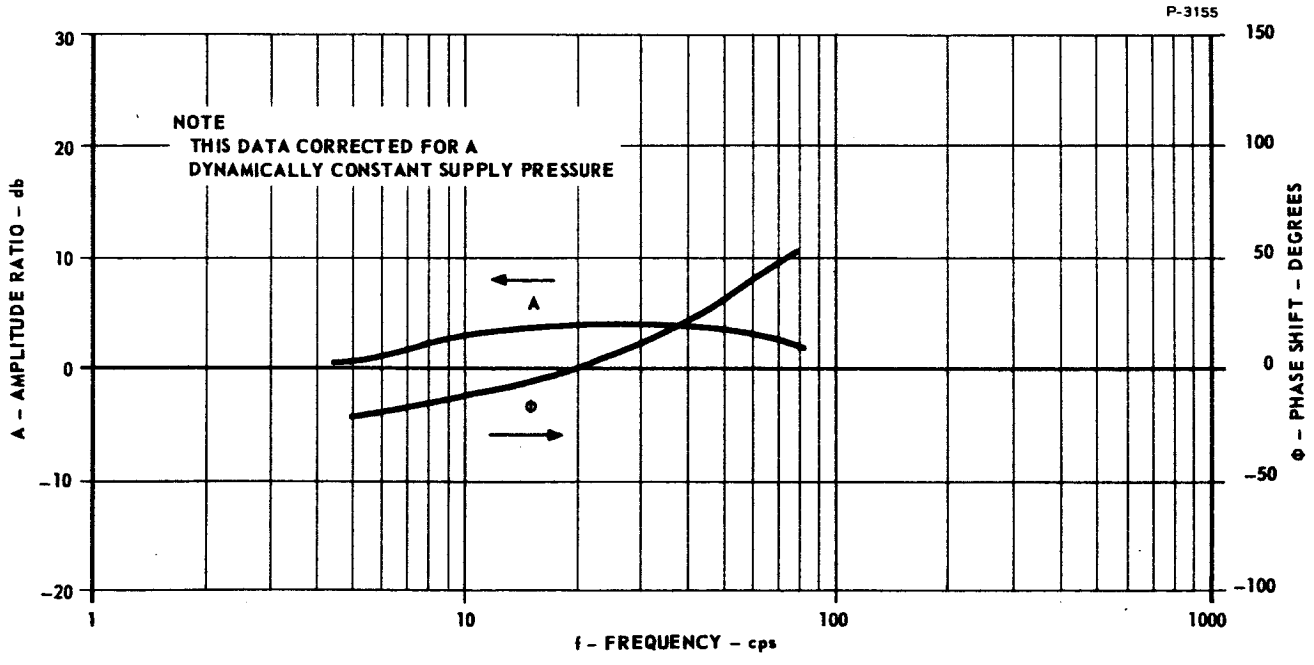

Figure 30 - Corrected Hot Dynamic Performance

VORTEX AMPLIFIER STAGING

The basic vortex amplifier when used for flow control has a flow gain of approximately 30 to 1 when utilizing the concept of bias flow. A gain of 200 to 1 is desirable. This can be achieved simply by staging two vortex amplifiers in series. The two-stage unit would consist of a power stage and a control stage, of which the power stage would be the larger by about one order of magnitude. A schematic of a staged vortex amplifier is shown in Figure 31. The supply pressure into the power stage is assumed as unity and is used as the reference for all other system pressures. The power stage control pressure requires a variation in pressure ratio of 1.3 to 1.5. At a control pressure ratio of 1.3, the power stage is biased to the high gain operating region. Increasing the control pressure ratio to 1.5 reduces the power stage flow to minimum value and modulates the probe or output flow from maximum recovered flow to zero flow. Power stage normalized performance is shown in Figure 31. All data is normalized against power stage supply pressure and power stage total flow at the bias point.

The control stage operates at a higher pressure than the power stage because its output is used as control flow to the power stage. Supply pressure to the control stage is established with a ratio of 1.9. This is sufficiently high to recover a maximum output control pressure ratio of 1.5, the maximum value of P_{c1}. The control stage can also be biased to operate in the high gain region. A minimum control stage control pressure ratio of 2.1 is used to obtain this bias. Increasing P_{c2} ratio from 2.1 to 2.5 results in modulation of the control stage over the desired operating range. The minimum output of the control stage is set to provide the flow required to set the power stage at the biased operating point.

The control stage configuration is different from the power stage. No probe is required, because this unit must supply power stage bias flow and consequently is not required to modulate output flow to zero. The control stage thus is much simpler in design.

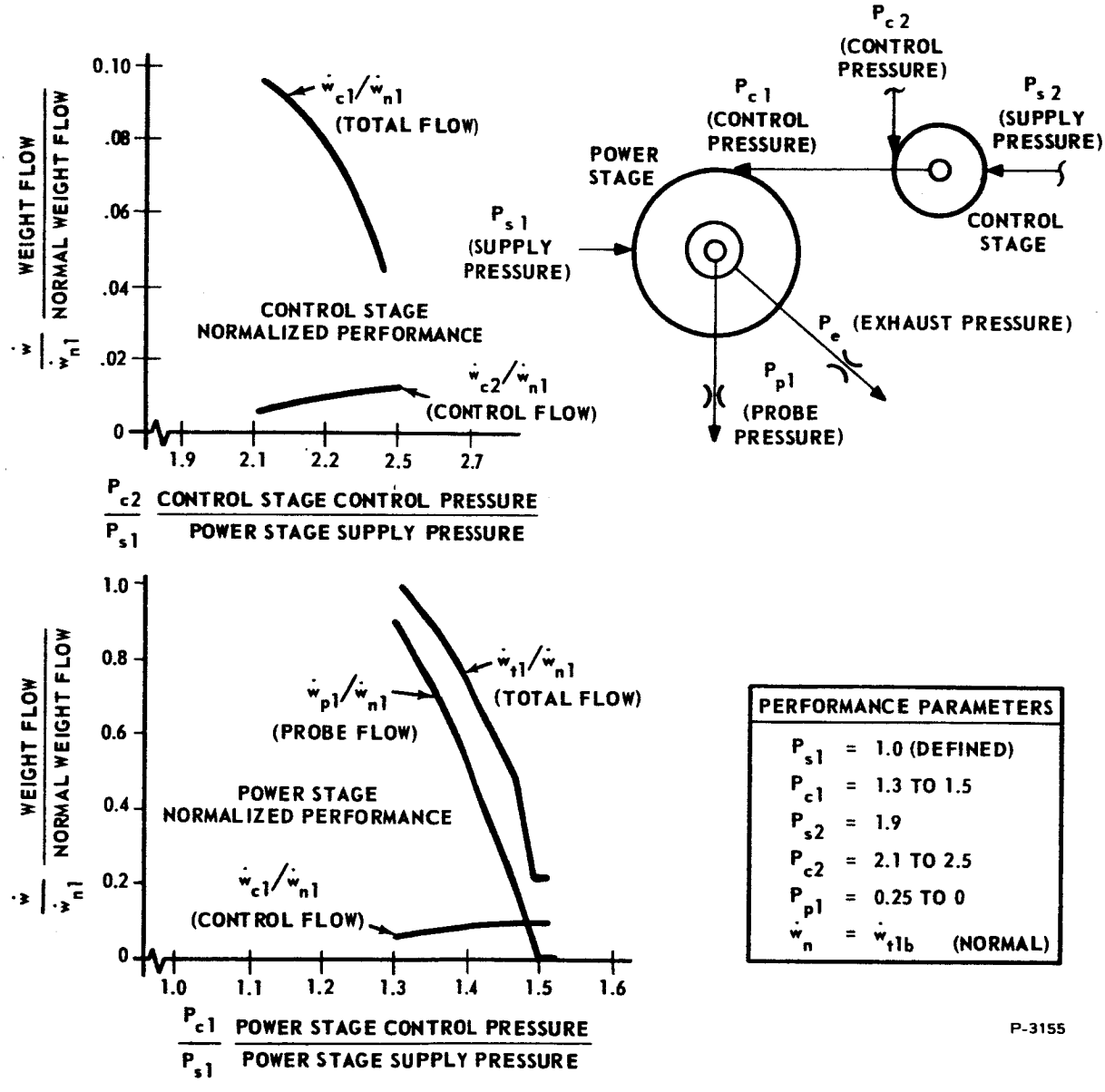

Figure 31 - Staged Vortex Amplifier Schematic

The control stage normalized performance is shown in Figure 31. The power stage control flow ratio is common to both curves. It is seen that only a small change in control stage control flow ($\dot{w}_{c2}/\dot{w}_{n1}$) is required and that the staging technique should produce gains in excess of 200:1.

HYDROGEN-OXYGEN GAS GENERATOR

A single hydrogen-oxygen gas generator was selected as the gas source for the Phase I vortex amplifier. Since gas is required at two pressure levels, i.e., supply gas and control gas, it was necessary to generate the gas at a high pressure and provide a hot gas pressure regulator to drop the gas pressure to the vortex amplifier supply pressure. A simple orifice was determined to be unsatisfactory in this application because of the 5 to 1 modulation range in total flow which would produce changes in supply pressure.

Gas Properties

The desired gas temperature is 1500°F. A hydrogen-rich reaction is used. The presence of free hydrogen in the exhaust products of the hydrogen-rich reaction assures a low molecular weight which is desirable for a high performance secondary injection thrust vector control system.

The hydrogen-rich reaction may be written as:

$$a\,H_2 + b\,0_2 \longrightarrow c\,H_2 + d\,H_2 0 + \text{Heat} \qquad (17)$$

The temperature resulting from this reaction is a function of the temperature of the hydrogen and oxygen prior to the reaction, the O/F ratio (weight 0_2/weight H_2, prior to reaction), and the reaction pressure.

The reaction pressure affects the reaction temperature obtained with a given O/F ratio because of the effects of disassociation and reassociation. These effects do not become significant until fairly elevated temperatures are reached. In Reference (2) it is shown that the effect of reaction pressure on reaction temperature can be ignored at reaction temperatures less than 3240°R and pressures less than 900 psia.

O/F Ratio. - Figure 32 shows the adiabatic bulk temperatures resulting from the combustion of an excess of hydrogen with oxygen for various temperatures at the inlet of the combustion zone. These

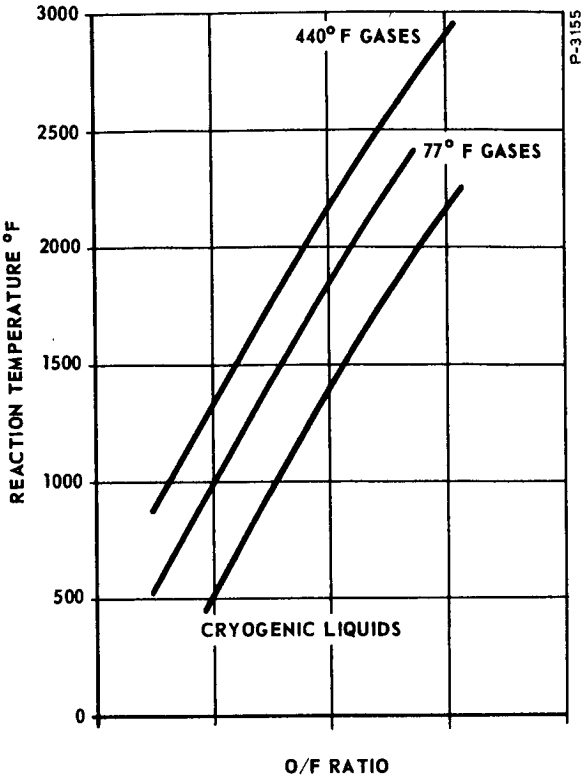

Figure 32 - Adiabatic Bulk Temperature

curves have been plotted from data given in References (3) and (4). This figure shows that the effect of initial temperature is significant and also shows that the bulk temperatures are quite sensitive to O/F ratio. It is seen that an O/F ratio of 0.8 is required to produce a bulk gas temperature of 1500°F, assuming that the propellants are initially at 77°F.

Molecular Weight. - With the hydrogen-rich reaction, assuming temperatures low enough to ignore disassociation effects, a simple relationship exists between f, the O/F ratio, and the apparent molecular weight, M. From equation (17), the following relationships may be written:

$$f = \frac{32b}{2a} \tag{18}$$

$$M = \frac{2c + 18d}{c + d} \tag{19}$$

$$a = c + d \tag{20}$$

$$d = 2b \tag{21}$$

Equations (18) through (21) may be combined to give:

$$M = 2(1 + f) \tag{22}$$

Letting

$$f = 0.8$$

$$M = 3.6$$

Figure 32 and equation (22) are combined to provide Figure 33, a plot of values of M versus adiabatic bulk temperatures.

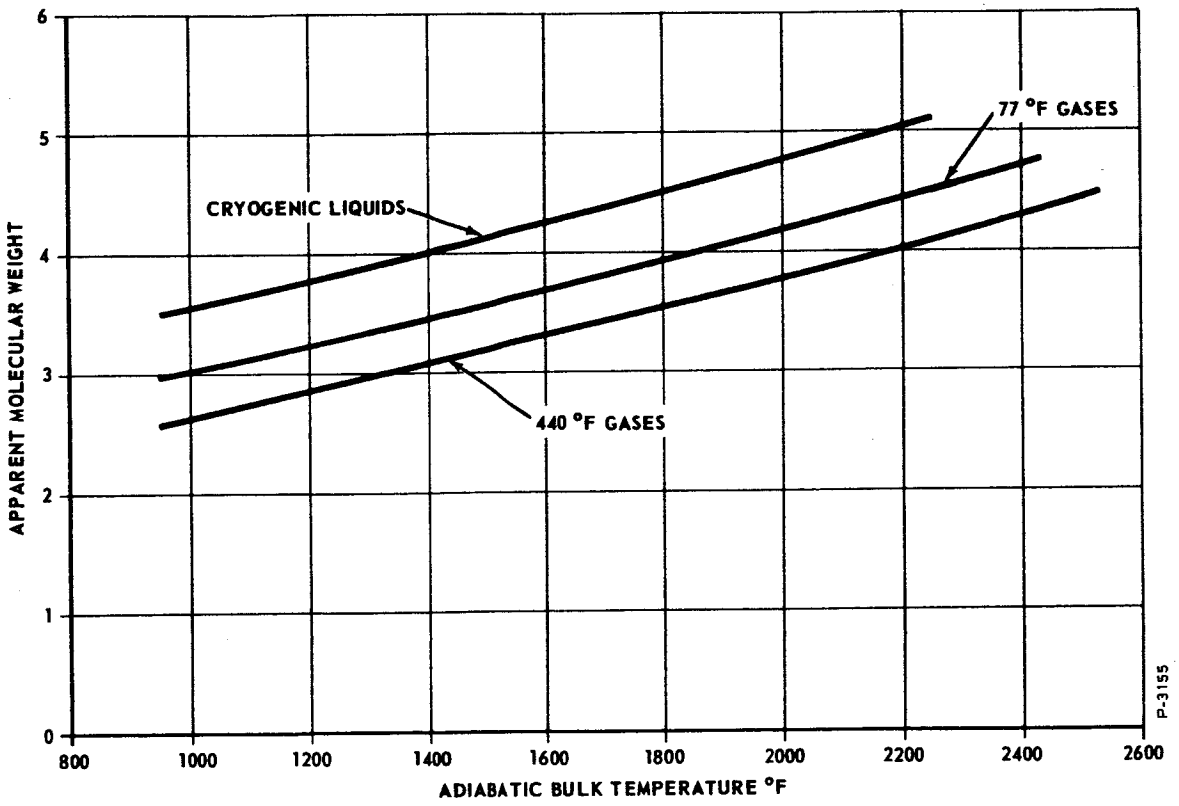

Figure 33 - Apparent Molecular Weight

Ratio of Specific Heats. - The specific heat of the mixture can be computed from:

$$C_{pm} = X_s C_{psm} + X_h C_{phm} \tag{23}$$

where:

C_{pm} = molar specific heat at constant pressure of mixture

X_h = mole fraction of hydrogen in mixture

X_s = mole fraction of steam in mixture

C_{psm} = molar specific heat of steam

C_{phm} = molar specific heat of hydrogen

From equation (17) the mole fraction may be expressed as:

$$X_h = \frac{c}{c + d} \tag{24}$$

and

$$X_s = \frac{d}{c + d} \tag{25}$$

Substitution of equations (18), (20) and (21) into (24) and (25) gives:

$$X_h = 1 - \frac{f}{8} \tag{26}$$

$$X_s = \frac{f}{8} \tag{27}$$

The specific heat at constant pressure on a weight basis, denoted C_{pw}, may be obtained from:

$$C_{pw} = \frac{C_{pm}}{M} \tag{28}$$

Values of C_{pw} have been computed from equations (23), (26), (27), and (28) using values of molar specific heats for steam and oxygen from Reference (2). The values of C_{pw} are plotted in Figure 34 as a function of temperature.

The specific heat ratio, k, may be computed from the molar specific heat of the mixture by means of the following equation from Reference (5).

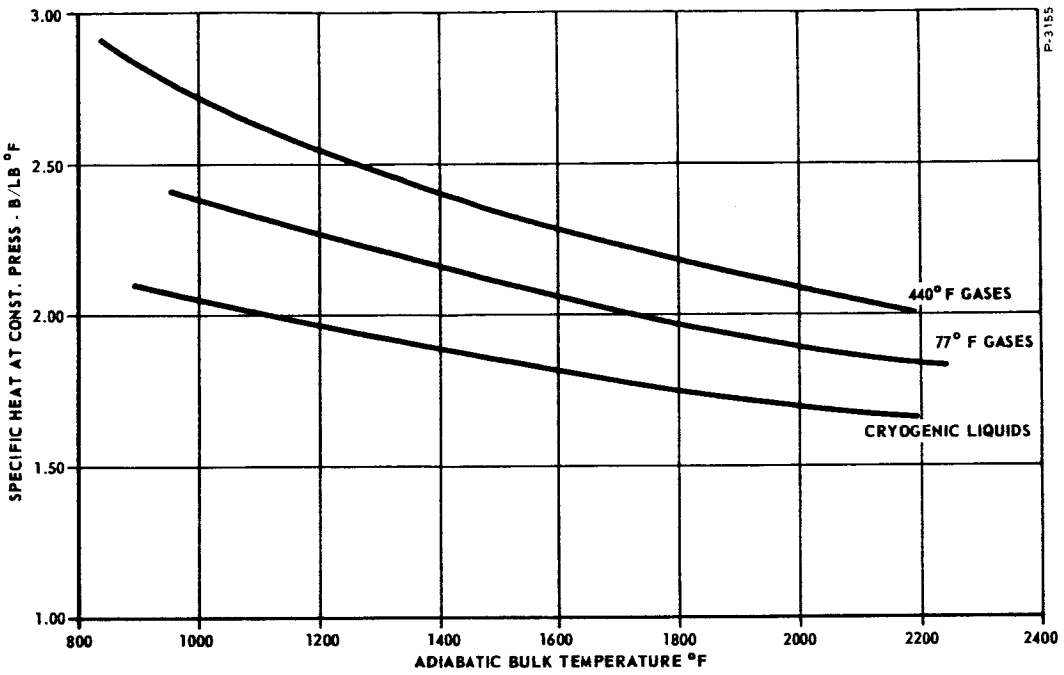

Figure 34 - Specific Heat at Constant Pressure

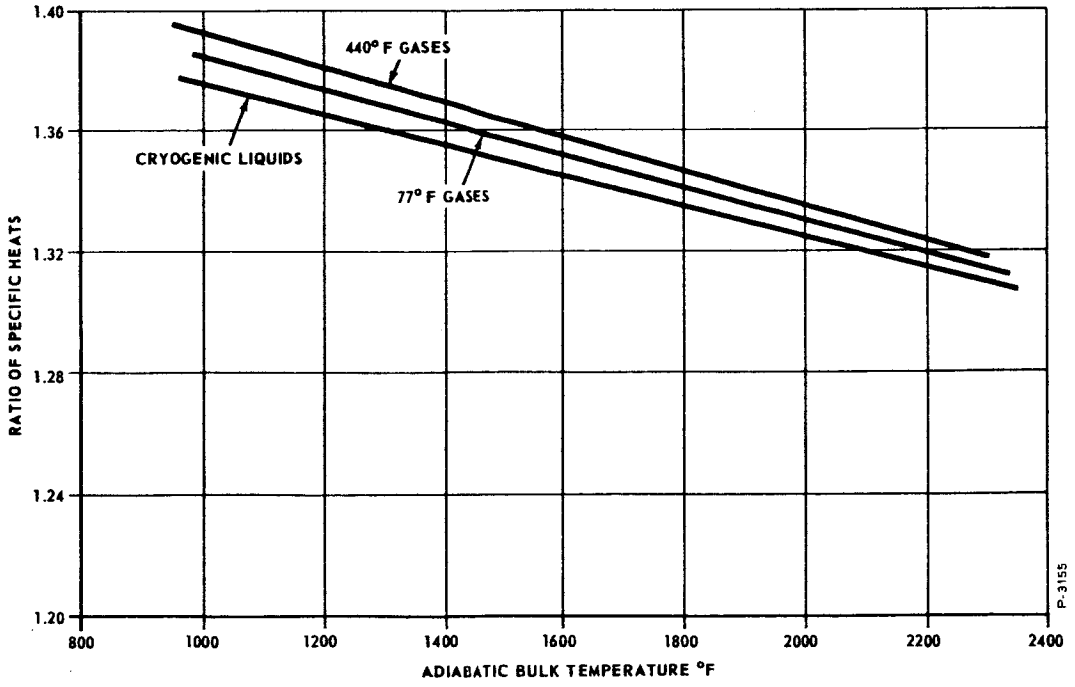

Figure 35 - Ratio of Specific Heats

$$k = \frac{C_{pm}}{C_{pm} - 1.99} \tag{29}$$

Values of k are plotted in Figure 35 as a function of temperature.

It was specified that the vortex amplifier be supplied with a hot gas at a temperature of 1500°F. Assuming that the gas generator is supplied with 77°F gases, the following data may be determined from Figures 32 through 35.

O/F ratio = 0.8 (Figure 32)

Apparent molecular weight = 3.57 (Figure 33)

Specific heat at constant pressure = 2.11 B/lb °F (Figure 34)

Ratio of specific heats = 1.358 (Figure 35)

The perfect gas constant can be computed from the molecular weight at the indicated conditions:

$$R = \frac{1544 \times 12}{M} \tag{30}$$

where:

$M = 3.57$

$$R = \frac{1544 \times 12}{3.57}$$

$R = 5190$ in/°R

The basic orifice weight flow equation is:

$$\dot{w} = \frac{C_d C_2}{\sqrt{T}} A P_u f_1 \left(\frac{P_d}{P_u} \right) \tag{31}$$

where:

C_d = discharge coefficient

C_2 = thermodynamic gas constant $\sqrt{°R}/sec$

T = gas temperature (°R)

A = flow area (in^2)

P_u = upstream pressure (psia)

P_d = downstream pressure (psia)

f_1 = sonic flow function

The thermodynamic gas constant is computed as follows:

$$C_2 = \sqrt{\frac{k\,g}{R\left(\frac{k+1}{2}\right)^{(k+1)/(k-1)}}} \qquad (32)$$

where:

k = 1.36

R = 5190 in/°R

g = 386 in/sec^2

C_2 = 0.185 $\sqrt{°R}/sec$

These gas parameters were used in the vortex amplifier development program.

Gas Generator Design

The hydrogen-oxygen gas generator which has been used as a hot gas source for the test work described in this report, uses a design based on the vortex combustor principle. The hydrogen, which is greatly in excess of stoichiometric requirements, is injected tangent to the combustion chamber wall. The resulting hydrogen vortex serves to cool the wall. The oxygen is injected along the axis of the combustion chamber. The flow paths are indicated schematically in Figure 36.

The design point for the gas generator is based upon the following operating conditions:

Chamber Pressure P_g = 850 psi

Mean Temperature T_g = 1960°R (1500°F)

O/F Ratio f = 0.8

Total flow $\dot{w}_t$ = 0.5 lbs/sec

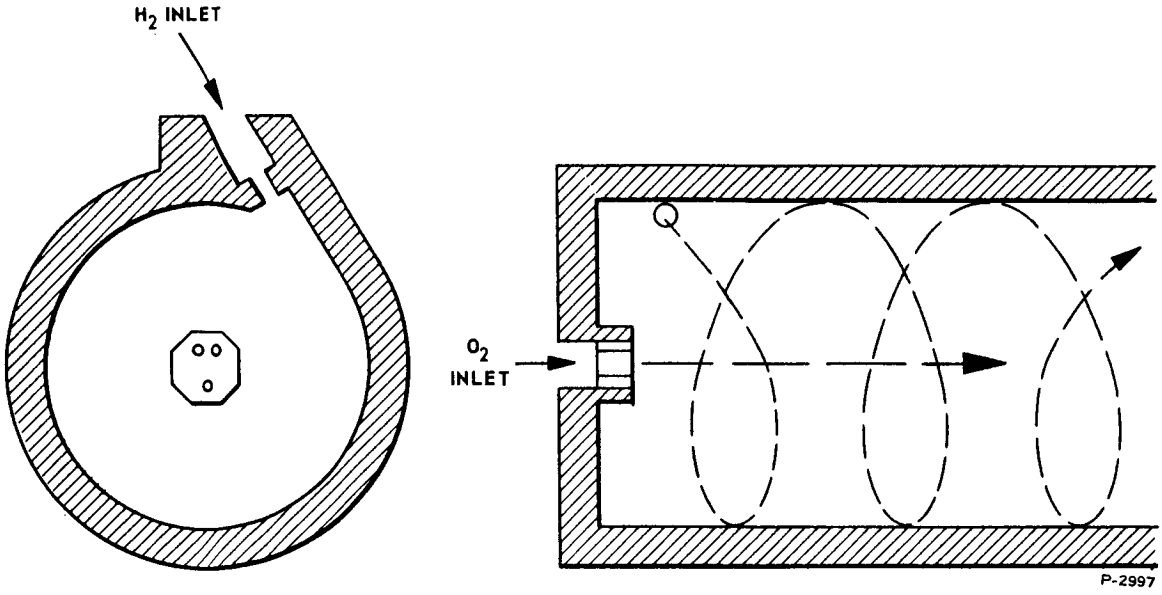

Figure 36 - Vortex Combustor Schematic

Photographs of the original gas generator configuration assembled and disassembled are shown in Figures 37 and 38. Since these photographs were taken, some modifications have been made. One consisted of the additions of a ring slipped into the injector housing to reduce the number of original hydrogen inlet ports. This step was taken as a result of the reduction of the maximum flow requirement from 0.7 to 0.5 lb/sec and also to increase the inlet port pressure drop, which was initially too low. Another modification consisted of replacing the oxygen inlet, which was a 3/8-inch tube connection, with a two-inch flanged connection. This port is also used as the nitrogen inlet to the system for cold gas tests. For hot gas tests, a flanged plug containing the oxygen injector and a 3/8-inch tube connection is used. Also, the four-port oxygen injector shown in Figure 38 has been replaced by a three-port injector as a result of system tests.

The significant dimensions of the gas generator are as follows:

Mean Chamber Length = 11.00 inches

Chamber Diameter = 5.5 inches

Number of 0_2 Injection Ports = 3

0_2 Injector Port Diameter = 0.08 inch

Number of H_2 Injection Ports = 3

H_2 Injector Port Diameter = 0.210 inch

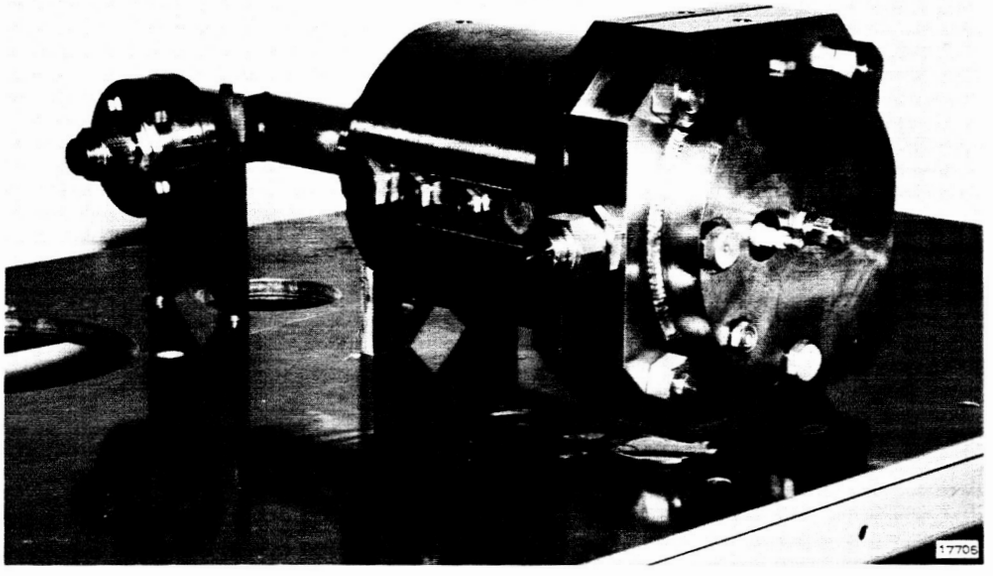

Figure 37 - Hydrogen - Oxygen Vortex Gas Generator (5.5 Inch Dia.)
Assembled View

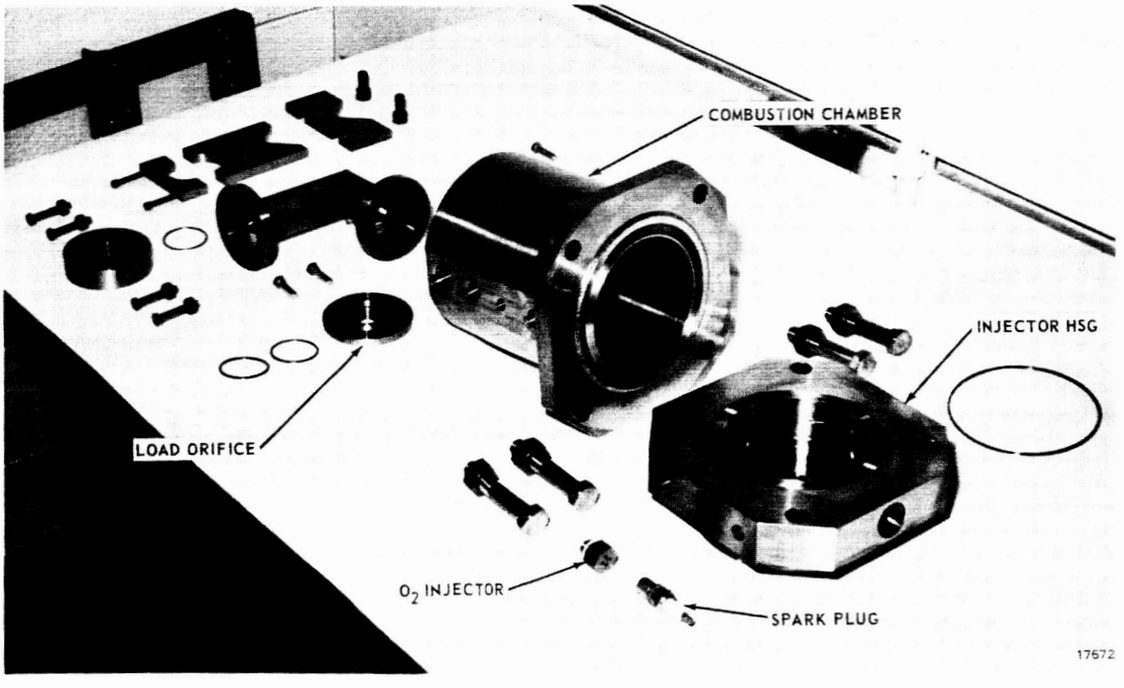

Figure 38 - Hydrogen - Oxygen Vortex Gas Generator (5.5 Inch Dia.)
Disassembled View

The gas generator was originally sized for an L* of 1100 inches. This conservative value was selected because the gas generator is basically test equipment and it was preferred to obtain a stable hot gas pressure while holding gas generator development efforts to a minimum. Because of the reduction in flow and increase in pressure after the chamber was sized, the L* value at the nominal flow rate of 0.5 lb/sec is now 1870 inches. A much lower value could be used.

Control of Gas Generator

Figure 39 is a schematic of the control system for the gas generator. The purpose of the control system is to modulate the hydrogen flow to give the desired hot gas pressure at some point in the system and to modulate the oxygen flow to maintain the O/F ratio constant.

The hydrogen and oxygen are stored in gaseous form in trailers. Pressure regulators at the trailer outlets maintain the supply pressures between 1200 and 1300 psig.

The hydrogen flow to the gas generator is controlled by a pressure regulator modified for external feedback. The sensed pressure is the gas generator chamber pressure P_g. The gas dome is supplied with nitrogen at a pressure level which gives the desired value of P_g = 850 psia.

The oxygen flow is also controlled with a dome loaded pressure regulator, modified for external feedback. The sensed pressure is the gas generator oxygen inlet pressure. The regulator acts to maintain the gas generator oxygen inlet pressure approximately equal to the regulator dome pressure. The oxygen flow is slaved to the hydrogen flow by maintaining the oxygen regulator dome pressure equal to the hydrogen pressure at the gas generator inlet. This, in effect, maintains both gas generator inlets at the same pressure, and the O/F ratio will be maintained at a constant value, which will be determined by the ratio of the effective areas of the gas generator injector ports.

There are potential hazards associated with applying hydrogen pressure directly to the oxygen regulator dome, where it would be separated from the oxygen by a single diaphragm. This is avoided by generating a nitrogen pressure equal to the gas generator hydrogen inlet pressure. The hydrogen inlet pressure is applied to the back

NOTES:

P_G = HOT GAS PRESSURE IN COMBUSTION CHAMBER

P_H = HYDROGEN PRESSURE

P_O = OXYGEN PRESSURE

P_S = VORTEX AMPLIFIER SUPPLY PRESSURE

SUBSCRIPT 1 REFERS TO PRESSURE IN STORAGE TRAILER

SUBSCRIPT 2 REFERS TO PRESSURE UPSTREAM OF FIRST SHUTOFF VALVE

SUBSCRIPT 3 REFERS TO PRESSURE UPSTREAM OF SECOND SHUTOFF VALVE

SUBSCRIPT 4 REFERS TO PRESSURE AT PRESSURE REGULATOR INLET

SUBSCRIPT 5 REFERS TO PRESSURE AT GAS GENERATOR INLET

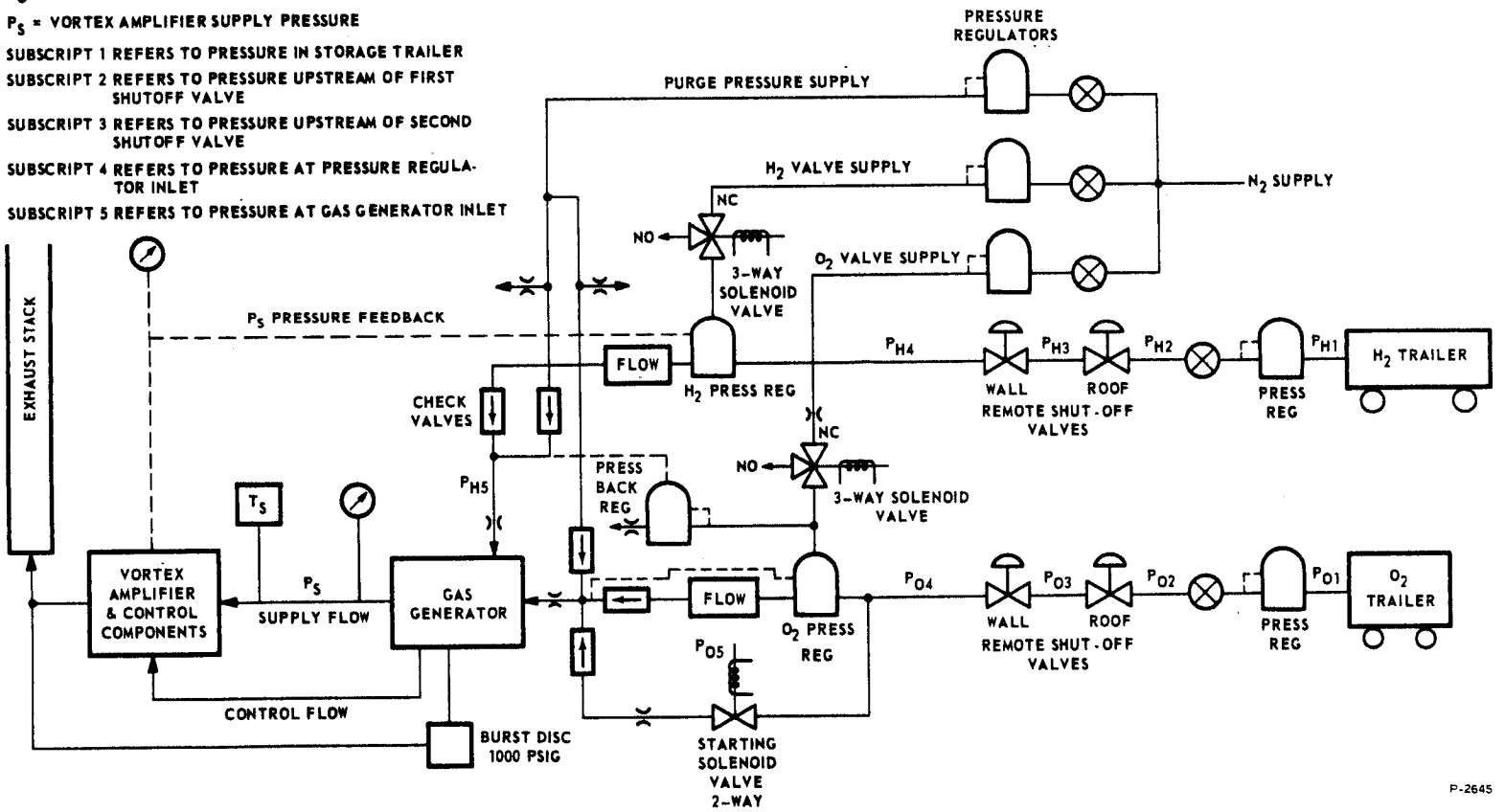

Figure 39 - Schematic of Hydrogen-Oxygen Gas Generator Control and Supply System

pressure regulator, which maintains its own inlet pressure approximately equal to the dome pressure. The back pressure regulator is supplied with nitrogen through a flow limiting orifice. The controlled back pressure is then applied to the oxygen regulator dome. Tests have shown that this control scheme is reasonably accurate at gas generator inlet pressures above 600 psig.

Ignition of the gas generator is achieved with an automotive spark plug (L-10). Since the spark plug is located in a hydrogen cooled region in back of the oxygen injector, ignition will not occur if hydrogen flow is started before the oxygen flow. The starting procedure provides for establishing an oxygen flow and activating the spark plug prior to starting hydrogen flow. When the hydrogen flow is started, ignition occurs as the hydrogen-oxygen interface moves across the spark plug. Since the oxygen pressure regulator is slaved to the hydrogen pressure regulator, it will not open until a hydrogen flow has been established. The required starting flow is obtained by by-passing the oxygen pressure regulator with a normally closed solenoid valve and a flow limiting orifice.

Nitrogen is supplied directly to the hydrogen inlet of the gas generator to permit purging the system after a firing. Check valves are placed in each gas generator inlet to prevent back flow of gases from the combustor chamber.

Figure 40 is a schematic of the electrical controls for the gas generator system.

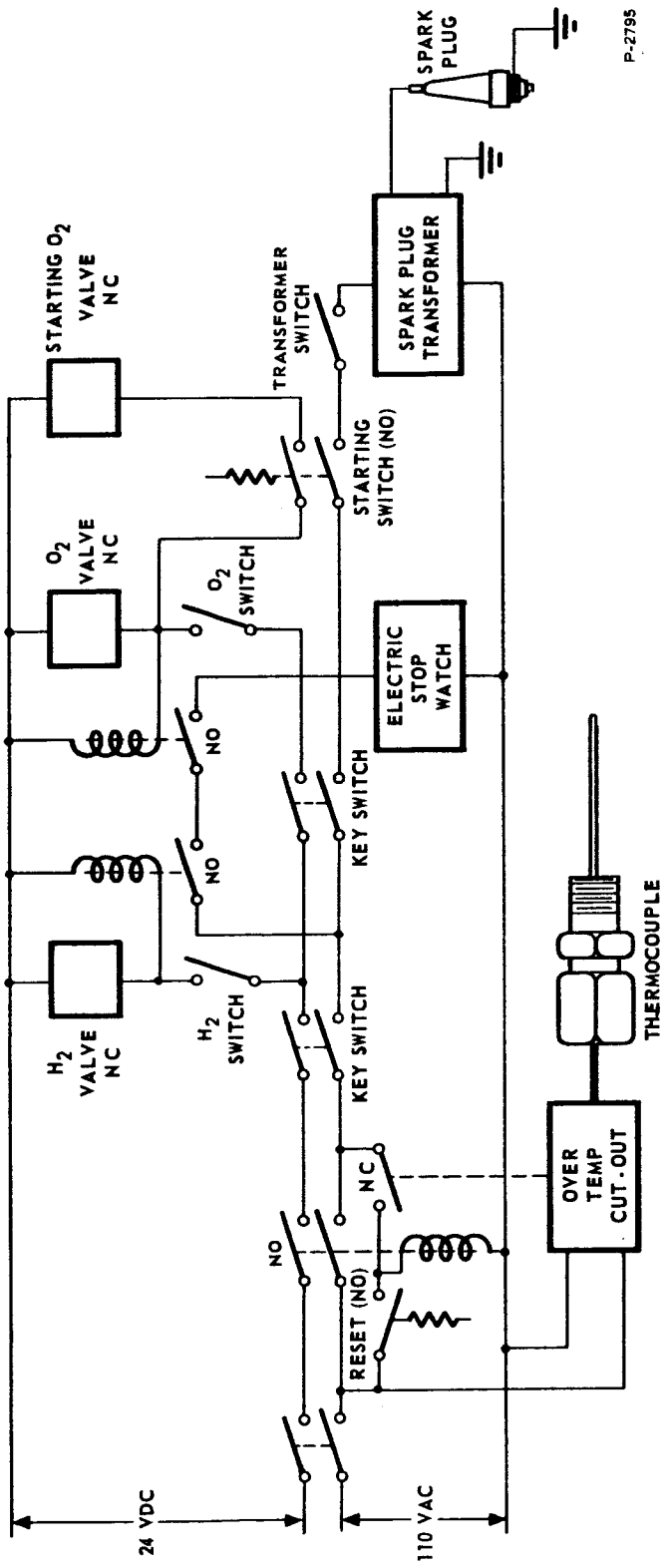

Figure 40 - Schematic of Electrical Controls for the Gas Generator System

CONCLUSIONS AND RECOMMENDATIONS

The fluid state vortex amplifier shows promise for future application to liquid propellant rocket engine secondary injection thrust vector control systems. The absence of moving parts, minimization of close fabrication tolerances, and elimination of dynamic seals results in a flow control device that is compatible with high temperature gas and that has high inherent reliability.

The vortex amplifier was developed for this application by first evaluating the performance of scale models operating with ambient temperature nitrogen gas. The development program culminated in the testing of a hot gas unit designed for a maximum flow rate 0.5 lb/sec. This test unit provided a total flow modulation range up to 5 to 1 with load flow modulation from 85 percent of total flow to near zero. A biasing technique was evaluated, which provides an overall flow gain (maximum load flow/variable control flow) of 30 to 1. The hot gas unit demonstrated a frequency response bandpass of 80 cps with inherent lead compensation. Testing was accomplished to evaluate the effects of change in pressure levels, back pressure and geometry changes. A significant realized advantage of the vortex amplifier is the similarity of performance when operating with gases having widely differing thermodynamic properties. The performance for the same unit with 1500 °F gas supplied from the hydrogen-oxygen gas generator is essentially the same as that with room temperature nitrogen gas. Although actual flow values change, gain, modulation ratio, etc., are virtually unaffected.

A theoretical analysis was conducted to establish models of the vortex amplifier performance. The analysis, although not exact, did provide a conceptual tool for evaluating performance and recommending changes in configuration for improved performance.

Feasibility of concept has been established by test performance. It is recommended that the staging of two vortex amplifiers be investigated for improved total system flow gain. A gain in excess of 200 to 1 should be possible with two units. The biasing technique required concurrent evaluation with staging tests.

The hydrogen-oxygen gas generator used for all hot gas testing was a workhorse unit. Realization of optimized system dynamics requires that the gas generator dynamics be matched to the vortex amplifier. A concept for a gas generator incorporating a unique vortex doublet injection scheme with demonstrated low L* is recommended. A complete system demonstration with a selected rocket engine applicable flow rate, in a simulated secondary injection thrust vector control system, should complete the total feasibility evaluation effort. This would provide complete information for comparison with existing methods of thrust vector control.

APPENDIX A

REFERENCE VORTEX AMPLIFIER PERFORMANCE REQUIREMENTS

This developmental program has been guided by a reference vortex amplifier performance requirement. This was deliberately kept flexible during the developmental phase. The initial requirements are summarized in Table A-1.

Table A-1 - Initial Vortex Amplifier Design Specification Requirements

Inlet fluid pressure	500 psi (Maximum)
Inlet fluid flow rate	1-5 pounds per second (pps)
Flow gain (Inlet fluid flow rate divided by the average control fluid flow rate)	100 (Minimum)
Frequency Response	Flat response with maximum variation of ± 10% up to 100 cycles per second (cps)
Amplifier pressure drop	100 psi (Maximum)
Single leg flow modulation	Near 0-5 pounds per second
Inlet fluid composition	50.5% by weight hydrogen 49.5% by weight water vapor
Control fluid composition	Same as inlet fluid or inert gas
Operating Life	1 hour (Minimum)
Inlet fluid temperature	1500°F (Maximum)

This basic preliminary design specification was modified as actual performance data was realized and resulted in normalized performance curves shown in Figures A-1 and A-2 for the basic vortex amplifier and also for operation using bias flow. Table A-2 summarizes pertinent performance requirements for the basic vortex amplifier and Table A-3 summarizes performance for operation with the bias flow.

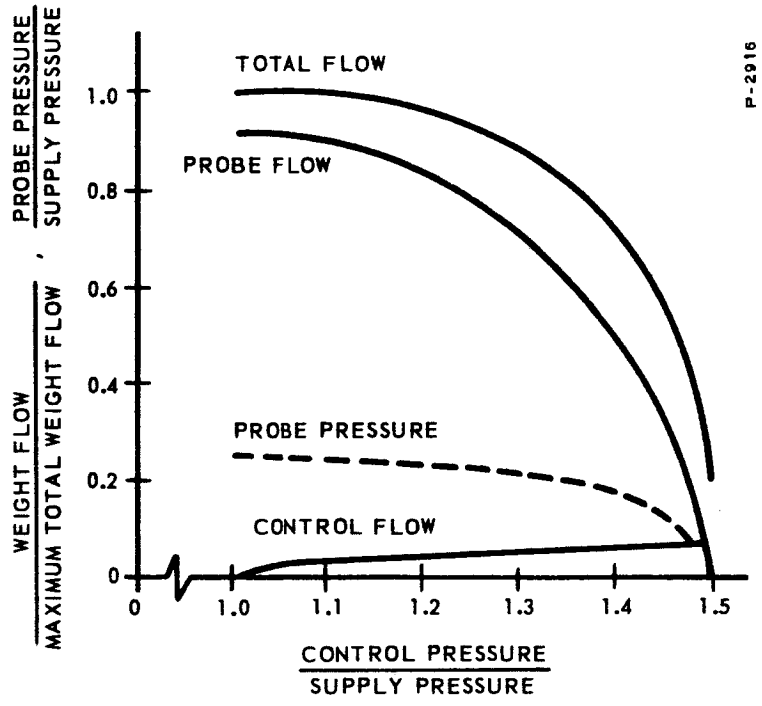

Figure A-1 - Normalized Static Performance

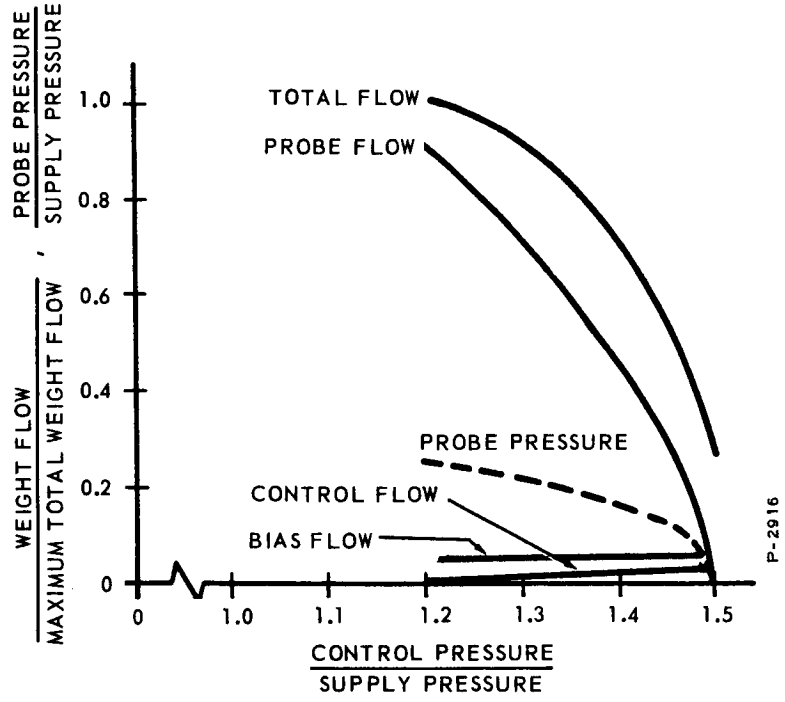

Figure A-2 - Normalized Biased Performance

Table A-2 - Reference Vortex Amplifier Static Performance

Flow Recovery	90%
Gain (Based on Probe Flow)	8
Control/Supply Pressure Ratio	1 - 1.5
Vortex Chamber Flow Turndown	5:1
Probe Flow Range	90% of Maximum to Near Zero
Probe Pressure Recovery	25% of Supply Pressure

Table A-3 - Reference Vortex Amplifier Biased Static Performance

Flow Recovery (Minimum)	90%
Gain (Based on Probe Flow)	30
Control/Supply Pressure Ratio	1.2 - 1.5
Vortex Chamber Flow Modulation	4:1
Probe Flow Turnoff	90% of Maximum Supply to Near Zero
Probe Pressure Recovery	25% of Supply Pressure
Bias/Supply Pressure Ratio	1.2

APPENDIX B

SCALE MODEL COLD GAS DEVELOPMENT TEST

BREADBOARD VORTEX AMPLIFIER NO. 1

A scale model vortex amplifier was designed and built early in the program for deriving design information for the Phase 1 vortex amplifier. This unit was equivalent in size to one-tenth the flow of the Phase 1 vortex amplifier. It was tested with nitrogen gas at a supply pressure of 200 psig. Figure B-1 is a layout and Figure B-2 shows the disassembled hardware. Figures B-3 and B-4 show the test setup. Two test series were run with this unit. Test series No. 1 was run with a probe pressure equal to 80 percent of supply pressure. After this series was completed, a second test series was accomplished with the probe exhausting into a constant probe pressure equal to 25 percent of supply pressure.

Significant vortex chamber dimensions were as follows:

D_o = 0.226 in. (Chamber Orifice Diameter)

$D_{(cham)}$ = 1.250 in. (Chamber Diameter)

This unit was fabricated from aluminum and brass and used "O"-Ring seals. The probe was axially positioned by a screw adjustment. All tests were operated between points of zero control flow and zero probe flow. Supply, control and bias flow measurements were made with calibrated orifices and pressure gages. The probe flow was measured with a glass tube flowmeter operating at atmospheric pressure. The exhaust flow was unrestricted.

Test Series Number 1

Testing accomplished during this series is summarized in Table B-1 and is described in the following sections with regard to the significant parameter change.

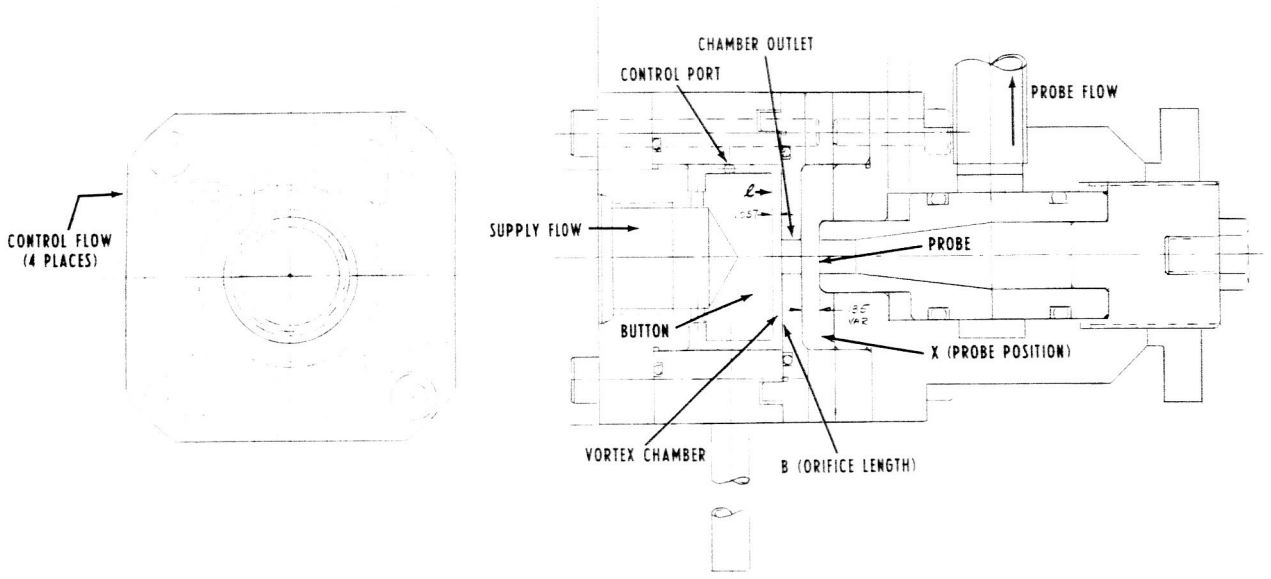

Figure B-1 - Layout-Breadboard Vortex Amplifier No. 1

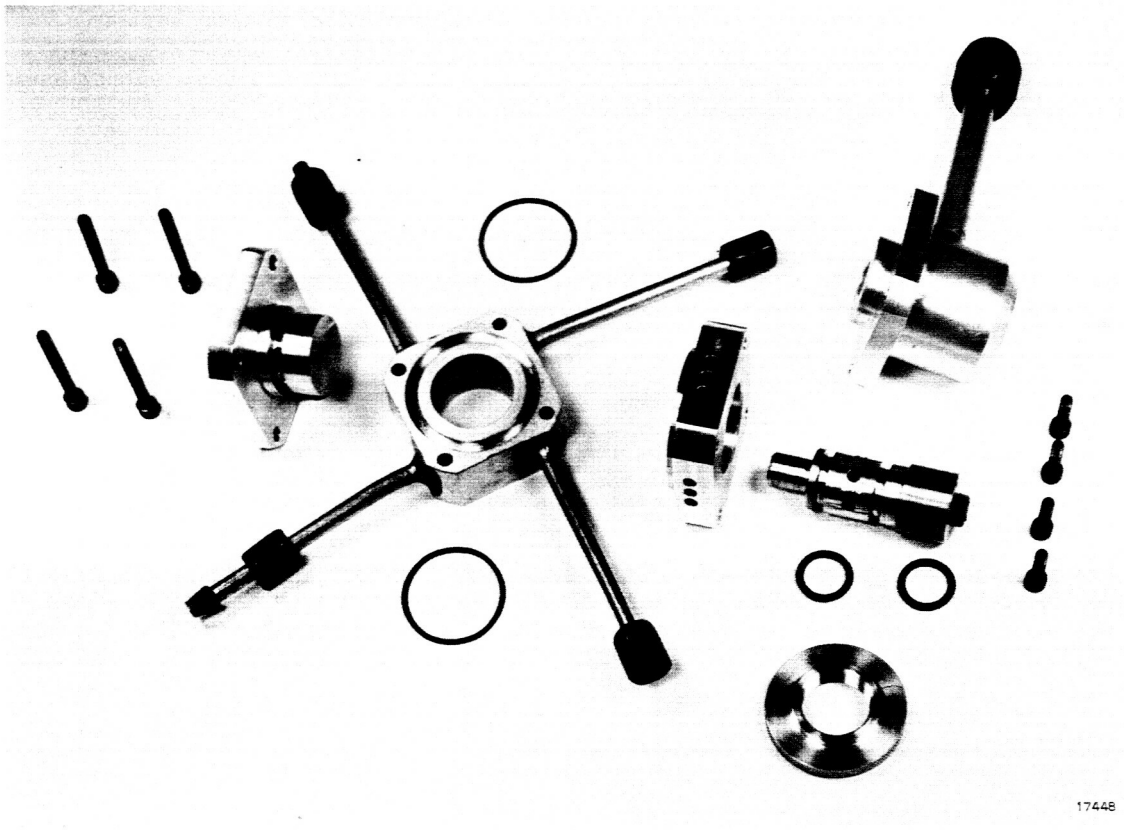

Figure B-2 - Breadboard Vortex Amplifier No. 1 - Disassembled View

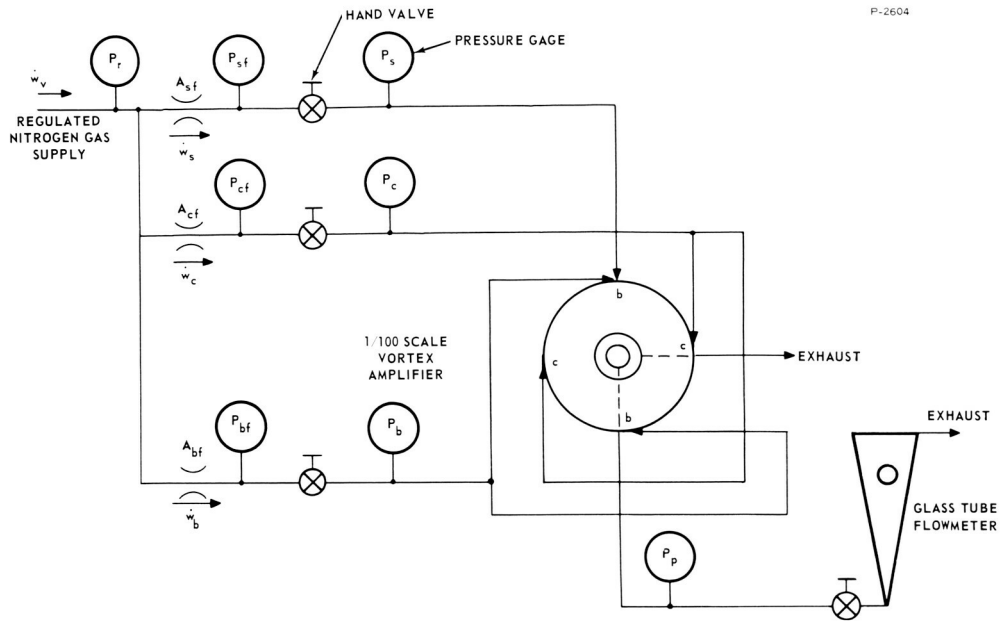

Figure B-3 - Test Schematic - Breadboard Vortex Amplifier

Figure B-4 - Test Stand - Breadboard Vortex Amplifier

Table B-1 - Summary of Test Series No. 1

Figure No.	Major Parameter Investigated	Test Description	Test Conclusions
B-5, B-6	Probe Position	Probe positions of 0.025 in. and 0.015 in. investigated	Operate at 0.015 in. to preserve recovery and still turn down
B-6, B-7 B-8	Multiple Control Ports	One, two and four control ports each 0.067 in. dia. investigated for ability to modulate probe flow	Probe flow modulation dependent on momentum, a combination of control pressure and flow
B-9, B-10	Probe Pressure	Lower probe pressures were run to determine effect on probe flow modulation	Low probe pressures adversely effect probe shutoff capabilities
B-11, B-12	Small Control Ports	Four small control ports were made with same flow area of one of the previous control ports	Amplifier modulation not effected by number of control ports
B-13, B-14	Orifice Length	Vortex chamber orifice length shortened in effort to improve turn down at low probe pressures	Reverse happened; however, recovery greatly improved
B-15, B-16 B-17, B-18	Bias	Fixed bias flow added to bring vortex amplifier to region of maximum gain	Bias worked satisfactorily at probe pressure for which it was set

P-2648

Probe position. - The axial position of the probe in relation to the vortex chamber outlet (Dimension "x" in Figure B-1) was adjustable. It was known that this parameter has a significant effect on the power recovery performance of jet pipe valves; it was therefore made adjustable to evaluate this application. It was found that the probe had to be located extremely close to the vortex chamber outlet in order to obtain good weight flow recovery in the probe at high probe back pressures. Figures B-5 and B-6 show the effect of varying this parameter. The probe was located at 0.025 inch in Figure B-5 and at 0.015 inch in Figure B-6. The probe and vortex chamber outlet diameters are both 0.226 inch. It was concluded on the basis of weight flow recovery in the probe at zero control flow, that the probe spacing should be 0.015 inch for this configuration and it was found that even with this close spacing, it was possible to decrease the probe flow to zero.

Multiple control ports. - The breadboard vortex amplifier was fabricated with the control body containing four control ports, each 0.067 inch in diameter. It is possible to pressurize any one or any combination

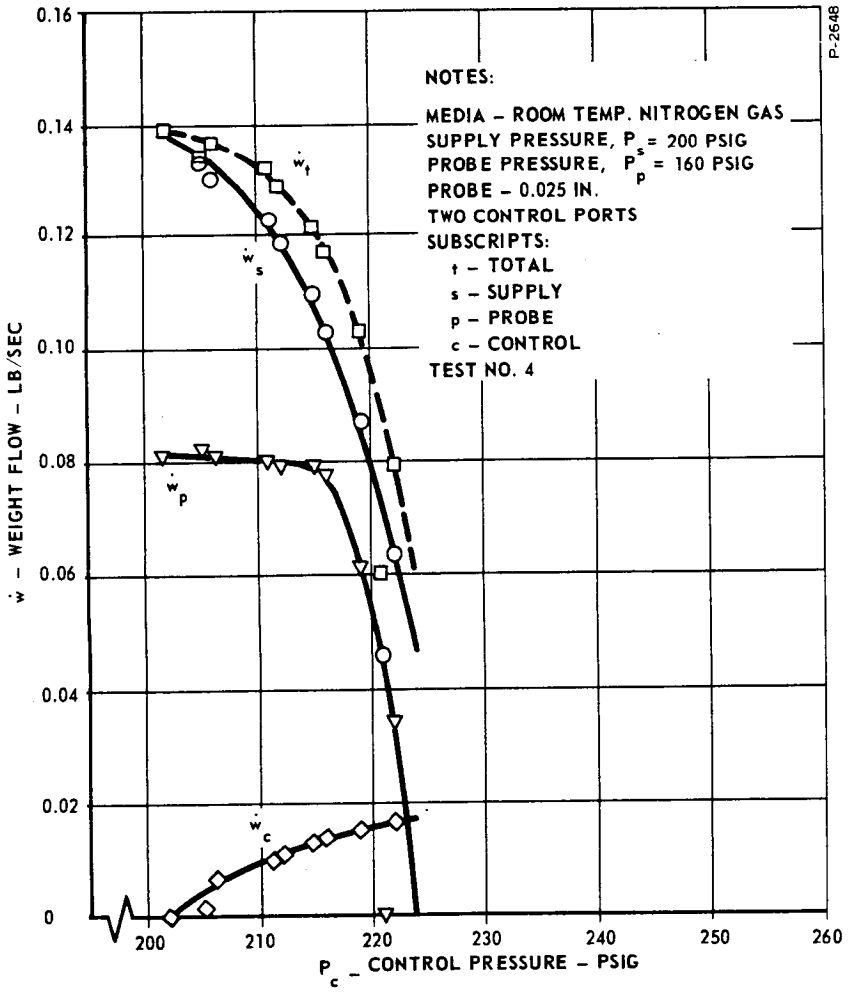

Figure B-5 - Probe Position Test-X - 0.025 inch

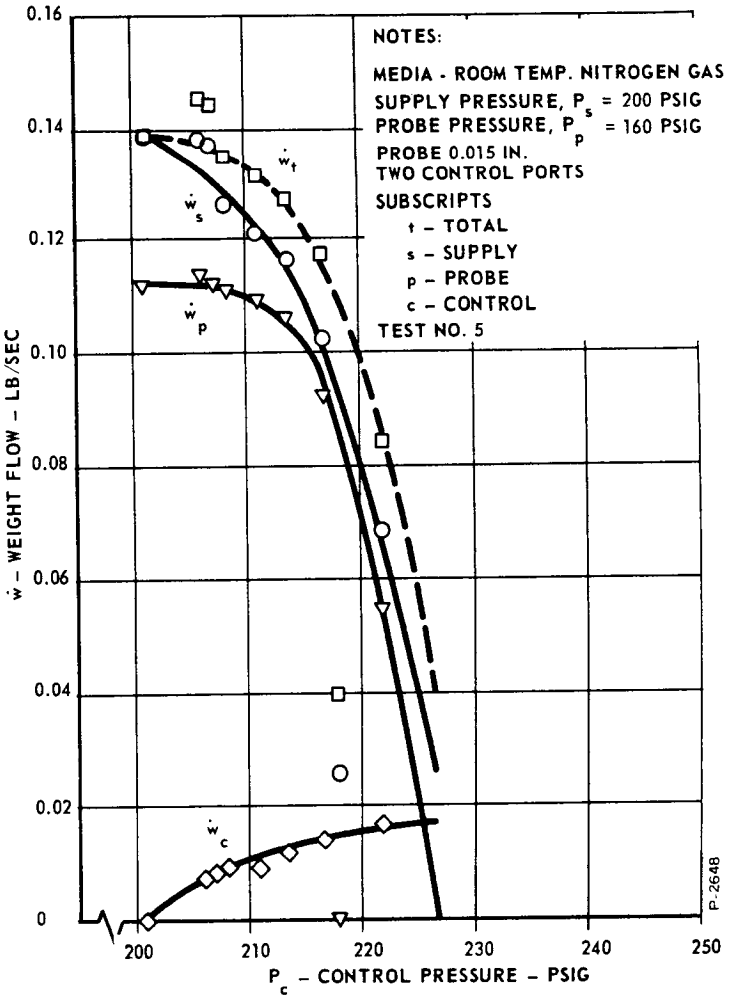

Figure B-6 - Probe Position Test-X - 0.015 inch

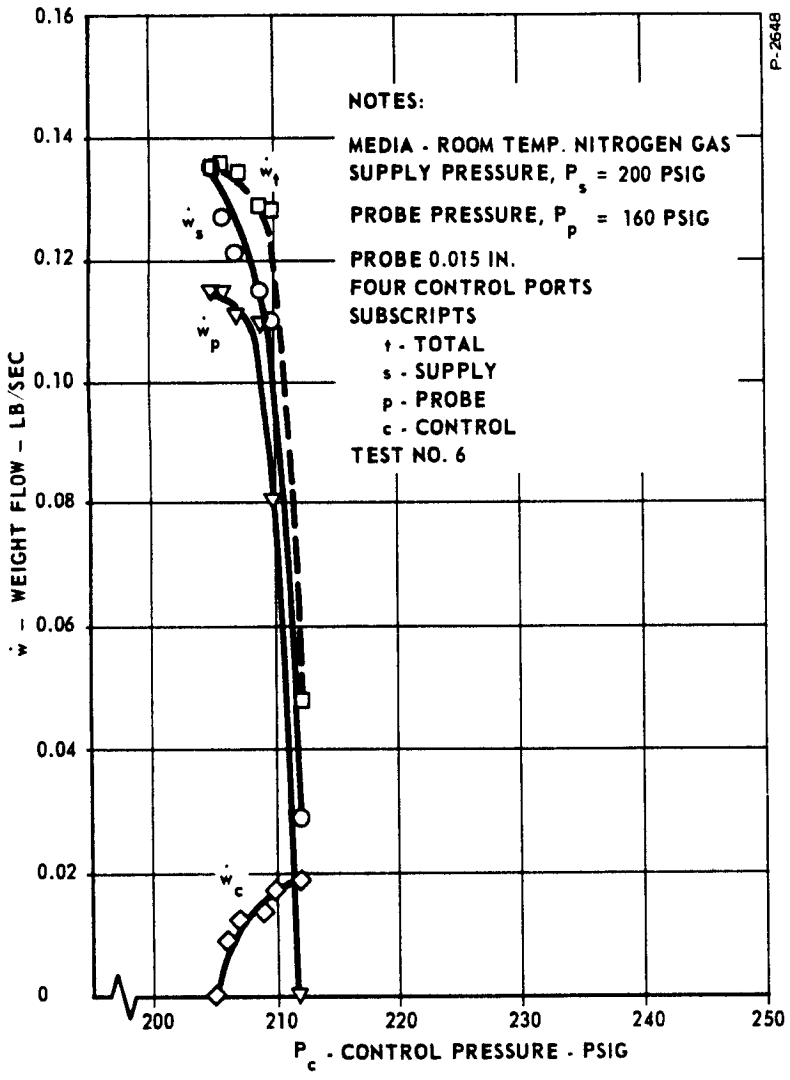

Figure B-7 - Multiple Control Port Test - Four (4) Control Ports

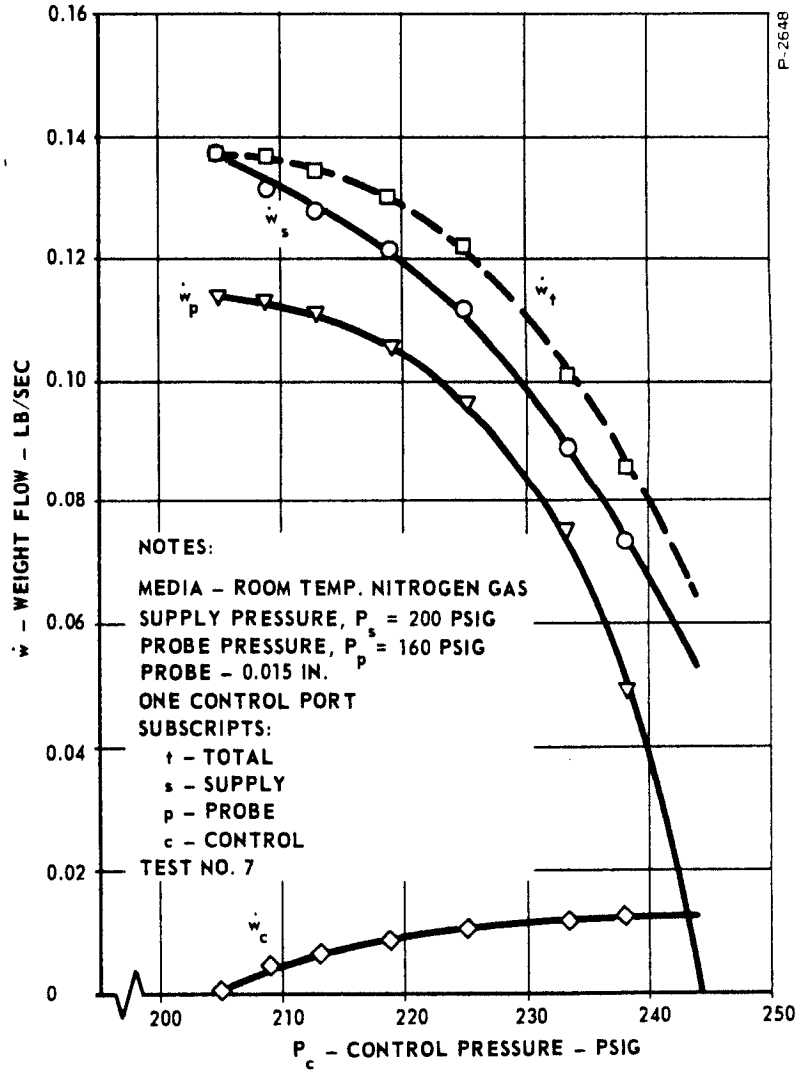

Figure B-8 - Multiple Control Port Test - One (1) Control Port

of these ports. Figures B-6, B-7 and B-8 show the effect of using one, two, and four of these control ports. Comparing the extreme cases (Figures B-7 and B-8 with four control ports and one control port respectively), it is seen that four control ports require a relatively large control flow rate and small control pressure, whereas the use of one control port requires a large control pressure and only a small control flow rate. There is a tradeoff between control flow and control pressure required to achieve zero probe flow. Basically, it is a momentum phenomenon that produces a swirl in the vortex chamber and momentum can result with either low velocity large flow rate or a high velocity small flow rate. With regard to this specific application, it is desirable to use minimum control flow rate to maximize flow gain. This results in a relatively high control pressure. There is a practical limit on maximum control pressure available, and it becomes necessary to design to this limit to minimize control flow rate.

Probe pressure. - A high probe pressure decreases the probe flow recovery, $\dot{w}_p / \dot{w}_t$, but also decreases the amount of control momentum required to effectively divert the probe flow to exhaust. Decreasing the probe pressure improves probe weight flow recovery and requires an increased control momentum to achieve probe flow diversion. The results of experimentation with reduced probe pressures are shown in Figures B-9 and B-10. These tests were run with a probe pressure of 106 psig and probe positions of 0.015 inch and 0.025 inch, respectively. Two control ports were used to supply control flow in both cases. It is noted that large control flows and pressures were required to achieve shutoff. It is also seen from Figure B-10 that extending the probe helped achieve probe flow turnoff at lower control flows. At lower back pressures, zero probe flow could not be achieved because the control flow required exceeded the flow capacity of the test stand.

Small control ports. - A new control port body was fabricated with four control ports having a total area equal to the area of one control port in the original control port body. The thinking at this point was that the control flow should be ported into the vortex chamber in several locations to couple control momentum with supply flow more efficiently. The creation of a strong vortex flow field and the resulting increased angle of the vortex cone exiting from the vortex chamber would increase the flow gain. Figures B-11 and B-12 show the test results. Figure B-11, utilizing four small control ports, each 0.034 inch in diameter, compares directly with Figure

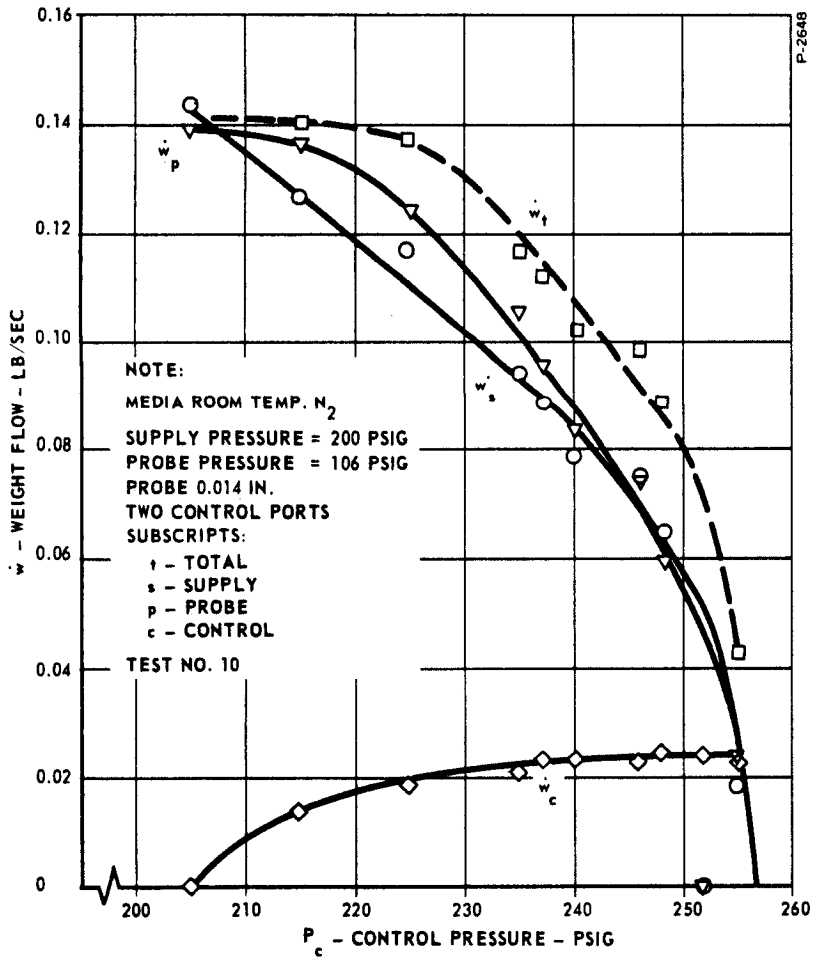

Figure B-9 - Reduced Probe Pressure
Test-X = 0.015 inch

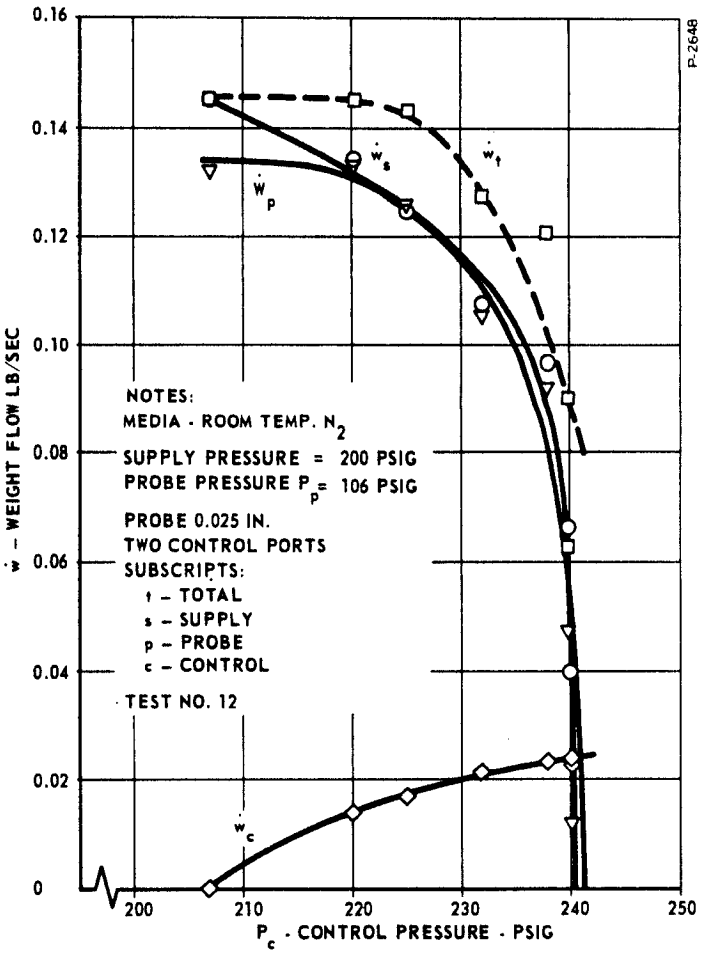

Figure B-10 - Reduced Probe Pressure
Test-X = 0.025 inch

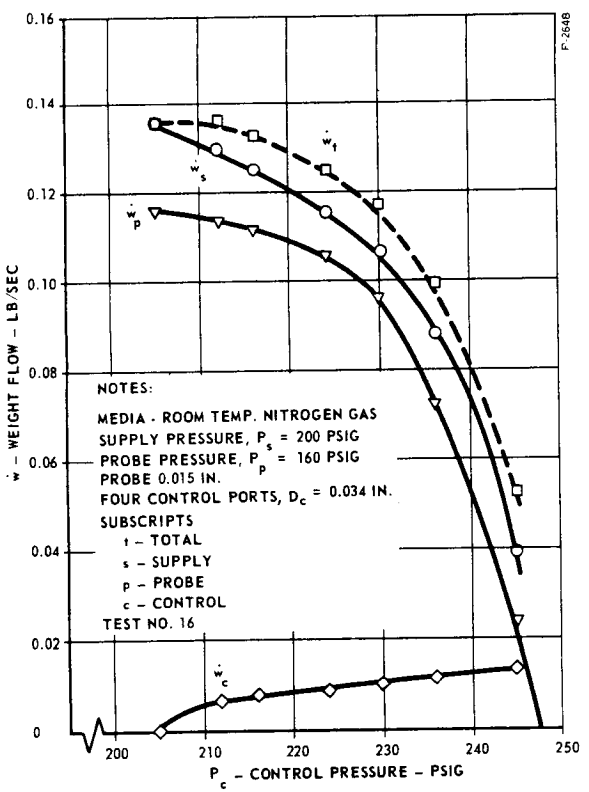

Figure B-11 - Small Control Port
Test - P_p = 160 Psig

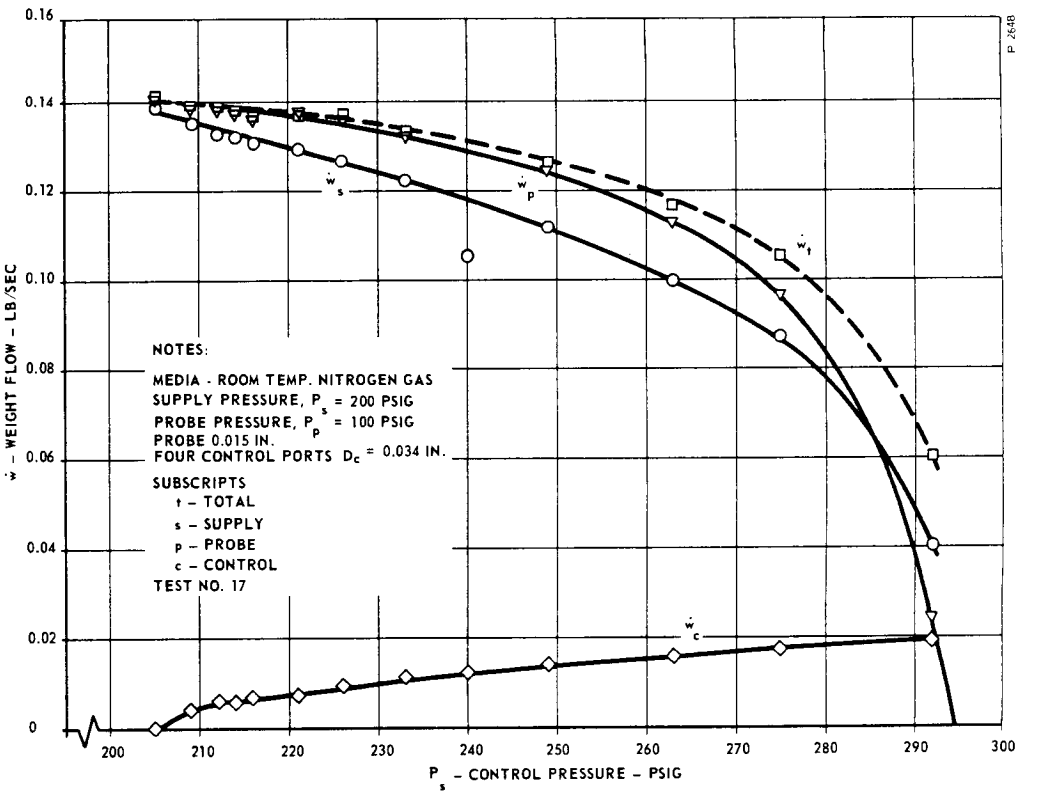

Figure B-12 - Small Control Port
Test P_p = 100 Psig

B-8 where one large control port was used. Both tests were run at a constant probe pressure of 160 psig. There does not appear to be any significant difference between the curves, indicating that the number of control ports used does not have a significant influence on the gain of a vortex amplifier of this particular size. Parameters which are significant are the control flow area, probe pressure, control pressure and control flow. The two curves are almost identical in performance.

The same results and similar conclusions were drawn from the test run with the same hardware at reduced back pressure. It was reasoned that possibly larger size vortex amplifiers operating on low density gas would operate more efficiently with multiple control ports, and for this reason, a general conclusion was not made at this point. The experimental evidence obtained indicated that one large control port is as efficient as several small ones. From a manufacturing viewpoint, and also to achieve minimum volume in the control circuit for good dynamic performance, the single control port is more desirable.

A general conclusion drawn at this point was that flow modulation at low probe pressure is not greatly influenced by either the control flow porting technique or by the position of the probe. The advantage obtained in achieving zero flow by extending the probe is offset by the low weight flow recovery.

Orifice length. - A new exhaust port body was fabricated with the dimension "B" (Figure B-1) reduced from 0.125 inch to 0.031 inch. Tests with this configuration are plotted in Figures B-13 and B-14. Comparison should be made with Figures B-11 and B-12 which show that probe flow modulation was adversely affected because more control momentum was required. Probe flow recovery was greatly improved, however, and the configuration change will be utilized. Since an opposite effect to that predicted occurred, the results were analyzed in detail. The improved recovery is believed to be the result of an improved jet profile exiting from the vortex chamber. The short orifice length provided an approximate thin plate configuration which is known to flow with better jet definition. The cleaner jet bridges the probe gap more efficiently and more flow is recovered in the probe. It is further noted in Figure B-13, that the probe flow increased at small control flows. This phenomenon is attributed to the ability of the control flow to direct and collimate the jet from the vortex chamber,

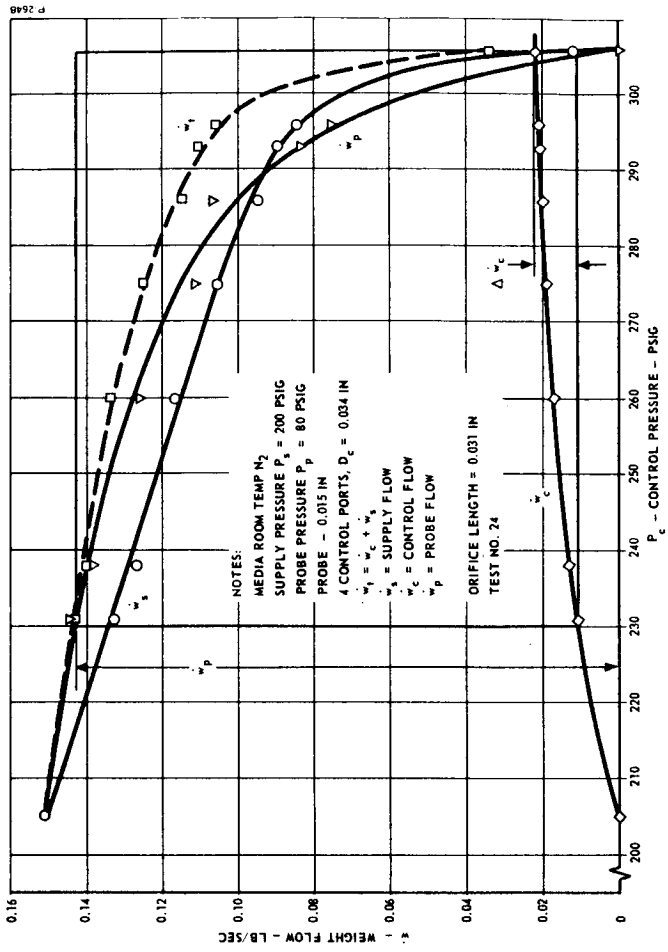

Figure B-14 - Short Orifice Test - P_p = 80 Psig

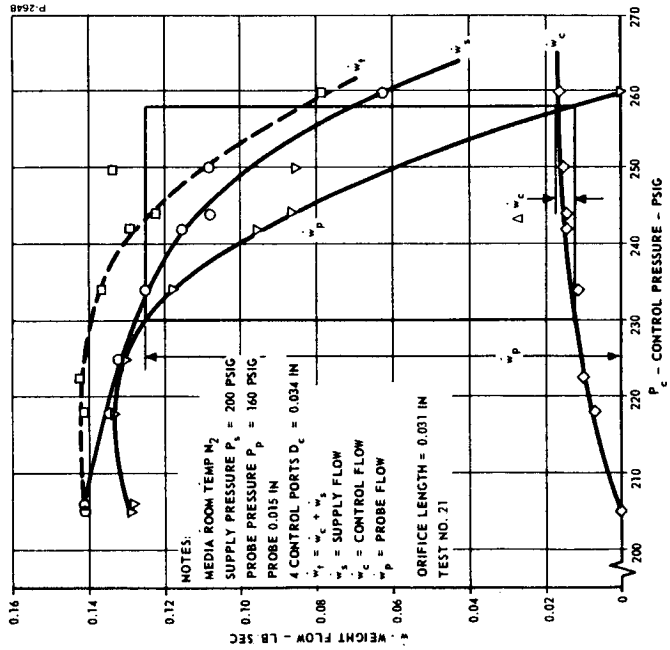

Figure B-13 - Short Orifice Test - P_p = 160 Psig

so that the jet diameter at the entrance to the probe is minimized and more flow is captured. The fact that flow modulation required more control flow can possibly be explained as a correllary to the above described phenomenon.

Biasing. - Biasing of the vortex valve is a technique whereby a fixed amount of control flow is introduced into the vortex chamber, in order to impart a residual swirl to the vortex field. It has been noted in all previous testing that the probe flow does not immediately turn down when control flow is introduced. The purpose of biasing is to set an operating point at the start of the high gain flow characteristic, so that the amount of additional control flow required is minimized. For this test, two control ports were used for biasing and two control ports were used for variable control flow. Tests were run with high and low probe pressures with both control bodies. These four tests are shown in Figures B-15, B-16, B-17 and B-18. In both cases, the bias flow and pressure were set to an operating point producing a 10 percent reduction in probe flow at a back pressure of 160 psig. This bias flow was fixed throughout the test and all tests were made with different constant back pressures.

An excessive amount of control pressure was required for the test shown in Figure B-16 where small control ports were used. This configuration must be rejected because the maximum control pressure must be limited to approximately 150 percent of the supply pressure. Comparing Figures B-17 and B-18, it is seen, that, while biasing greatly aids the performance at high probe pressure, it actually hurts the low probe pressure performance since the control pressure must be raised very high in order to accomplish flow modulation. This control pressure is then higher than it would have been if all four control ports were supplying variable control flow. It was experimentally shown that the control pressure and bias pressure for two control ports each must arithmetically average to that maximum control pressure required for use with four control ports.

In summary, it can be said that operation over a wide range of probe pressure has only been partially investigated and additional breadboard valve testing was required. It was decided that the fluid mechanics of the flow modulation phenomenon had to be investigated more thoroughly, both analytically and experimentally, in an effort to determine an optimum configuration. The last configuration tested

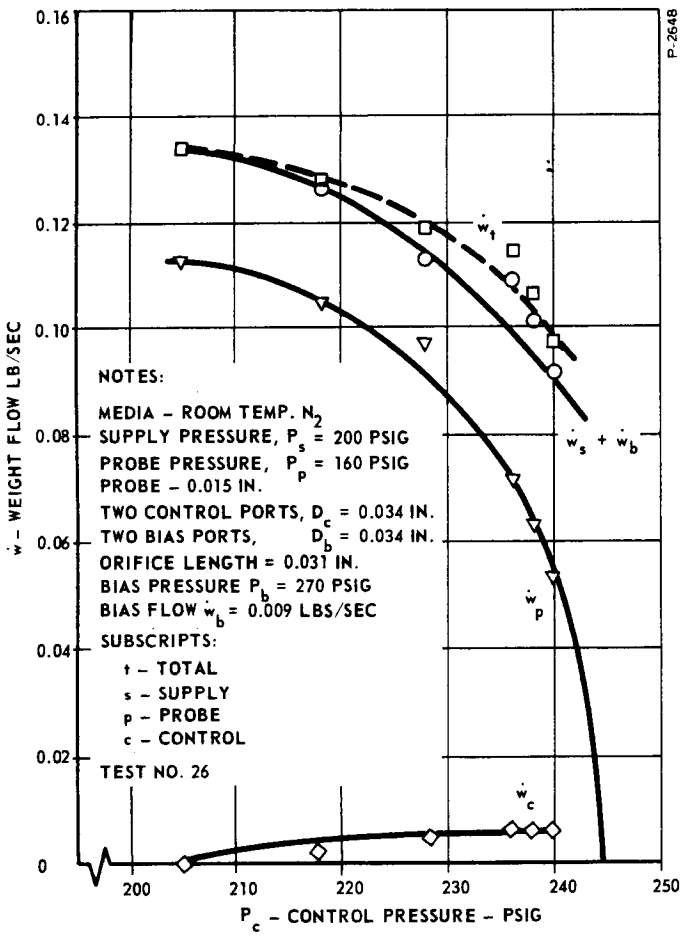

Figure B-15 - Small Control Port Bias Test - P_p = 160 Psig

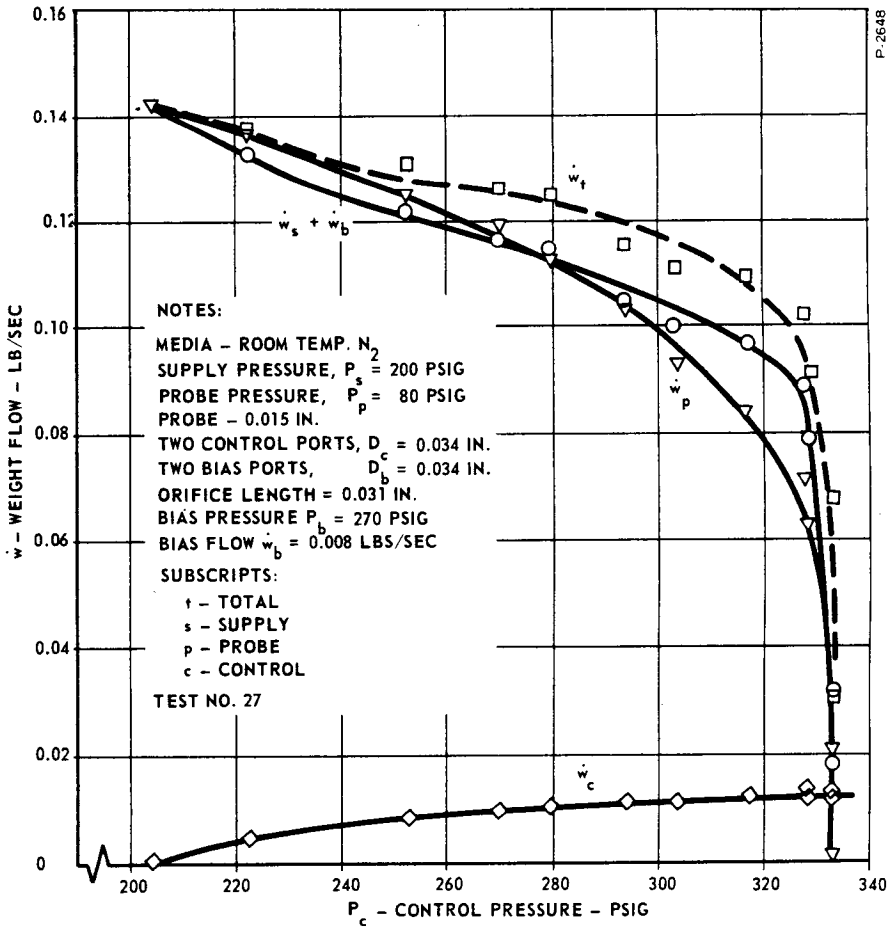

Figure B-16 - Small Control Port Bias Test - P_p = 80 Psig

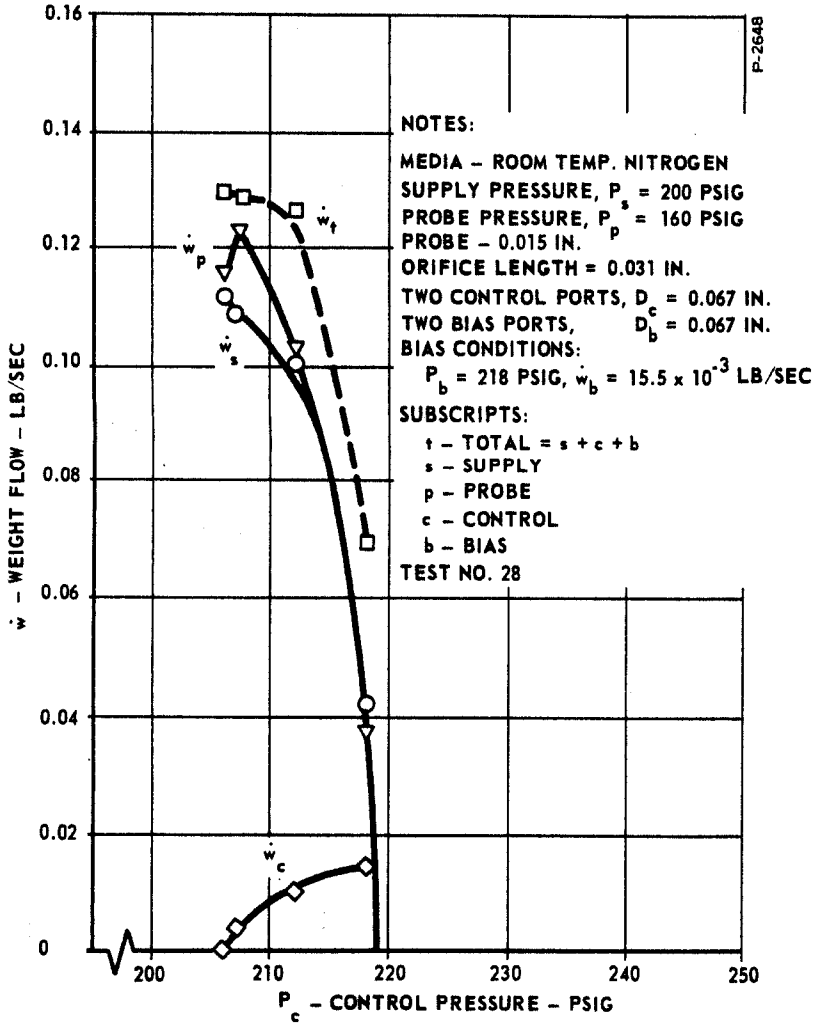

Figure B-17 - Large Control Port Bias Test - P_p = 160 Psig

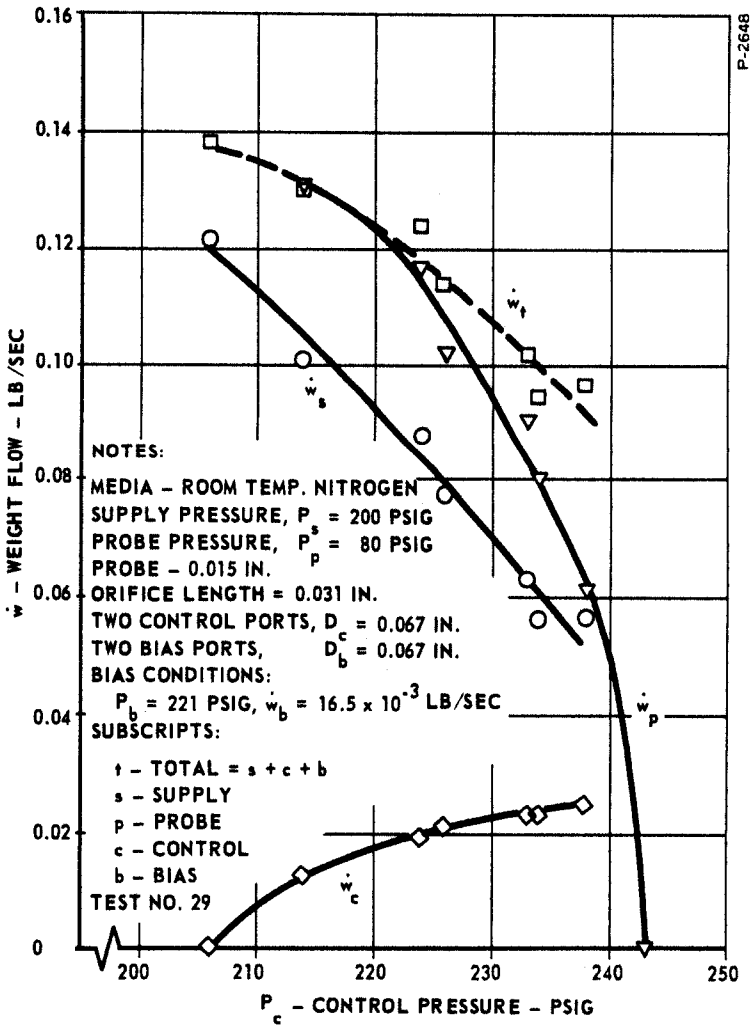

Figure B-18 - Large Control Port Bias Test - P_p = 80 Psig

(short orifice length) utilizing the biasing technique was considered the best configuration at this time, and it formed the model for the Phase 1 vortex amplifier design.

Test Series Number 2

This series of tests was accomplished using the same basic hardware as the first series, with several modifications. A primary objective was to maximize flow gain. Flow gain, as defined in the initial reference specification, was to be a minimum of 100 and is equal to the inlet fluid flow rate, divided by the average control fluid flow rate. The intent of this specification was to limit the amount of control flow required to modulate the gas flow used for secondary injection thrust vector control. This flow for the vortex amplifier should be based on output or probe flow, rather than input flow. This specification was rephrased and flow gain is now interpreted as the ratio between maximum probe flow and the change in control flow required to reduce probe flow to near zero. This definition is more inclusive, since it applies to the delivered flow and implies good flow recovery. This definition of flow gain applied to the data shown in Figure B-13 of the first test series, and assuming the use of bias control flow, results in a flow gain of 31 to 1. (See Figure B-19.)

This is considerably less than the value of 100 desired, but is reasonably good for a vortex amplifier. This gain resulted with a probe pressure of 160 psig. Figure B-14 shows typical data using a probe pressure of 80 psig. Assuming use of the same bias control flow, Figure B-20 shows a flow gain of 13 to 1. This indicates that a reduced probe pressure decreases flow gain.

An effort was made to increase the gain. Physical changes, shown in Figure B-21 were made to the probe flow receiver and to the button and vortex chamber outlet diameter.

These design parameters are considered significant in changing the flow gain. Specifically, the button was rounded to introduce the swirling gas to the vortex chamber without an abrupt change in flow section. The vortex chamber outlet diameter was chamfered on the downstream side to essentially provide a thin plate orifice. This modification allows the swirling gas to enter the exhaust chamber immediately after leaving the vortex chamber. This prevents any decrease in

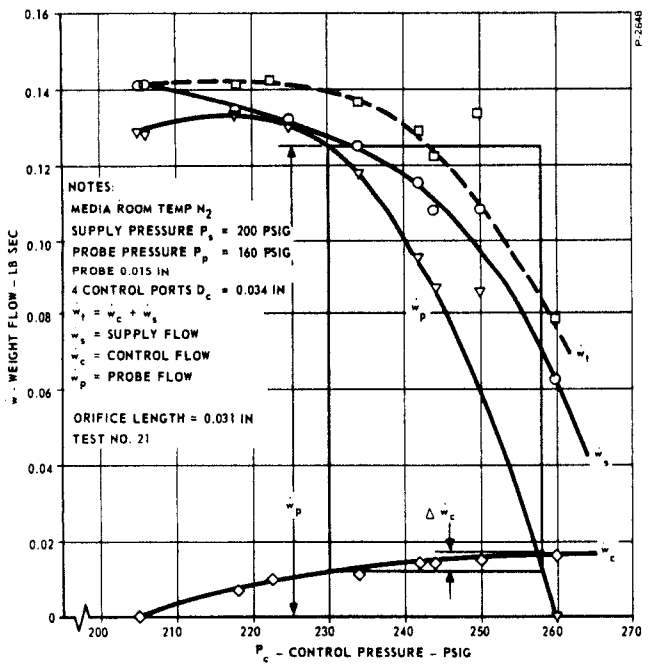

Figure B-19 - Bias Effect on Gain at P_p = 160 Psig

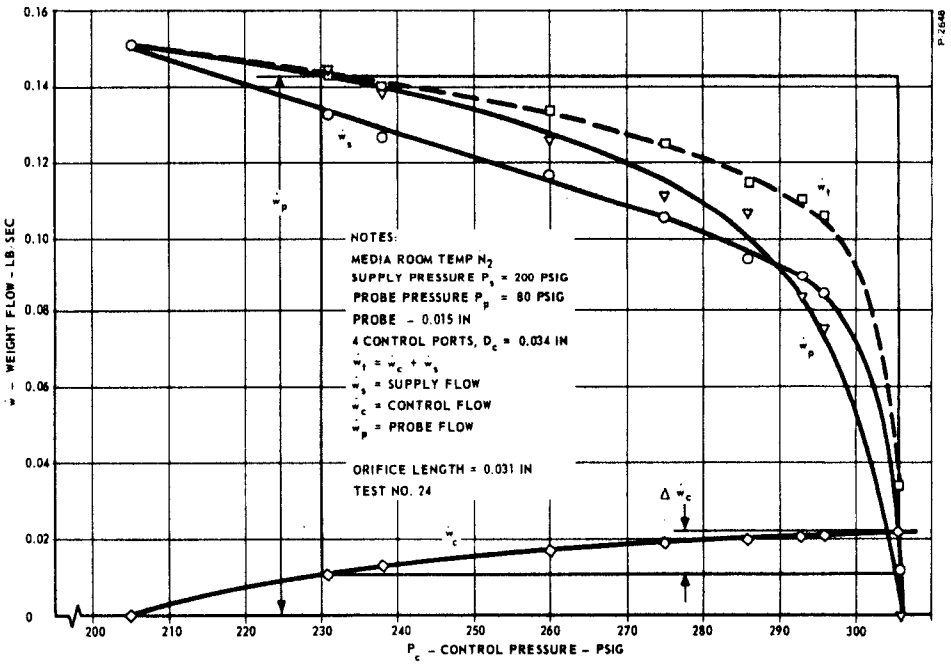

Figure B-20 - Bias Effect on Gain at P_p = 80 Psig

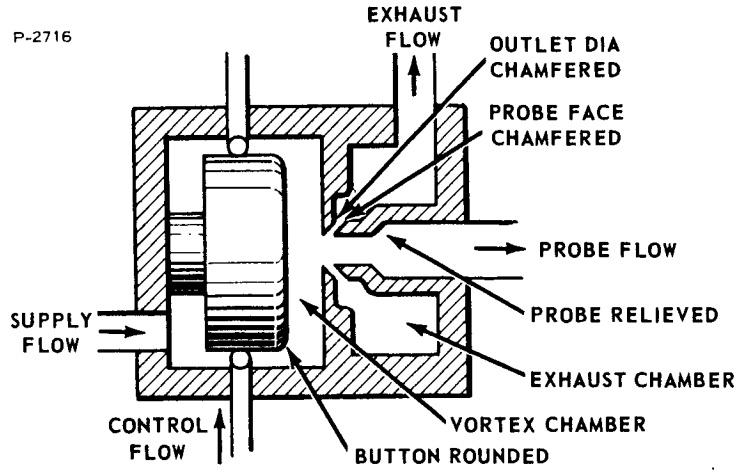

Figure B-21 - Modifications - Breadboard No. 1

swirl, due to losses in a long orifice. The probe face was chamfered to minimize restrictions, due to vena contracta in the exhaust path. These two changes allow the gas to be diverted more easily to exhaust with increasing vortex swirl. The probe was internally relieved to prevent restriction of probe flow for improved weight flow recovery. A one-to-one relationship between vortex chamber outlet orifice and probe diameter was maintained.

The performance results of these modifications are shown in Figure B-22. The gain was definitely improved. With a probe pressure of 160 psig, it was possible to show a flow gain of 101 to 1. At a probe pressure of 80 psig, the gain was 28.4 to 1. This shows a 3 to 1 improvement in gain. Another significant improvement was a flow recovery of 89.4 percent, with a probe pressure of 160 psig. This weight flow recovery represents a power recovery of 7.48 percent. The control to supply pressure ratio used to decrease probe flow to zero was 1.26. This change was later found to limit gain, because the effective diameter ratio is reduced. These ratios are satisfactory and the configuration changes have been incorporated into the Phase 1 vortex amplifier.

Secondary injection simulation. - The objectives of the breadboard tests thus far were to determine the performance and optimum values of the design parameters for the vortex amplifier for various back pressures. A simulation test was now performed for a secondary injection thrust vector control system, where the probe pressure would vary with flow. A typical secondary injection thrust vector control

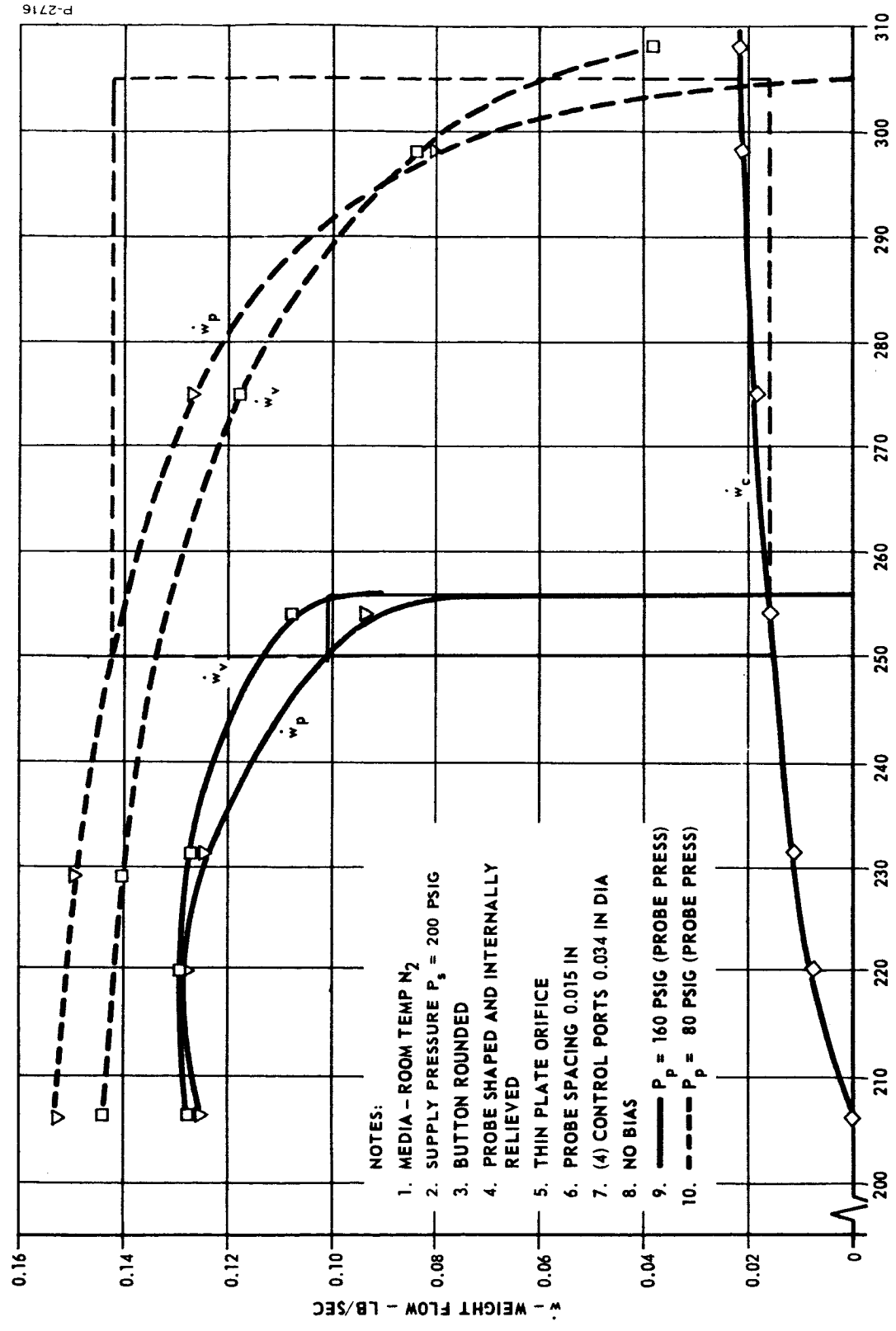

Figure B-22 - Breadboard Tests at High and Low Back Pressure

system is shown schematically in Figure B-23. Vortex amplifier supply flow is assumed to be engine bleed. An auxiliary gas generator is used for control flow. A servovalve is used to modulate the control flow to the vortex amplifier. Probe flow is injected near the exit plane of the primary propulsion nozzle. All exhaust flow from the vortex amplifier, at a relatively low pressure, is exhausted through an auxiliary thrust nozzle for recovery of available impulse. It should be noted that Figure B-24 shows only one possible system configuration and only part of that system. Hot gas could be supplied from a separate gas generator or turbine exhaust gas could be utilized. There would be at least four secondary injection ports on the nozzle to achieve thrust vectoring in two coordinate axes.

A test, simulating secondary injection thrust vector control, was made by operating with a back pressured, fixed area, restriction at the outlet of the vortex amplifier. Figure B-24 shows the results of this simulation.

The supply pressure corresponding to engine chamber pressure was set at 200 psig. With maximum probe flow, the probe pressure was set to 160 psig, with a hand valve serving as the restriction. This setting was not disturbed for the remainder of the test. A back pressure of 40 psig was placed on the hand valve to simulate a pressure in the nozzle at the point of injection. This represented a chamber to nozzle pressure ratio of 3.9, which was considered reasonable. This test resulted in full probe flow turnoff. The initial probe weight flow recovery was 79.2 percent, at a pressure recovery of 81.3 percent, for a power recovery of 64.5 percent. Probe flow turnoff was achieved with a control to supply pressure ratio of 1.5. A vortex chamber flow turndown of 2.67 was realized.

BREADBOARD VORTEX AMPLIFIER NO. 2

The breadboard amplifier No. 1 was used to establish initial design parameters for the hot gas Phase 1 vortex amplifier. This configuration was unfortunately not flexible enough for additional cold gas testing required to support the hot gas testing. It was decided to design and build a more universal unit. This is referred to as Breadboard amplifier No. 2. The design of this unit is shown in Figure B-25.*

*Refer to Figure 12 for an assembled view.

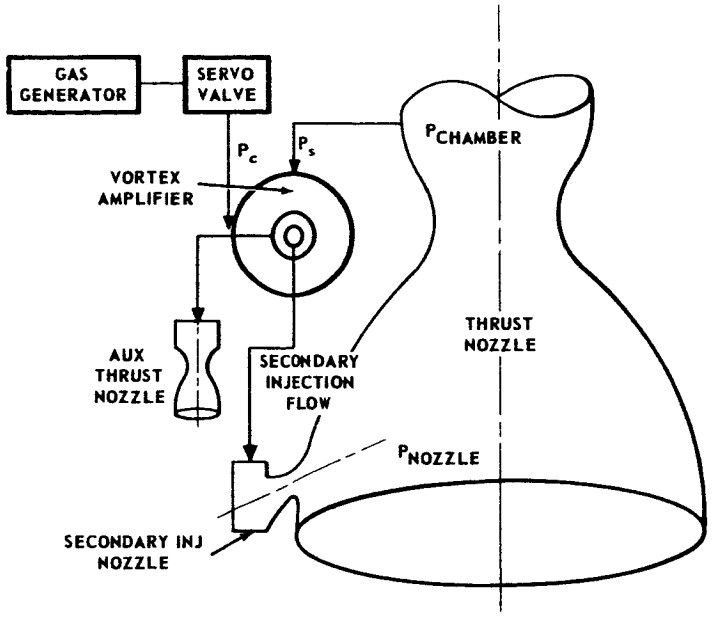

Figure B-23 - Typical Secondary Injection Thrust Vector Control System

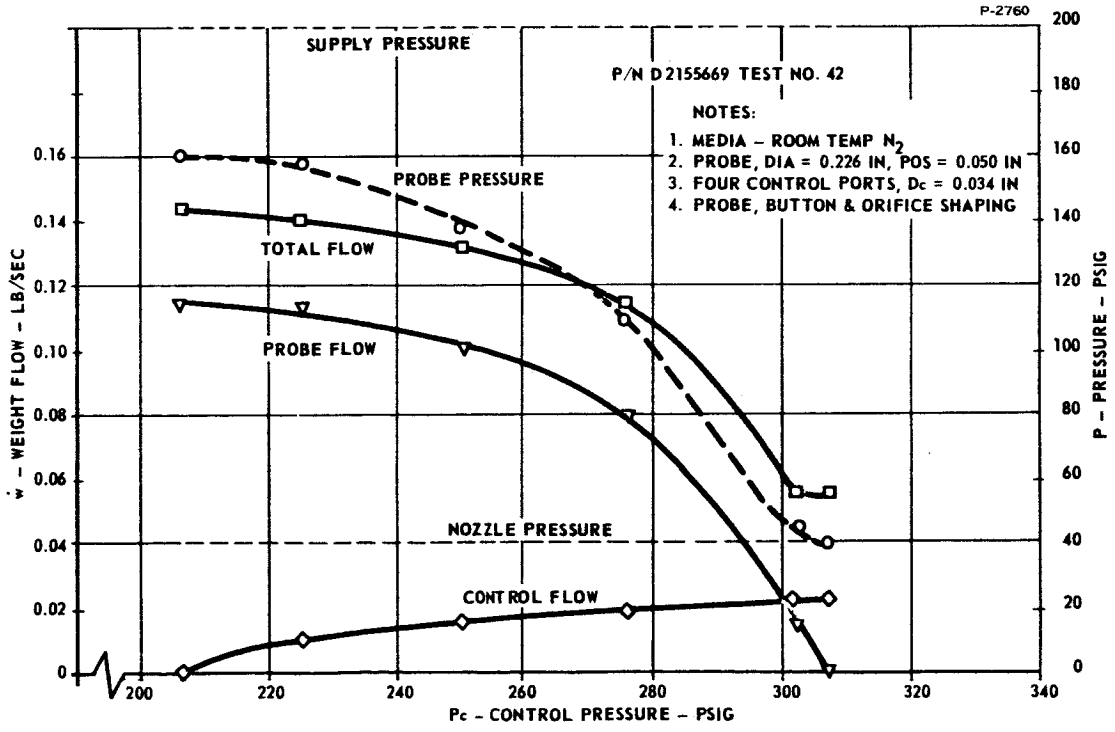

Figure B-24 - SITVC Simulated Performance

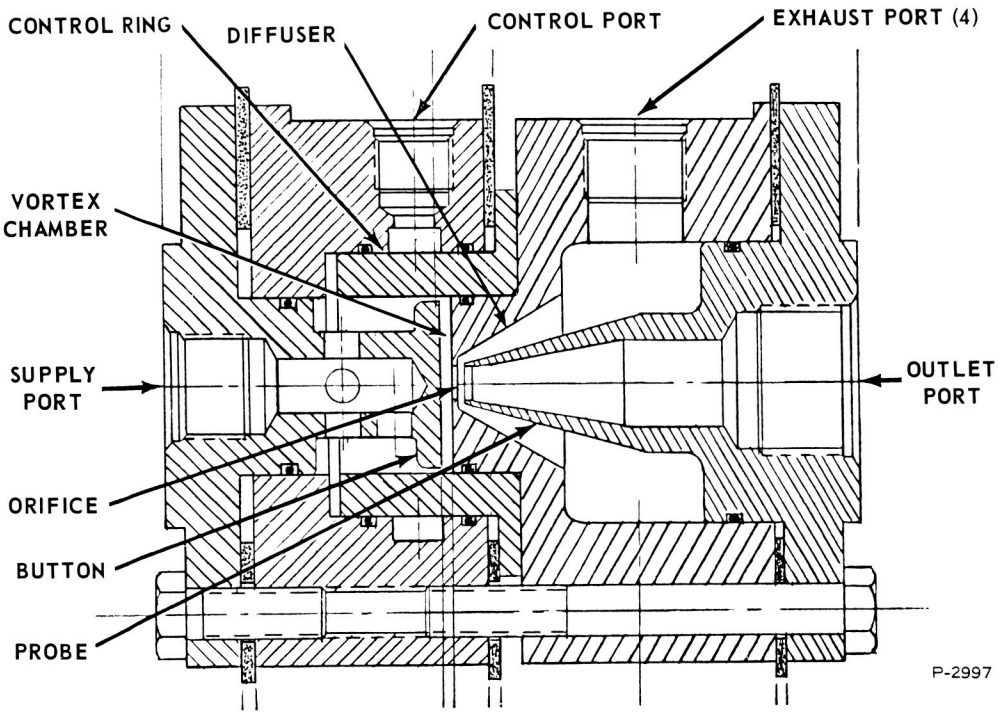

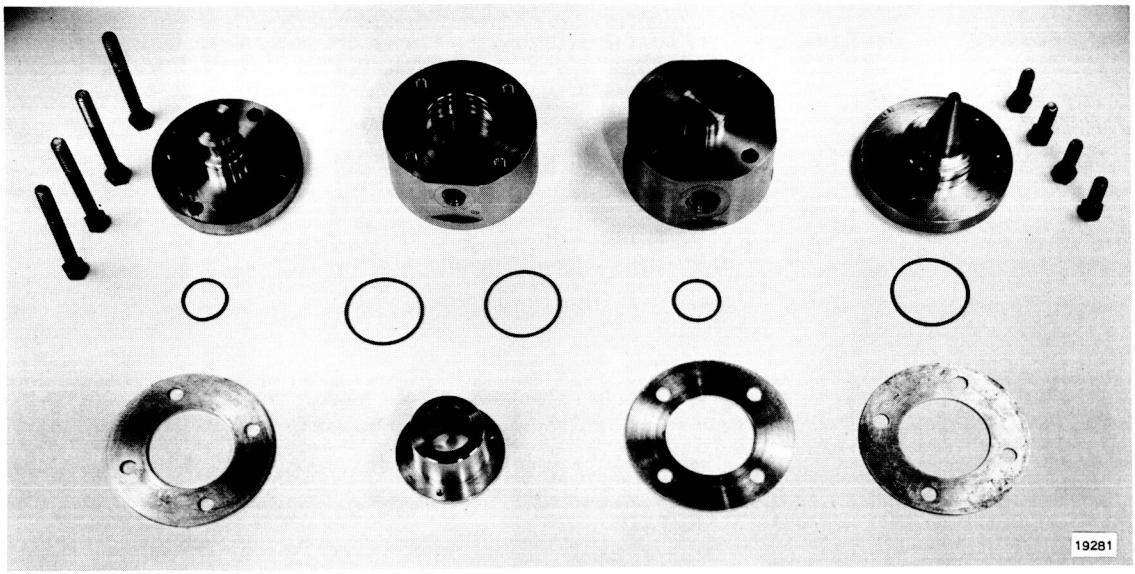

Figure B-25 - Breadboard Vortex Amplifier No. 2 - Layout and Disassembled Parts

This was again sized as a tenth scale model of the Phase 1 vortex amplifier. Principle areas of investigation were: a comparison of the effect of diameter ratio (vortex chamber outer diameter to outlet diameter) on performance; the effect of exhaust back pressure; and the effect of variation in supply pressure.

The test schematic is shown in Figure B-26, and the test installation is shown in Figure B-27. The supply flow and control flow were determined by measuring the pressure drop across the calibrated orifices A_{sf} and A_{cf}. The probe flow was measured with glass tube flowmeters. Two flowmeters were required for accurate determination of the complete range of probe flow. Valves V_1 and V_2 were used to set the control pressure recovery of 25 percent of the supply pressure, and this setting was maintained to simulate a fixed orifice load. Valve V_4 was used for varying the exhaust back pressure.

Baseline Testing

The initial configuration had a ratio of chamber outlet diameter to chamber length, D_o/ℓ, of 2.38. The spacing between the probe and vortex chamber wall, x, was 0.050 inch. The purpose of this initial test was to determine the correct probe spacing. The performance curves are shown in Figure B-28. All pressure ratios are plotted as absolute pressures. Detailed information on the test configuration is provided on each curve.

The Breadboard No. 2 configuration includes a significant change in probe geometry. The ratio of probe diameter to vortex chamber outlet orifice diameter was increased to 1.1. It was reasoned that the flow recovery would be improved and greater probe spacings could be used, resulting in a larger exit area for the exhaust flow.

Instability resulted in the region where the slope of the flow curve becomes negative and also at very low flows. The probe flow at zero control flow (maximum probe flow recovery), was greater than unity and the probe flow could not be decreased to zero. The next step was to increase the probe spacing, sacrificing flow recovery in an effort to improve probe flow modulation range. A value of 85 percent flow recovery was used as a reference point. To determine the proper probe spacing, a curve of spacing versus flow recovery at zero control flow was run. This is shown in Figure B-29. A probe spacing of

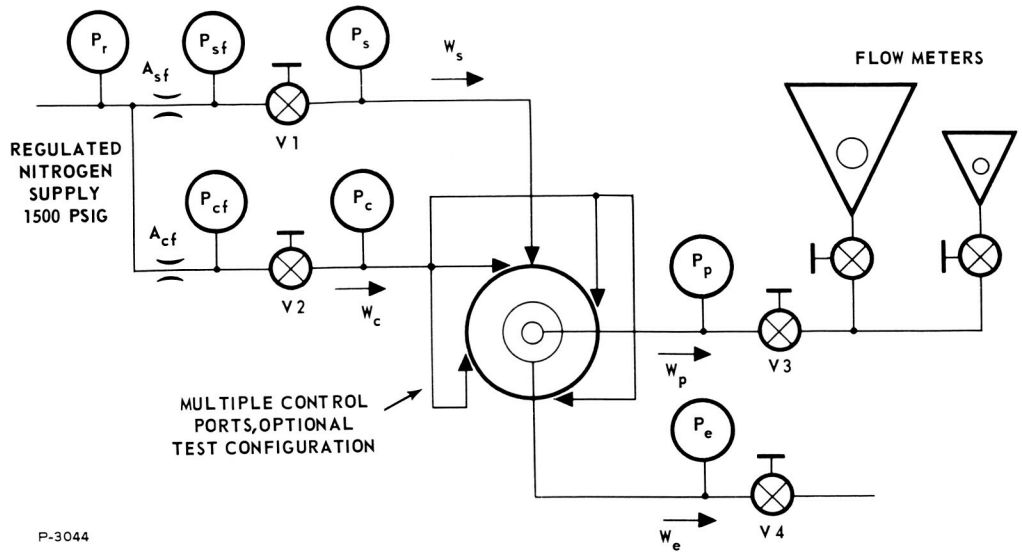

Figure B-26 - Test Schematic - Breadboard No. 2

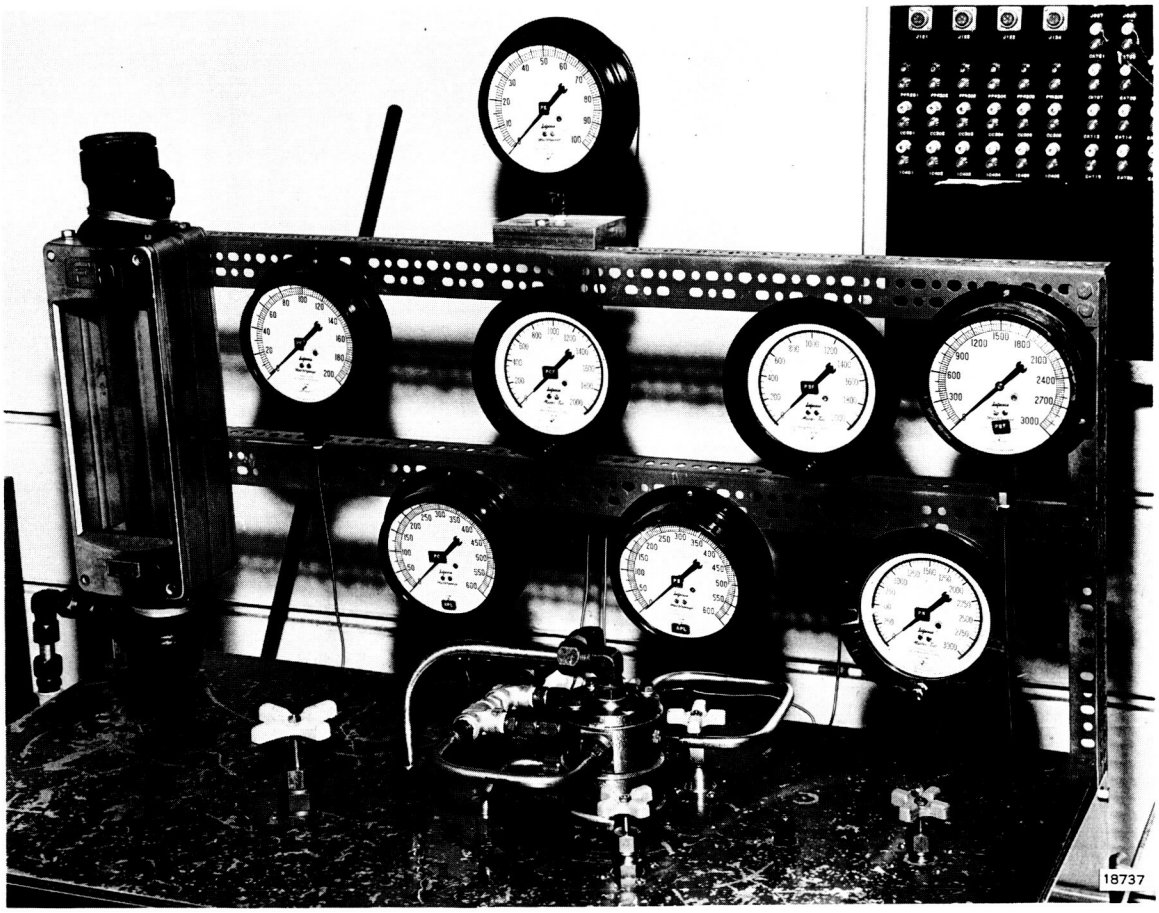

Figure B-27 - Test Setup

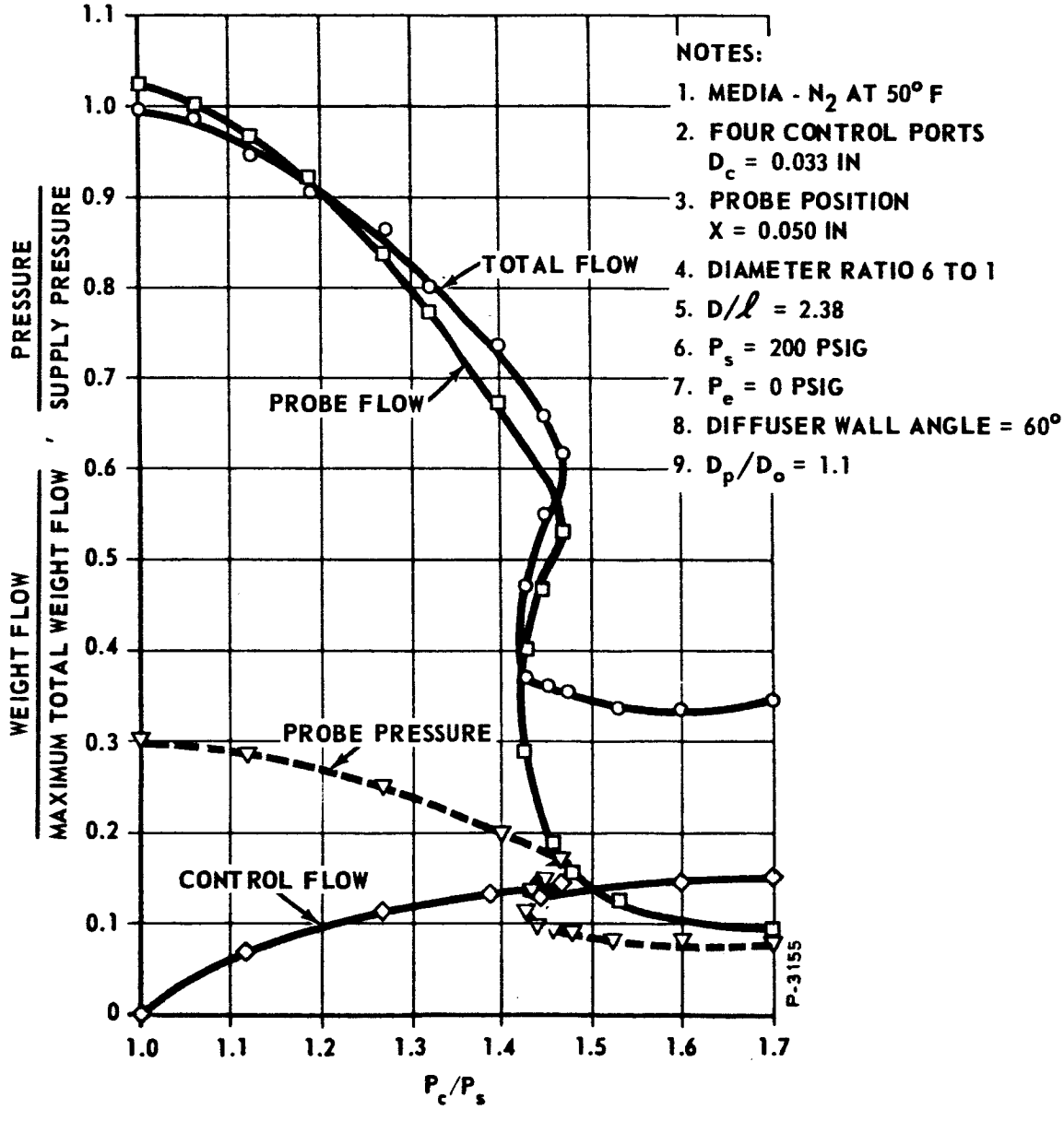

Figure B-28 - Initial Performance

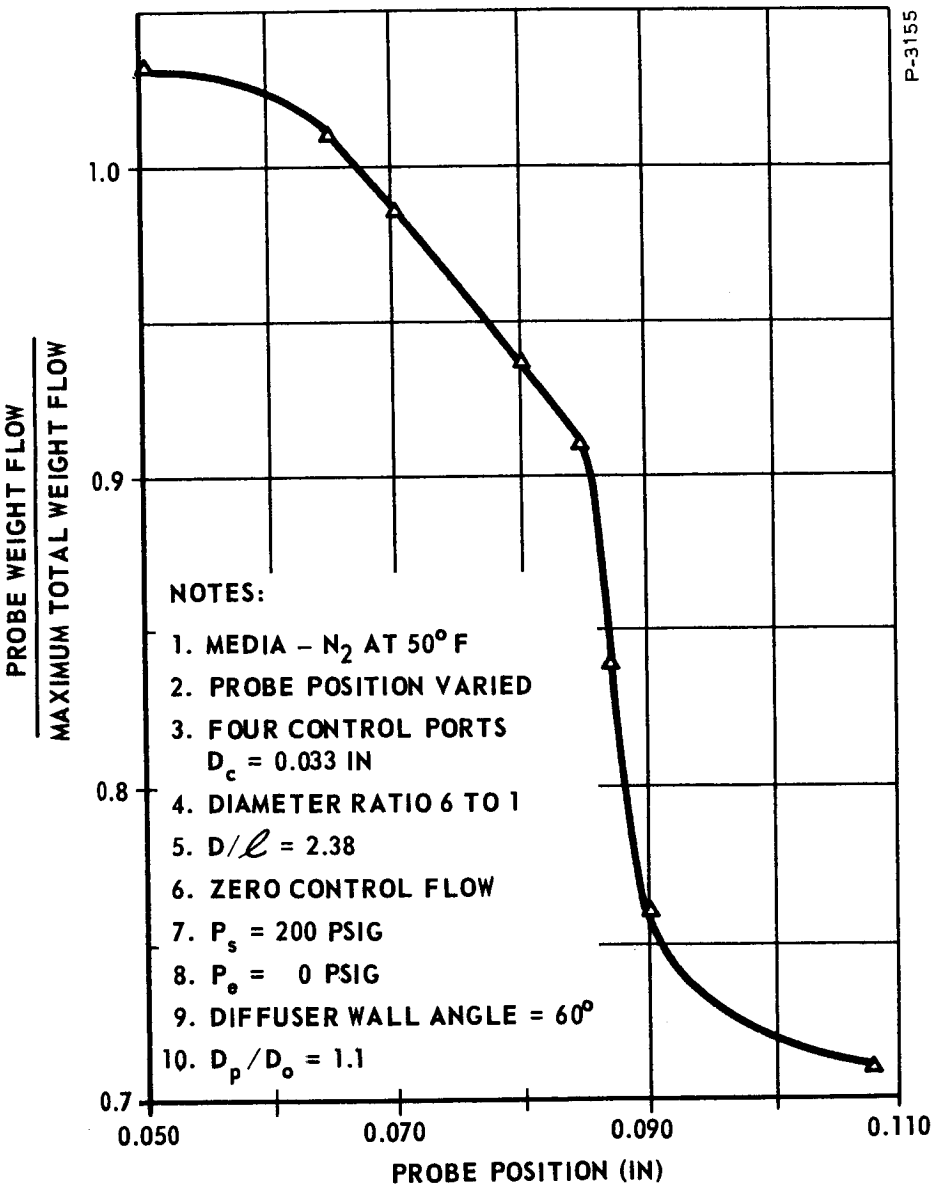

Figure B-29 - Probe Flow Versus Probe Position

x = 0.087 inch was selected. It should be noted that the slope of the curve is quite steep in the region of interest and that the flow recovery is sensitive to spacing. This must be considered in the design of amplifiers operating with hot gas.

Vortex Chamber Diameter Ratio

With the probe properly located, the comparison testing of a 6:1 and 8:1 vortex chamber to outlet orifice diameter was accomplished. The performance using a 6:1 diameter ratio is shown in Figure B-30 and the 8:1 diameter ratio performance is shown in Figure B-31. A comparison of the two curves shows no significant difference. The 6:1 diameter ratio curves have somewhat higher gain, but this is attributed to the fact that the control ports in the 6:1 control ring were slightly larger, allowing a higher control flow at a given control pressure. Very low probe flows could not be measured in these tests with a single flowmeter, thus the curves do not show decrease of probe flow to zero. The low flow region was evaluated after installing a second parallel low range flowmeter and zero probe flow was verified.

The maximum probe flow recovery for these tests was less than 80 percent. The reason for this parameter being lower than predicted is attributed to two causes. First, the flow recovery is sensitive to probe spacing, and, second, it was found that wall attachment of the exiting flow occurred in the exhaust diffuser. The flow leaving the chamber attached to the diffuser wall thus decreases the probe flow recovery under zero swirl condition. The diffuser wall half-angle was increased from 30 to 60 degrees, which eliminated this effect. This was an oversight in the design and previous experience has correlated this observation.

The reversal in slope of the flow turndown curves shown in Figure B-30 and B-31 can be predicted by analysis. This slope reversal results when using large vortex chamber lengths. This unstable region must be avoided in an amplifier of this type, so that the ratio of outlet orifice diameter to chamber length was increased to 3.0. This provided the desired positive slope and stability.

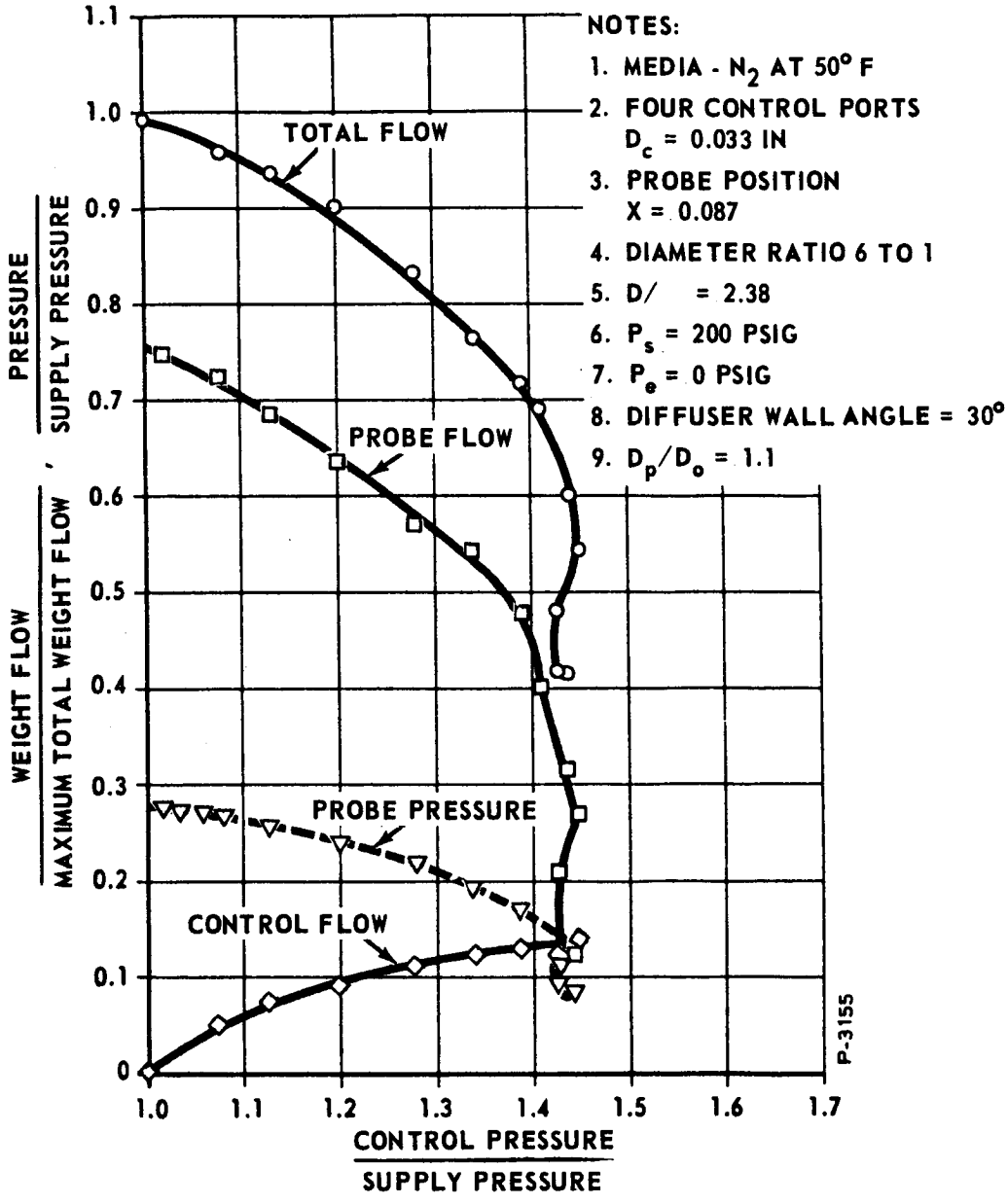

Figure B-30 - 6:1 Dia. Ratio Performance

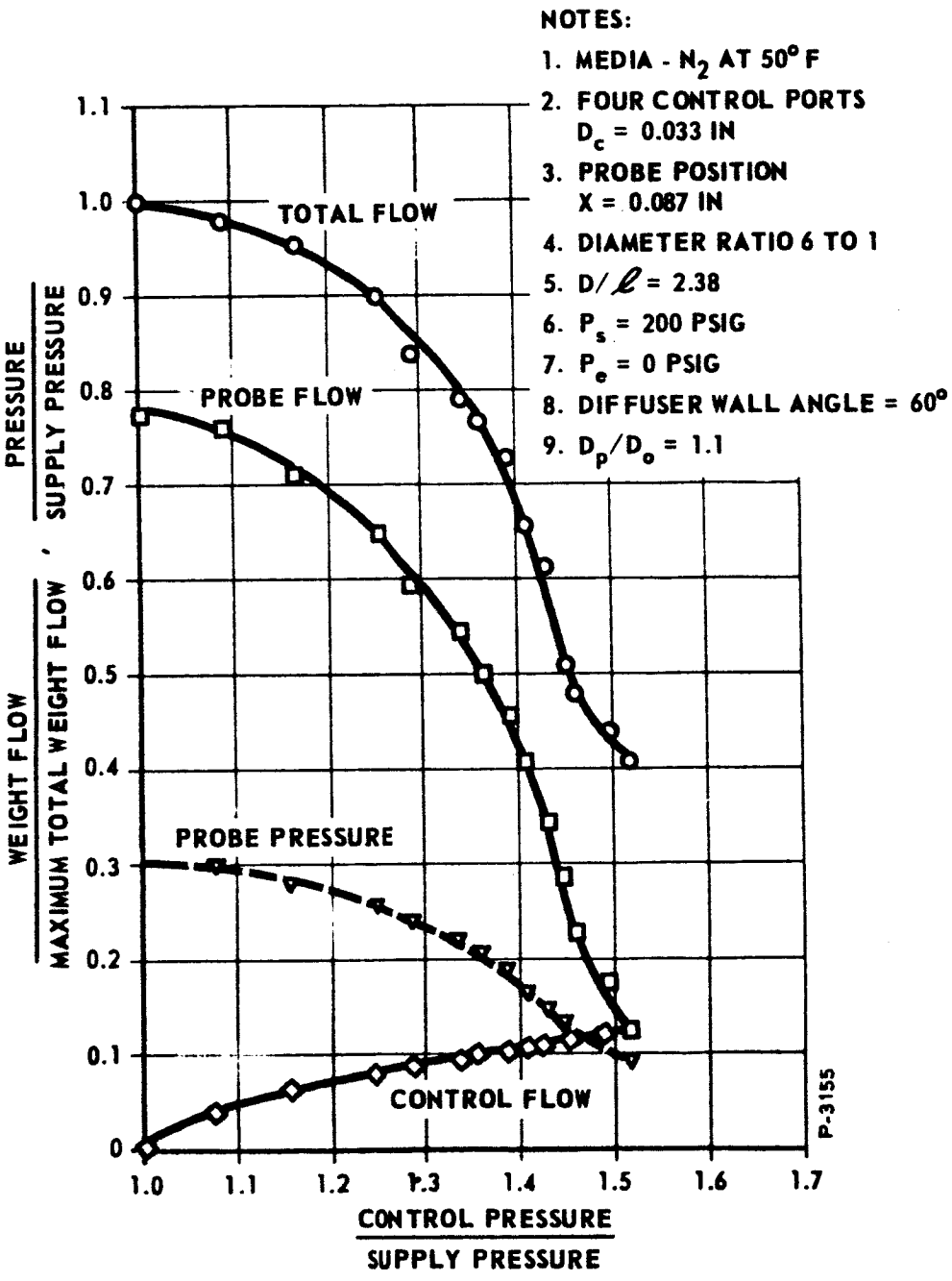

Figure B-31 - 8:1 Dia. Ratio Performance

Exhaust Back Pressure

The effect of exhaust back pressure on performance was investigated next. The exhaust back pressure valve was completely closed for the first test, shown in Figure B-32. This shows the relationship between control pressure and exhaust back pressure. This curve indicates the maximum possible back pressure at all control pressures of interest. This then is an upper limit, at least based on this series of tests, and the exhaust back pressure must be considerably lower to allow modulation of probe flow to zero. Accordingly, Figures B-33 and B-34 show performance at P_e = 24 psig and P_e = 38 psig. These curves can be compared with Figure B-36, which was run at zero back pressure.

The significant effect of exhaust back pressure on performance is to increase the probe flow recovery. This is desirable; however, the opposite effect occurs when maximum probe flow modulation is desired and the modulation range is not improved. A probe spacing varying from 0.087 inch to 0.188 inch is desired to provide sufficient area for the exhaust gas. The initial flow recovery was decreased to 90 percent; however, it was still not possible to achieve full probe flow modulation to zero. This performance is shown in Figure B-33. With an exhaust back pressure of 38 psig, it was still not possible to achieve full probe flow shutoff, even when the probe spacing was increased to 0.218 inch. This is shown in Figure B-34. The probe flow curve matched the total flow curve very closely, indicating a very small exhaust flow.

This particular vortex amplifier configuration is reasonably insensitive to exhaust back pressure; however, best results are achieved with this pressure maintained at a low value. Experimentation and study are needed in this area to develop a configuration less sensitive to exhaust back pressure. The final application of the vortex amplifier to secondary injection thrust vector control requires that the exhaust flow be utilized for additional axial thrust contributed and a nominal exhaust back pressure is required.

Variation In Supply Pressure

Figures B-35, B-36 and B-37 show the performance for supply pressures of 100, 200, and 250 psig. All of the tests showed the capability for decreasing the probe flow to zero, by increasing the control pressure sufficiently. A probe spacing of 0.146 inch was used at 100 psig

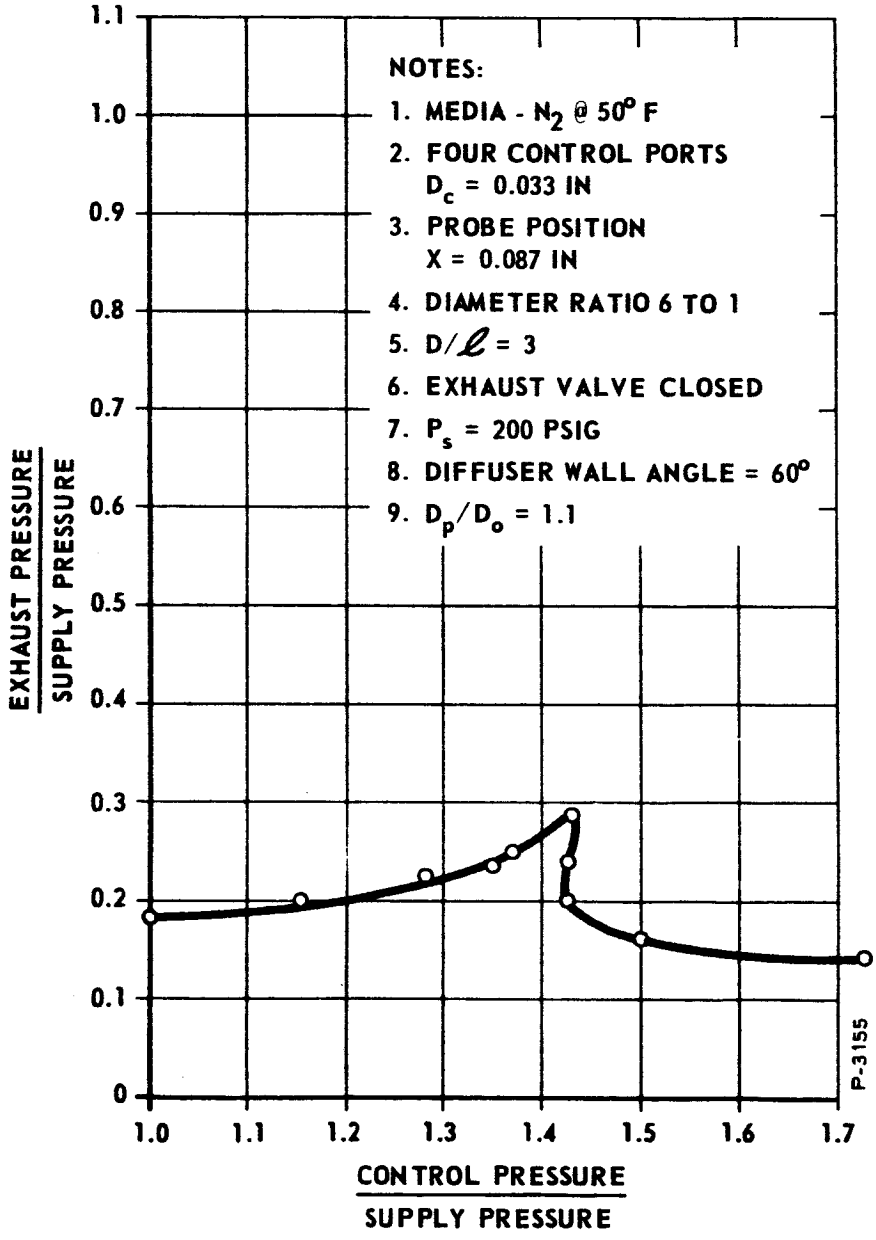

Figure B-32 - Maximum Exhaust Back Pressure

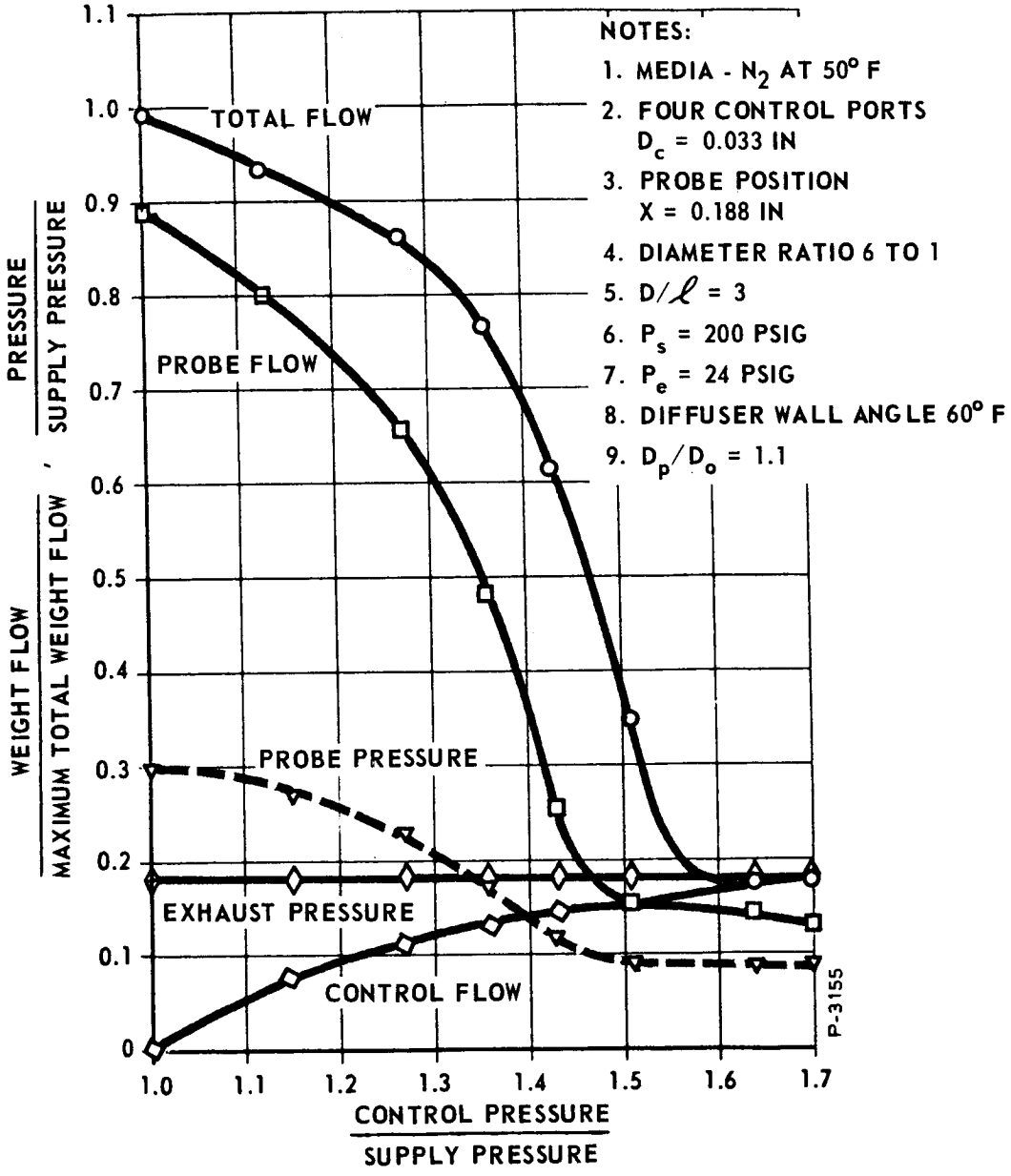

Figure B-33 - Exhaust Back Pressure = 24 Psig

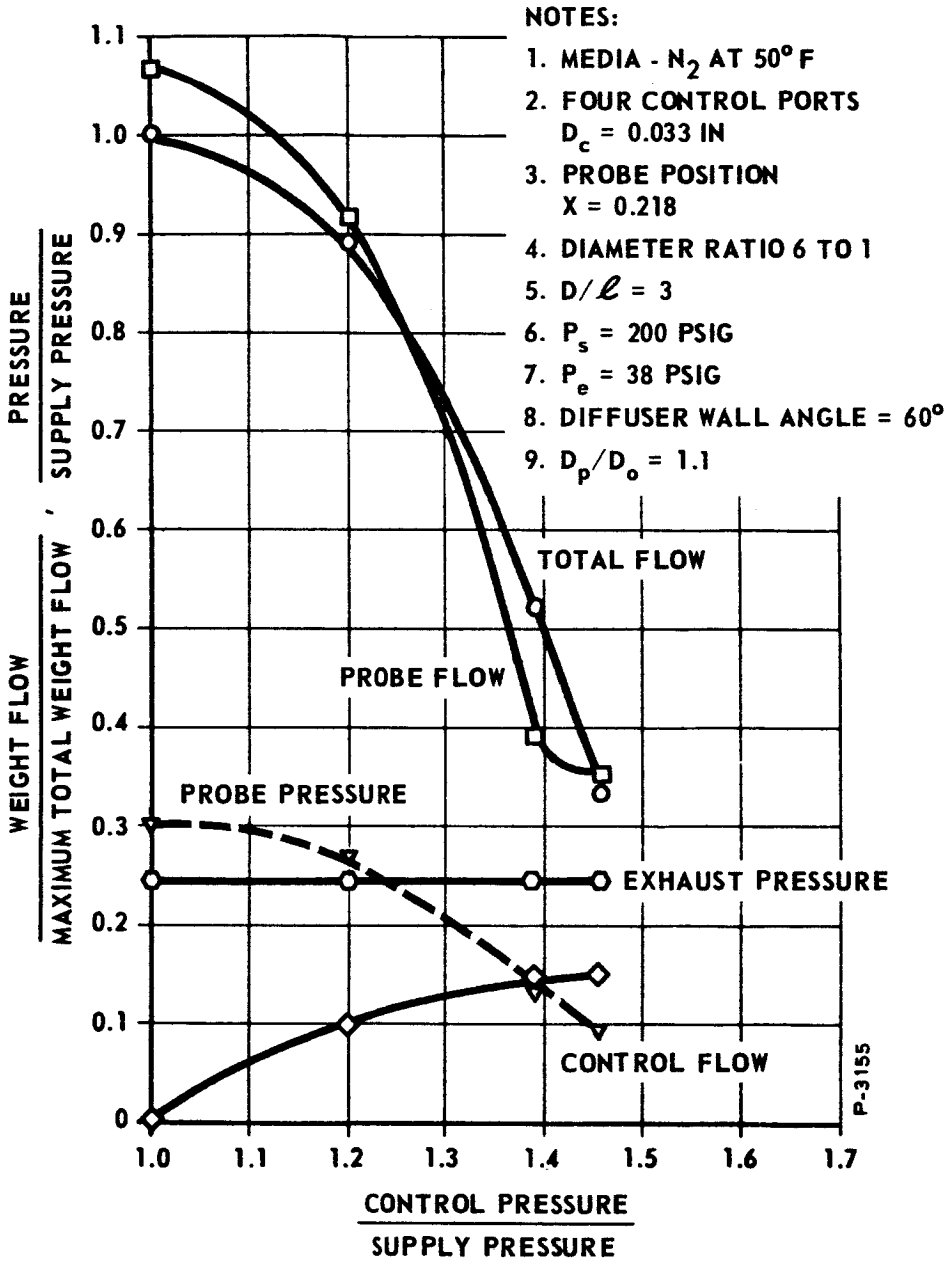

Figure B-34 - Exhaust Back Pressure = 38 Psig

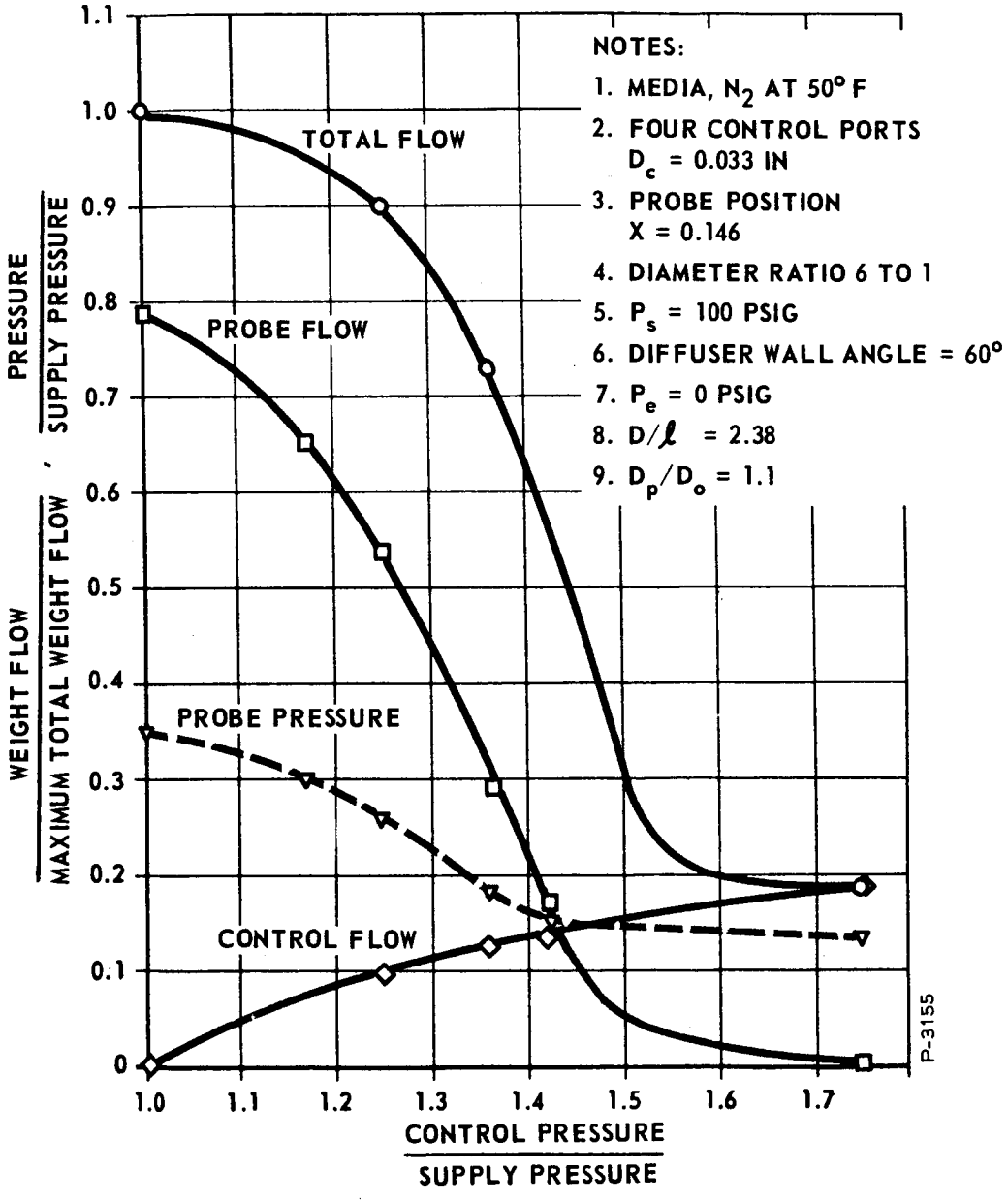

Figure B-35 - Supply Pressure = 100 Psig

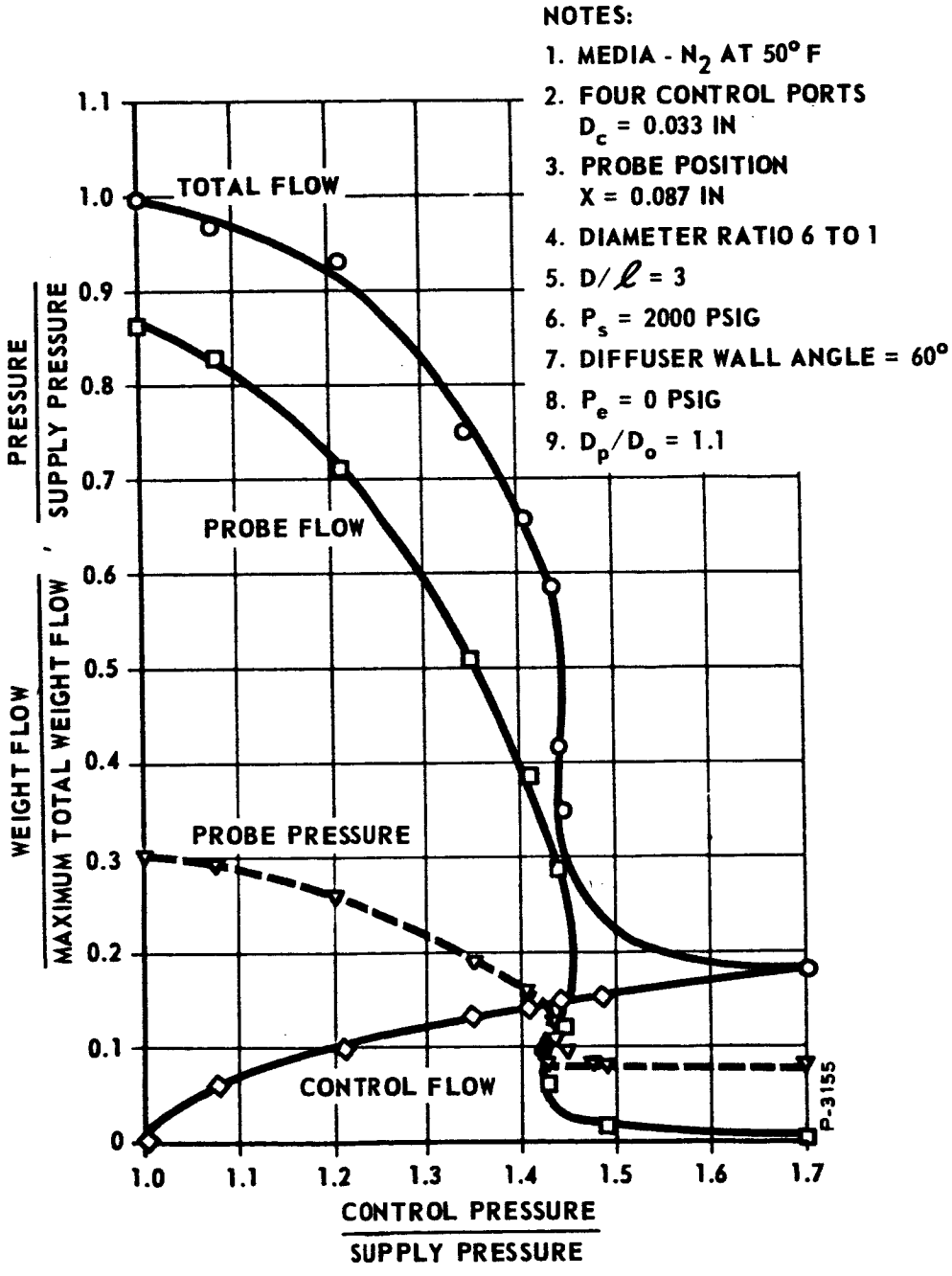

Figure B-36 - Supply Pressure = 200 Psig

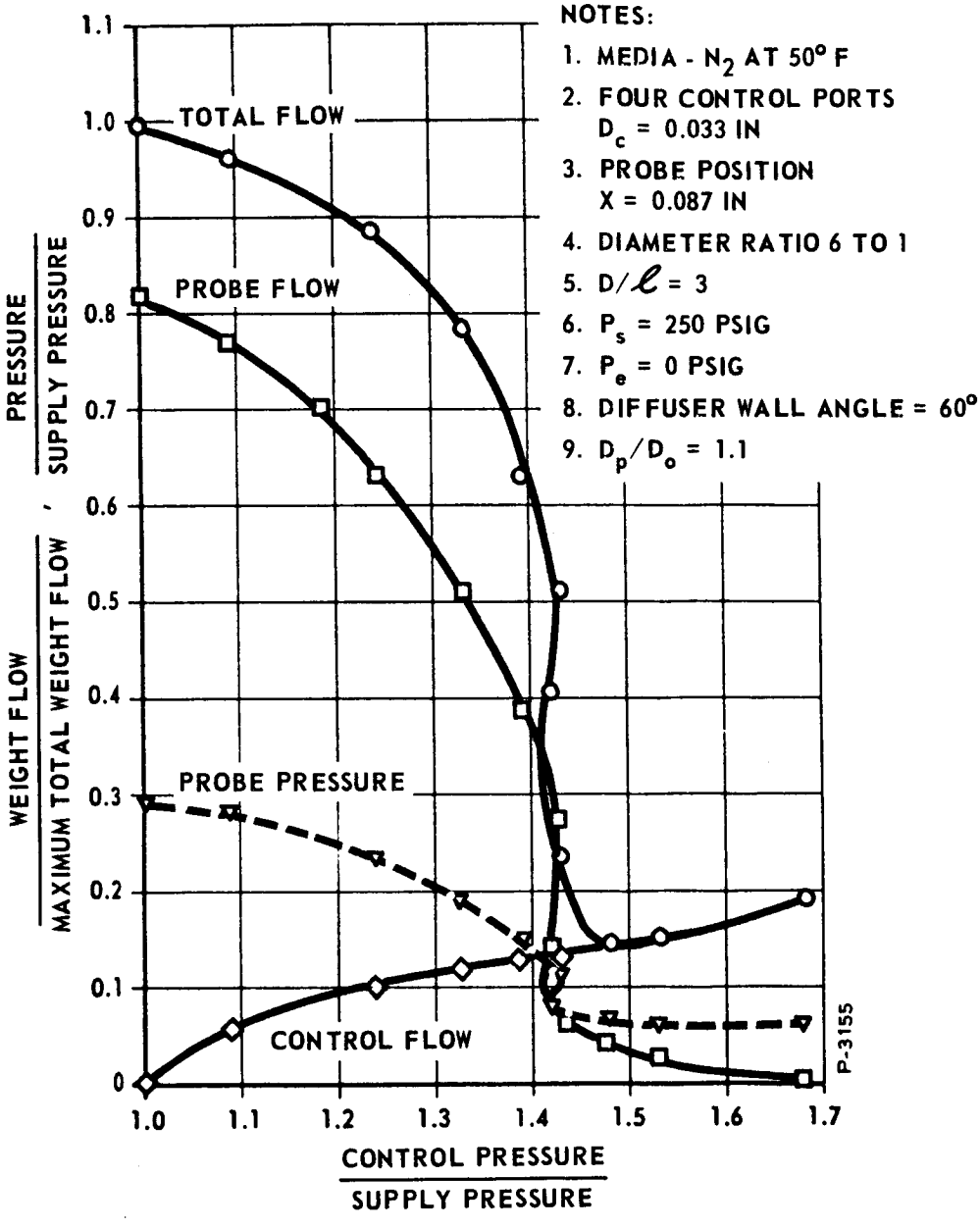

Figure B-37 - Supply Pressure - 250 Psig

supply pressure, compared to a spacing of 0.087 inch at the other pressures. The probe flow modulation at maximum turndown exhibits a gain saturation characteristic for all three pressures. The performance with P_s = 100 psig is quite different when compared with the other two pressure settings, indicating that the configuration was being operated off the design point. At P_s = 200 psig and P_s = 250 psig, the performance is similar and required no shifting of the probe spacing to achieve similar performance.

Relative Probe Flow Receiver Diameter

The last test with this size control ports is shown in Figure B-38. The initial probe flow recovery was 82 percent and probe flow was essentially zero at P_c/P_s ratio of 1.48. A vortex chamber flow turndown greater than 3 was attained.

It was reasoned that better performance would result if the probe diameter was made even larger and the probe spacing increased. Accordingly, the ratio of probe diameter to vortex chamber outlet diameter was increased from 1.1 to 1.2. The diameter of each control port was reduced from D_c = 0.033 inch (4 holes) to D_c = 0.031 inch (4 holes) for improved gain. These ports are axially located slightly over the edge of the button and are tangent to the chamber wall and perpendicular to the center line of the vortex amplifier. The performance for this test configuration is shown in Figure B-39. A vortex chamber flow turndown of 8.1 resulted. The maximum probe flow recovery was 79 percent and complete probe flow shutoff was obtained at a P_c/P_s ratio of 1.6. The total flow gain was approximately 8 based on total flow and approximately 6 based on probe flow. This test was run without bias. The control pressure ratio, P_c/P_s, of 1.6 was higher than desired; however, the added velocity obtained from this higher ratio produces a considerably larger swirl momentum component and results in better performance.

The final test of this series was run, using the larger probe diameter. Some testing was done, varying the probe position, and it was found that a spacing of x = 0.102 inch gave the best overall probe performance. This is shown in Figure B-40. Excellent chamber and probe performance was attained, and Figure B-40, as well as Figure B-39, can both be considered as reference baseline performance. Using bias

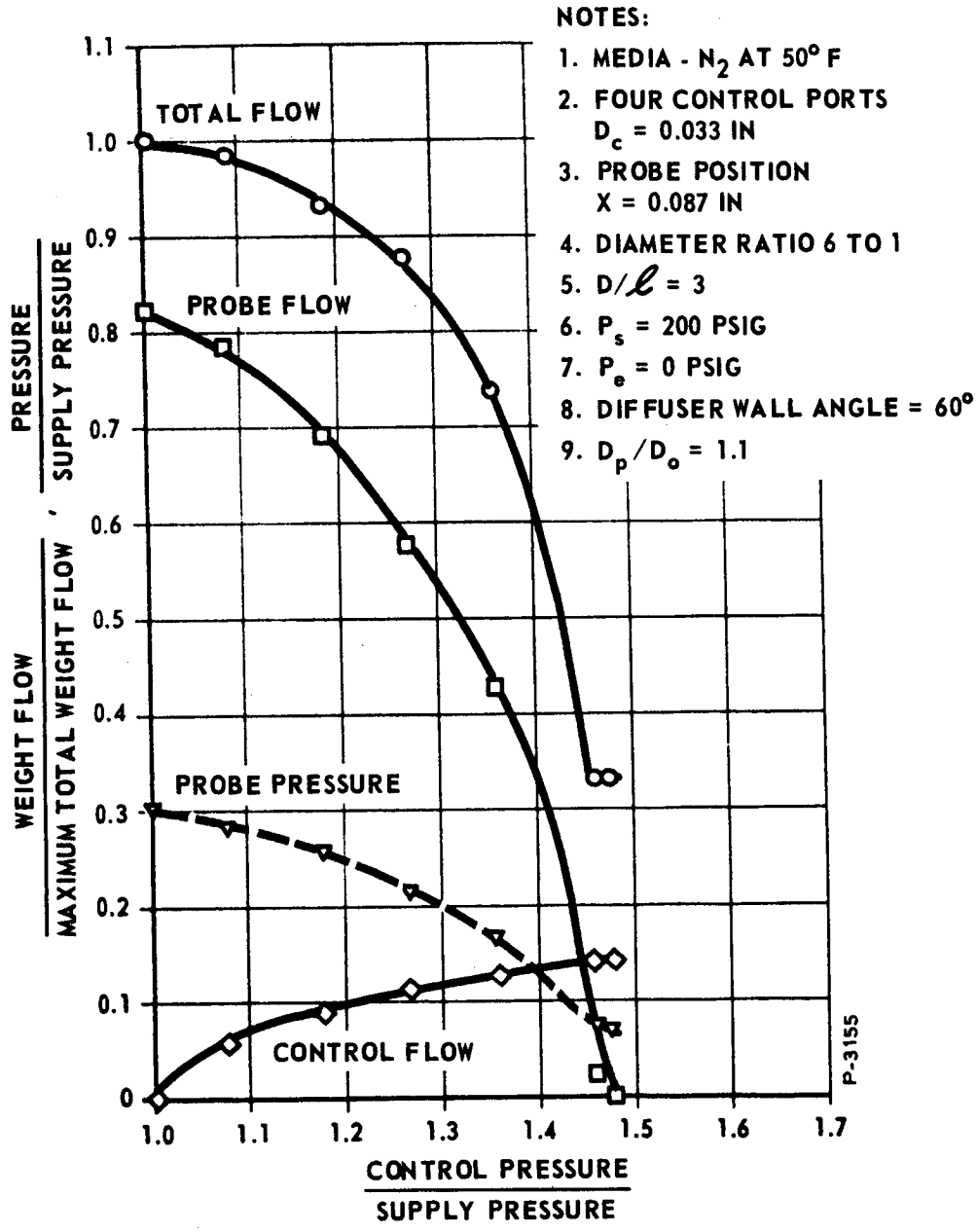

Figure B-38 - Large Probe Test

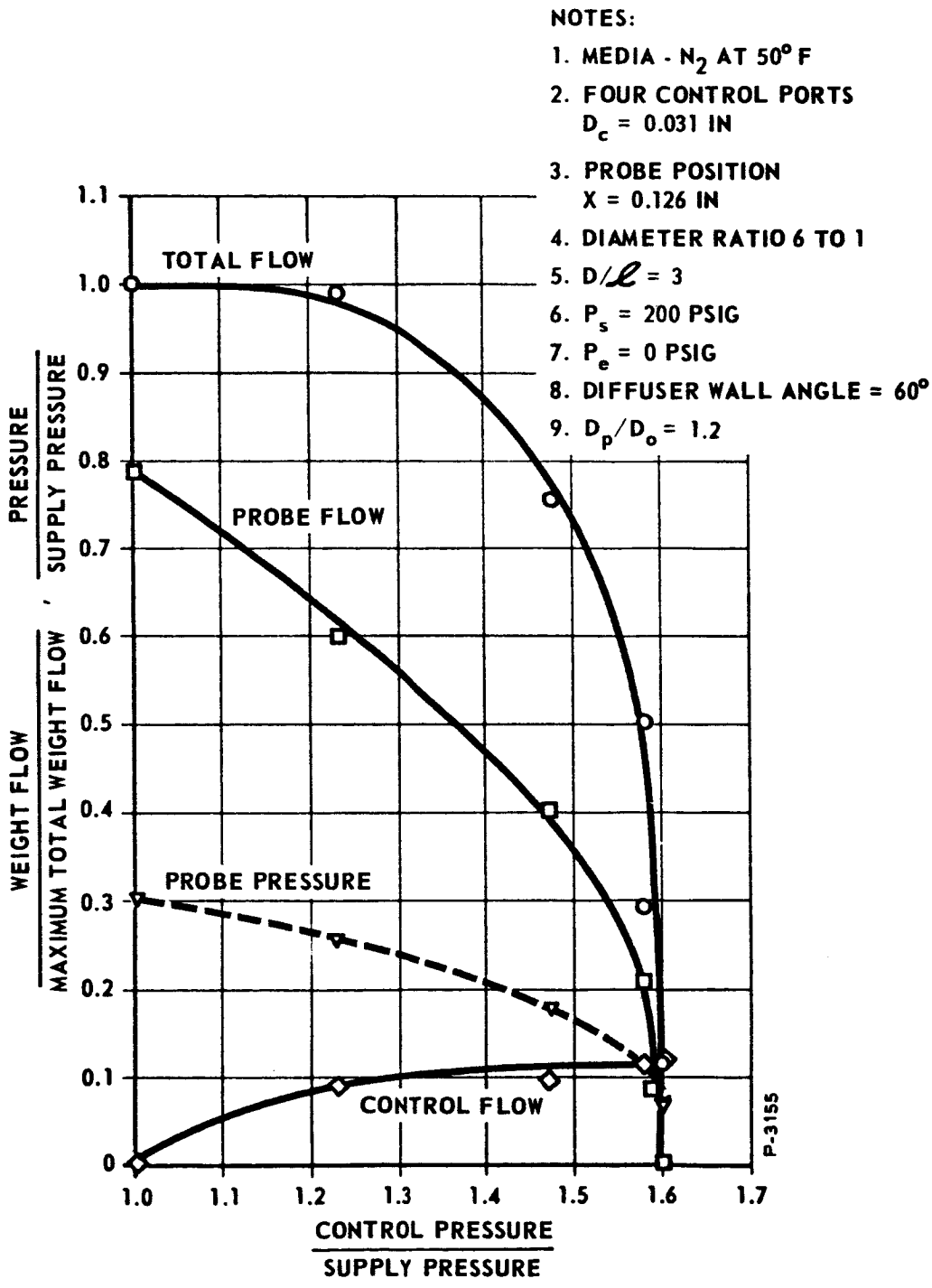

Figure B-39 - Final Test with Small Probe

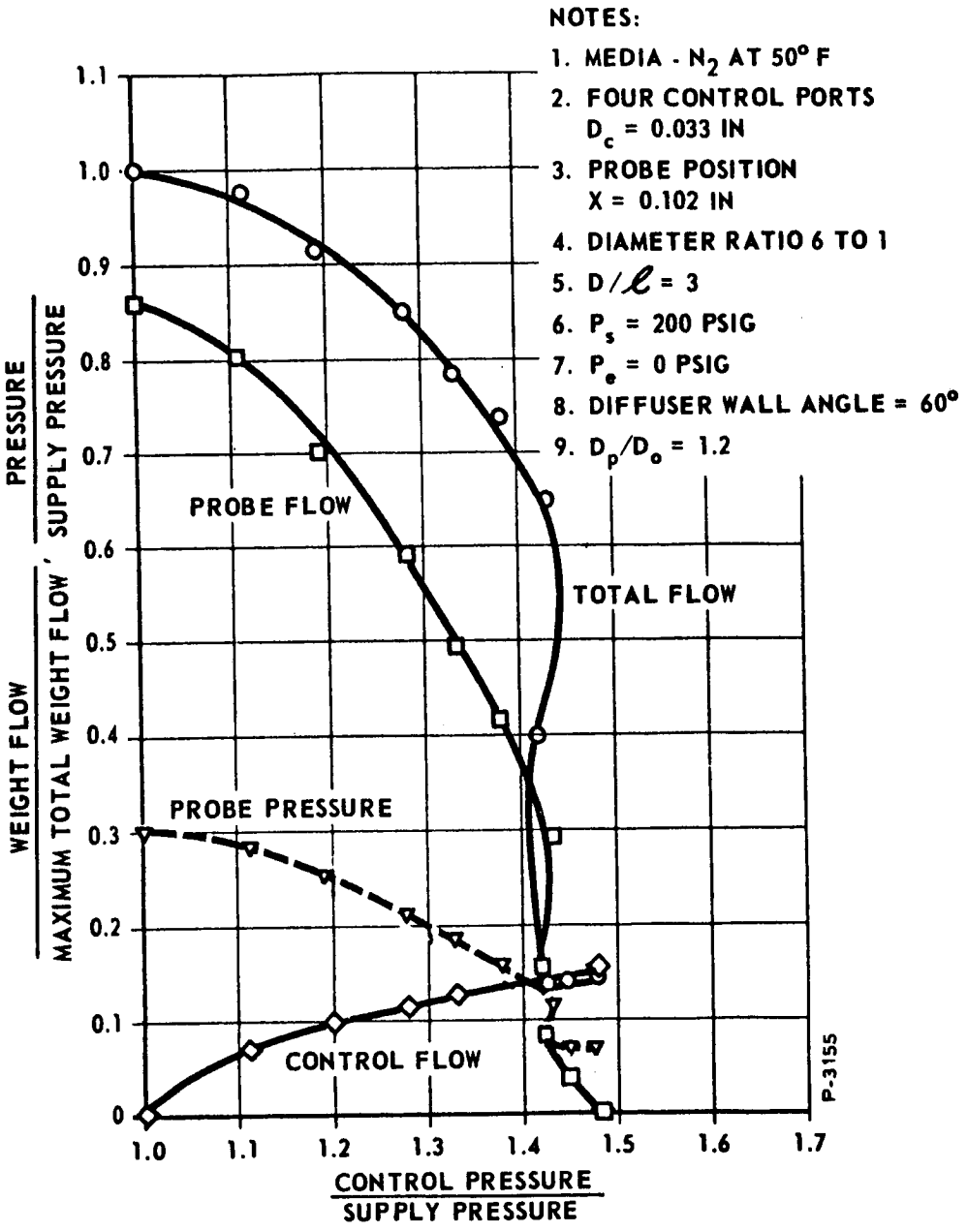

Figure B-40 - Final Test with Large Probe

flow and the performance shown in Figure B-40, it is possible to achieve 80 percent probe flow recovery and improve the total gain from 6.7 to 15.5 with complete probe flow turndown at low probe pressures.

The configuration details of the breadboard vortex amplifier that produce this performance were incorporated in the Phase 1 vortex amplifier hardware.

APPENDIX C

DYNAMIC ANALYSIS OF THE PHASE 1 VORTEX AMPLIFIER

Realization of the dynamic response of the vortex amplifier in the test installation is complicated by the dynamics of the gas generator and other peripheral test gear. An analysis of the complete system was attempted for initial correlation with cold gas performance. This analysis allows the separation of the vortex amplifier dynamics from the complete test system dynamics.

The basic problem in frequency response testing of the vortex amplifier was that the supply pressure could not be held constant while the control pressure was varied sinusoidally. In an actual secondary injection thrust vector control application, the supply flow can be obtained from rocket engine chamber bleed with the supply pressure held constant. This analysis allows the separation of the vortex amplifier dynamics from the complete test system dynamics.

A block diagram of the system dynamics is shown in Figure C-1.

Simple gain equations are used with single order dynamics to define the various elements. Equation (C-1) is the relationship between control pressure P_c, and probe pressure P_{pc}.

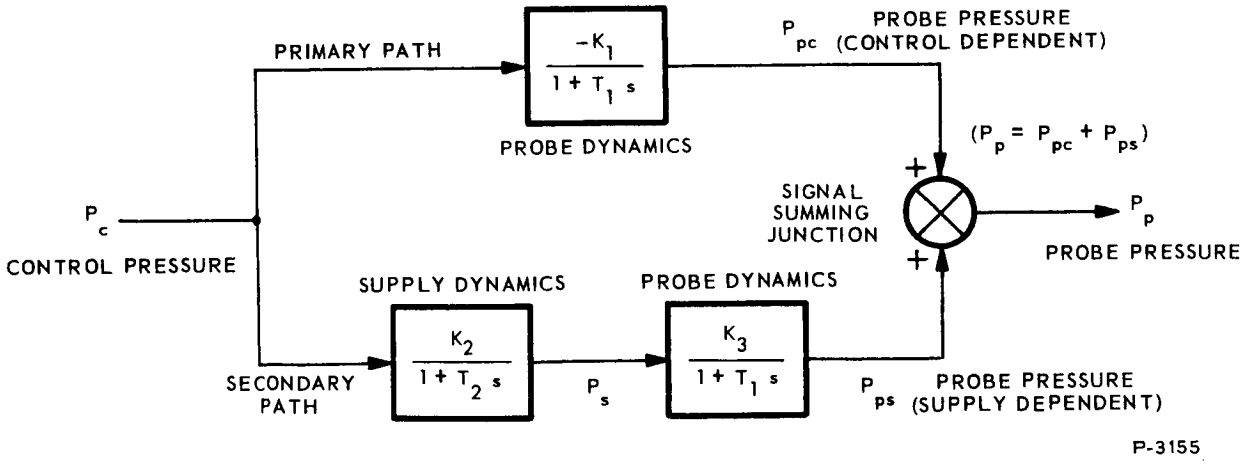

Figure C-1 - System Block Diagram

$$\frac{P_{pc}}{P_c} = \frac{-K_1}{(1 + T_1 s)} \qquad \text{(C-1)}$$

P_{pc} = probe pressure change resulting from change in P_c, control pressure

P_c = change in control pressure

K_1 = gain over small increment relating P_c to P_{pc}

T_1 = time constant between P_c and P_{pc}

Equation (C-2) is the relationship between the control pressure P_c, and supply pressure, P_s.

$$\frac{P_s}{P_c} = \frac{K_2}{1 + T_2 s} \qquad \text{(C-2)}$$

P_s = change in supply pressure

K_2 = gain, P_c to P_s

T_2 = time constant, P_c to P_s

Equation (C-3) is the relationship between supply pressure, P_s and probe pressure P_{ps}.

$$\frac{P_{ps}}{P_s} = \frac{K_3}{1 + T_1 s} \qquad \text{(C-3)}$$

P_{ps} = probe pressure change resulting from change in P_s, supply pressure

K_3 = gain, P_s to P_{ps}

T_1 = time constant, P_s to P_{ps} (Same time constant as in (C-1) since same flows and volumes are involved)

Solving equations (C-1) thru (C-3) to obtain $\frac{P_p}{P_c}$

$$P_{pc} = \frac{-K_1}{(1 + T_1 s)} P_c \qquad (C\text{-}4)$$

$$P_s = \frac{K_2}{(1 + T_2 s)} P_c \qquad (C\text{-}5)$$

$$P_{ps} = \frac{K_3}{1 + T_1 s} P_s \qquad (C\text{-}6)$$

Substituting equation (C-5) into (C-6):

$$P_{ps} = \frac{K_2 K_3}{(1 + T_1 s)\ (1 + T_2 s)} P_s \qquad (C\text{-}7)$$

but:

$$P_p = P_{pc} + P_{ps} \qquad (C\text{-}8)$$

Substitution of equations (C-4) and (C-7) into (C-8) results in:

$$\frac{P_p}{P_c} = \frac{1}{1 + T_1 s} \left[-K_1 + \frac{K_2 K_3}{(1 + T_2 s)} \right] \qquad (C\text{-}9)$$

Simplifying:

$$\frac{P_p}{P_c} = \frac{-(K_1 - K_2 K_3) \left[1 + \left(\frac{K_1 K_2}{K_1 - K_2 K_3} \right) s \right]}{(1 + T_1 s)\ (1 + T_2 s)} \qquad (C\text{-}10)$$

This is the final transfer function and it can be evaluated by substituting $s = j\omega$. The constants are evaluated from the static system characteristics.

$$K_1 = \frac{P_{pc}}{P_c} = \frac{87\text{-}72}{500\text{-}400} = 0.15 \frac{\text{psi}}{\text{psi}}$$

$K_1 = 0.15 \frac{\text{psi}}{\text{psi}}$ (Obtained from initial step response data)

$$K_2 = \frac{P_s}{P_c} = \frac{40}{100} = 0.4 \frac{psi}{psi}$$

$$K_2 = 0.40 \frac{psi}{psi}$$

$$P_s = 0.40\ P_c$$

$$P_p = K_4\ P_c$$

$$K_4 = \frac{P_p}{P_c} = \frac{82 - 72}{100} = 0.1 \frac{psi}{psi}$$

$$P_p = 0.10\ P_c \quad \text{(Obtained from step response data)}$$

$$P_s = 0.4\ P_c$$

$$P_c = 10\ P_p$$

$$P_c = 2.5\ P_s$$

$$10\ P_p = 2.5\ P_s$$

$$P_p = 0.25\ P_s$$

$$K_3 = 0.25 \frac{psi}{psi}$$

To evaluate the time constants, the following general analysis was made: See Figure C-2.

Assumptions:

(a) All orifices are sonic

(b) $C = \frac{C_d\ C_2}{\sqrt{T}}$

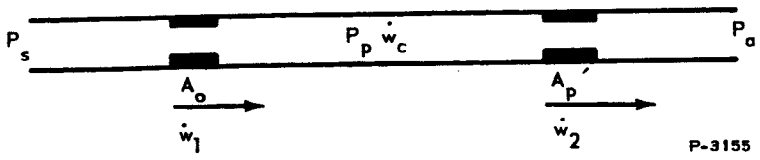

Figure C-2 - Series Orifice Schematic

where:

C_d = discharge coefficient

C_2 = thermodynamic gas constant

T = gas temperature

$$\dot{w}_1 = C A_o P_s \quad \text{(Inlet Flow)} \tag{C-11}$$

$$\dot{w}_2 = C A_p' P_p \quad \text{(Outlet Flow)} \tag{C-12}$$

$$\dot{w}_c = \frac{V P_s}{RT} \quad \text{(Compressibility Flow)} \tag{C-13}$$

$$\dot{w}_1 = \dot{w}_2 + \dot{w}_c \quad \text{(Continuity Equation)} \tag{C-14}$$

Substituting equations (C-11), (C-12) and (C-13) into (C-14):

$$\frac{P_p}{P_s} = \frac{A_o/A_p'}{1 + \frac{Vs}{k C A_p' RT}} \tag{C-15}$$

however:

$$C = \frac{C_d C_2}{\sqrt{T}}$$

$$\frac{P_p}{P_s} = \frac{A_o/A_p'}{1 + \frac{Vs}{k C_d A_p' R \sqrt{T} C_2}} \tag{C-16}$$

And in general form:

$$\frac{P_p}{P_s} = \frac{K}{1 + TS} \tag{C-17}$$

where:

$$K = A_o/A_p'$$

$$T = \frac{V}{k C_d C_2 A_p' R \quad T}$$

or

$$T = \frac{V}{k Q} \qquad \text{(C-18)}$$

This analysis justifies the use of a single order system to describe the dynamics of the vortex amplifier, since only volumes and flow rates are involved.

Time Constant Determination

T_1 is the time constant associated with the probe and T_2 is the time constant associated with the supply source.

$$T_1 = \frac{V_p}{k Q_p} \qquad \text{(C-19)}$$

where:

$V_p = 24 \text{ in}^3$ (Probe Volume, purposely made large to facilitate the measurement of probe pressure)

$\dot{w}_p = 1.715$ lb/sec

$P_p = 85$ psia

$k = 1.4$ (Ratio of specific heats for nitrogen)

$R = 662$ in/°R (Universal gas constant)

$T = 500$ °R

$$Q_p = \frac{\dot{w}_p R T}{P_p} = \frac{1.715 \times 662 \times 500}{85} = \frac{6670 \text{ in}^3}{\text{sec}} \qquad \text{(C-20)}$$

$$T_1 = \frac{24}{1.4 \times 6670} = 0.00257 \text{ sec}$$

$T_1 = 0.0026$ sec

$$T_2 = \frac{V_s}{k Q_s}$$

where

V_s = 52 in^3 (Actually measured)

V_{se} = 26 in^3 (Effective volume reduced because of volume separation)

$\dot{w}_s = \dot{w}_t - \dot{w}_c$ = 1.98 lb/sec

P_s = 425 psia

$$Q_s = \frac{1.98 \times 662 \times 500}{425}$$

$$Q_s = 1540 \frac{in^3}{sec}$$

$$T_2 = \frac{26}{1.4 \times 1540} = 0.012 \text{ sec}$$

T_2 = 0.012 sec

Substituting all values of K and T into equation (C-10)

$$\frac{P_p}{P_s} = \frac{-(0.15 - 0.40 \times 0.25)}{(1 + 0.0026\,s)\ (1 + 0.012\,s)} \quad 1 + \frac{(0.15 \times 0.012)}{0.15 - 0.40 \times 0.25}\ s \qquad \text{(C-21)}$$

$$\frac{P_p}{P_c} = \frac{-\ 0.05\ (1 + 0.036\,s)}{(1 + 0.0026\,s)\ (1 + 0.012\,s)} \qquad \text{((C-22)}$$

An evaluation of time constants:

$$T = 0.036 \text{ sec}, \quad f = \frac{1}{2\pi \times 0.036} = 4.4 \text{ cps}$$

$$T = 0.012 \text{ sec}, \quad f = \frac{1}{2\pi \times 0.012} = 13.2 \text{ cps}$$

$$T = 0.0026 \text{ sec}, \quad f = \frac{1}{2\pi \times 0.0026} = 60.2 \text{ cps}$$

Figure C-3 is a plot of equation (C-22). The data from an actual frequency response cold gas test is plotted in Figure C-4. A comparison of the two curves shows that there is a close correlation, indicating an accurate analysis.

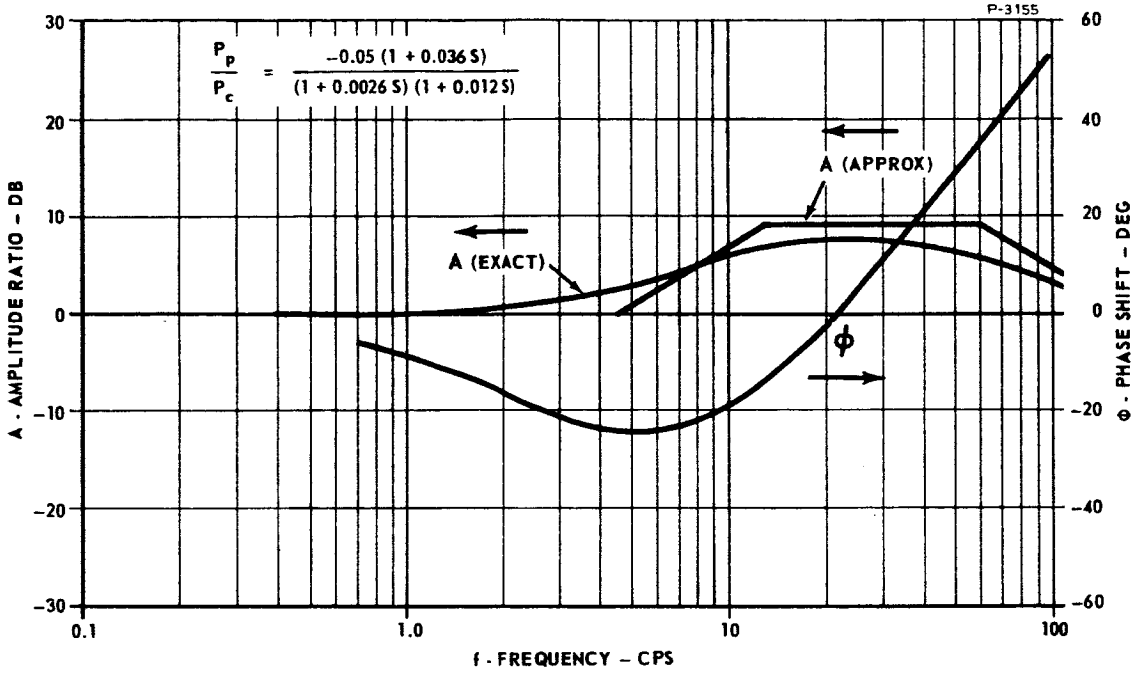

Figure C-3 - Theoretical Cold Gas Dynamic Performance - Varying Supply Pressure

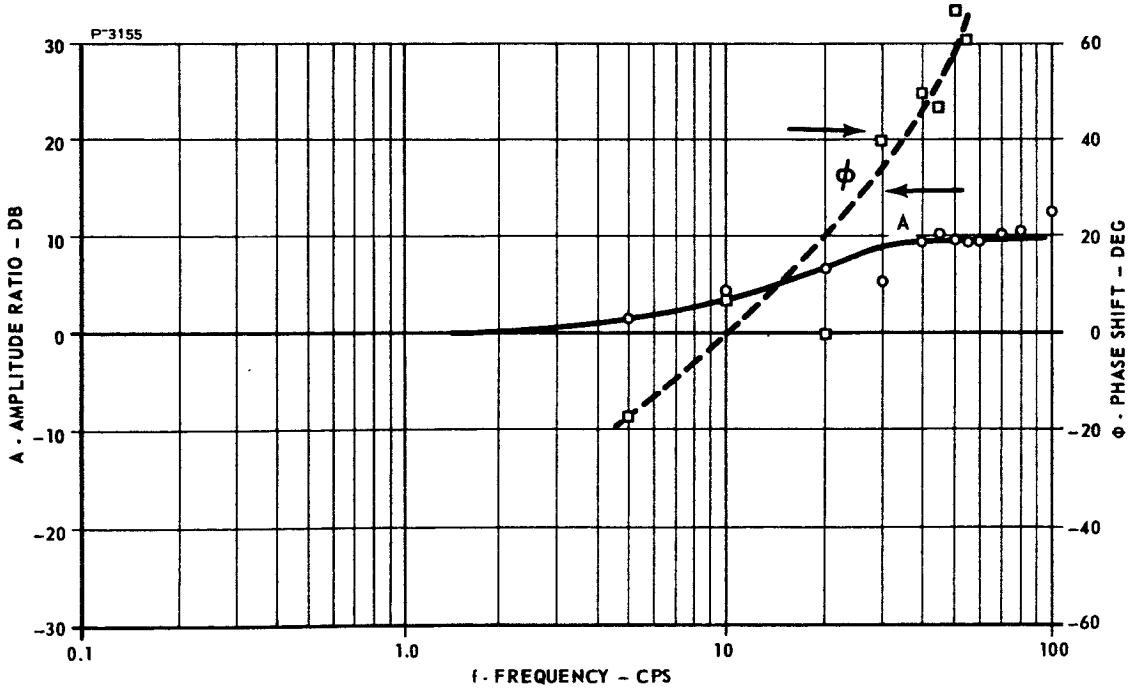

Figure C-4 - Cold Dynamic Performance

The next step is to eliminate analytically the effect of a varying supply pressure.

Let $T_1 = 0$ in equation (C-10).

$$\frac{P_p}{P_c} = \frac{-(K_1 - K_2K_3)}{(1 + T_2 s)} \left[1 + \left(\frac{K_1 T_2}{K_1 - K_2K_3} \right) s \right] \qquad \text{(C-23)}$$

Substituting constants

$$\frac{P_p}{P_c} = \frac{-0.05\ (1 + 0.036\ s)}{(1 + 0.012\ s)}$$

This equation is plotted in Figure C-5. The frequency response of the Phase 1 vortex amplifier, with constant supply pressure, can now be approximated by adding the performance shown in Figures C-4 and C-5. Figure C-6 is the final performance and represents the corrected data.

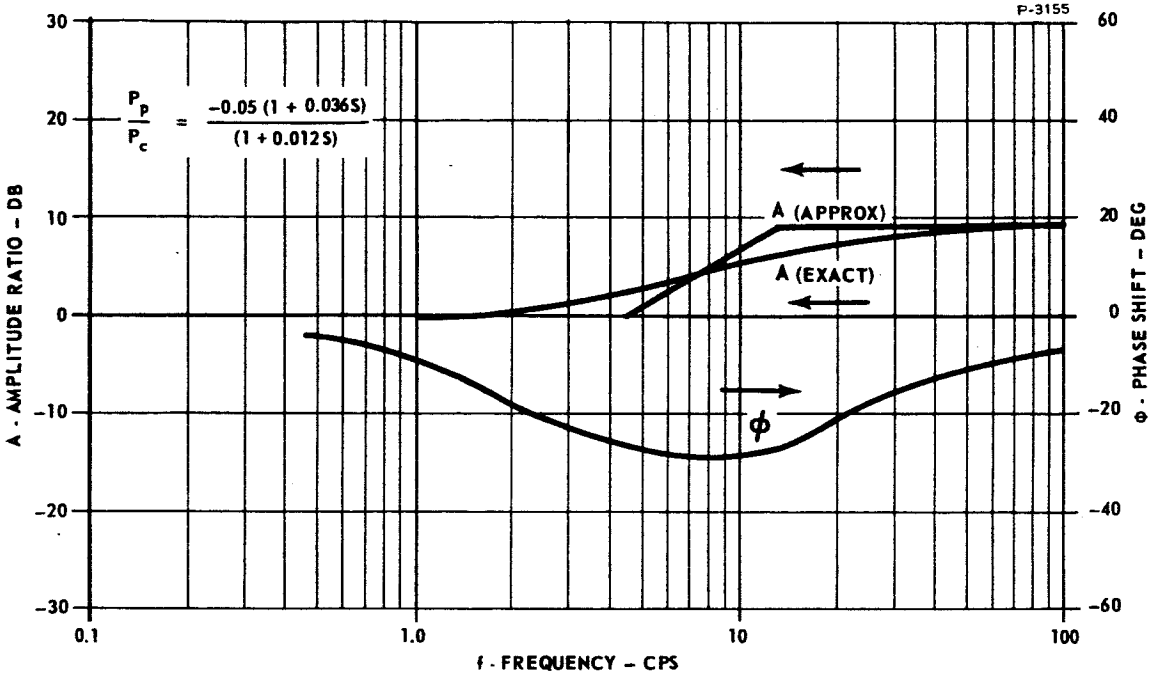

Figure C-5 - Theoretical Effect of Varying Supply Pressure

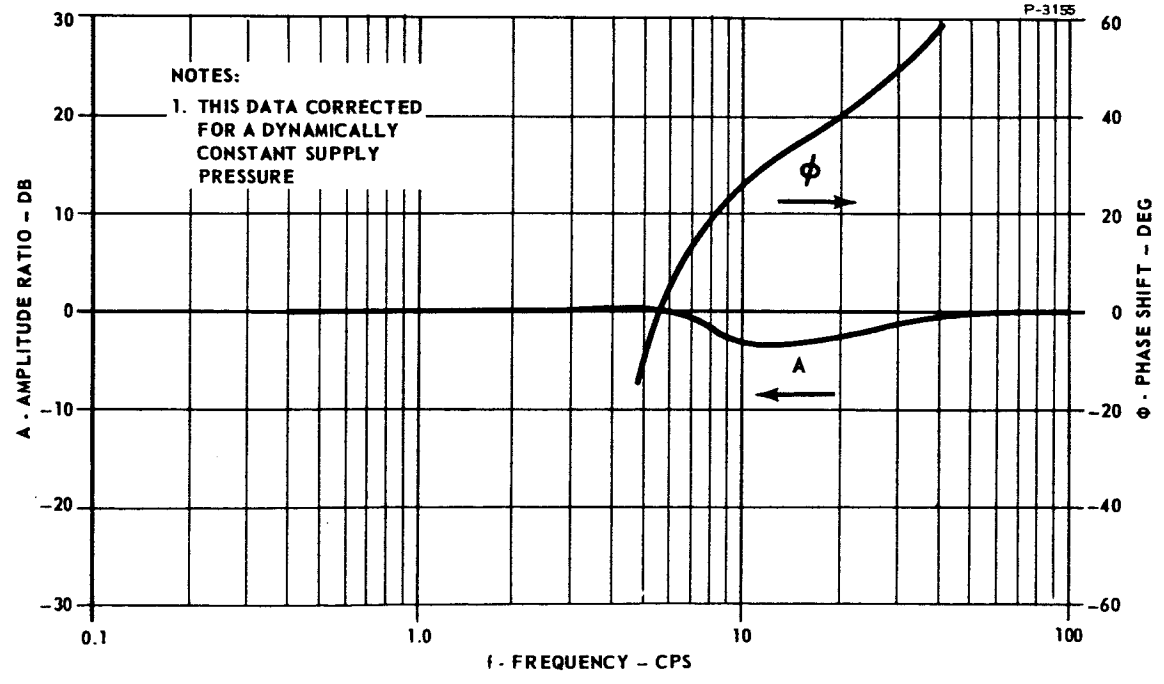

Figure C-6 - Corrected Cold Gas Dynamic Performance

APPENDIX D

THEORETICAL ANALYSIS

Derivation of an analytical model of the vortex amplifier and probe flow pickoff assures better technical judgments when physical parameters are varied for improved performance. It serves to minimize the cut and try approach and establishes trends.

Significant progress has been made in the formulation of a basic analytical model and in normalization of test data. The fluid mechanics technology required to define the vortex flow field is very complex, involving boundary layer effects and three-dimensional flow. A simple mathematical model is used in this analysis, which assumes free vortex theory for the vortex chamber. Geometric flow relationships were used for the probe model.

Reference (6) was used as the source of all equations for this analysis. Appendix A shows ideal performance curves, based on the specification requirements. It is the intent of this analysis to derive equations describing these curves. The analysis consisted of deriving expressions for a total vortex amplifier flow curve ($\dot{w}_o/\dot{w}_{om}$); a control flow curve, ($\dot{w}_c/\dot{w}_{om}$); and a probe flow curve ($\dot{w}_p/\dot{w}_{om}$). The total flow curve includes a region where free vortex theory determines performance at low vortex swirl conditions and a transition region where a combination of free and forced vortex theory more nearly approximates the actual performance. The design parameters for the Phase 1 vortex amplifier were used; consequently, the analysis is not general, but represents a given configuration operating with specific operation conditions. The complete total flow curve, using free vortex theory, shows that a reversal in curve slope can occur, i.e., negative resistance. In a theoretical loss-less system, after some initial flow modulation occurs, less and less control momentum is required for further modulation. In an actual vortex valve, the slope reversal can be eliminated by proper chamber design. In order to provide a continuous curve of theoretical total flow, a transition curve was arbitrarily fitted between the analytically derived portion of the total flow curve and the control flow curve.

The control flow curve ($\dot{w}_c/\dot{w}_{om}$) was obtained from a simple orifice flow theory, using a modification of Fliegner's formula described in Reference (6).

The exact mathematical derivation of probe flow ($\dot{w}_p/\dot{w}_{om}$) is a complex problem involving the use of control volumes and pressure gradients. In order to obtain a preliminary solution to the problem, it was assumed that the probe was not back pressured. Geometry of the hot gas Phase 1 vortex amplifier was used. The problem was to compute first the cone angle for various control pressures, and then, from geometrical considerations, compute the flow ($\dot{w}_p$) entering the probe. The resulting curve shows that it is theoretically possible to decrease the flow in an unloaded probe to zero.

This analysis has proven useful in providing direction to the test program. The total flow curve slope reversal can be justified. Insight was gained into designing a more optimum probe configuration. The general shape and location of the curves on the standard nondimensional coordinates agree reasonably well with experimental data, indicating that the mathematical model is accurate enough to be a useful tool.

Vortex Amplifier Analysis - No Probe Flow Receiver

This analysis is concerned with the basic vortex amplifier. A schematic diagram for identifying variables is shown in Figure D-1. Using the equations developed in Reference (6), it is possible to obtain relationships between control pressure P_c and total flow $\dot{w}_o$.

Using free vortex theory: (See Glossary, p. 131)

$$\frac{P_o}{P_i} = e^{K M_{to}^2} \tag{D-1}$$

$$P_i = P_o e^{-K M_{to}^2}$$

where:

$$P_o = 415 \text{ psia (Pressure at outer wall)} \tag{D-2}$$

$$K = \left[\frac{k}{2}\left(\frac{r_o}{r_i}\right)^2 - 1\right] \tag{D-3}$$

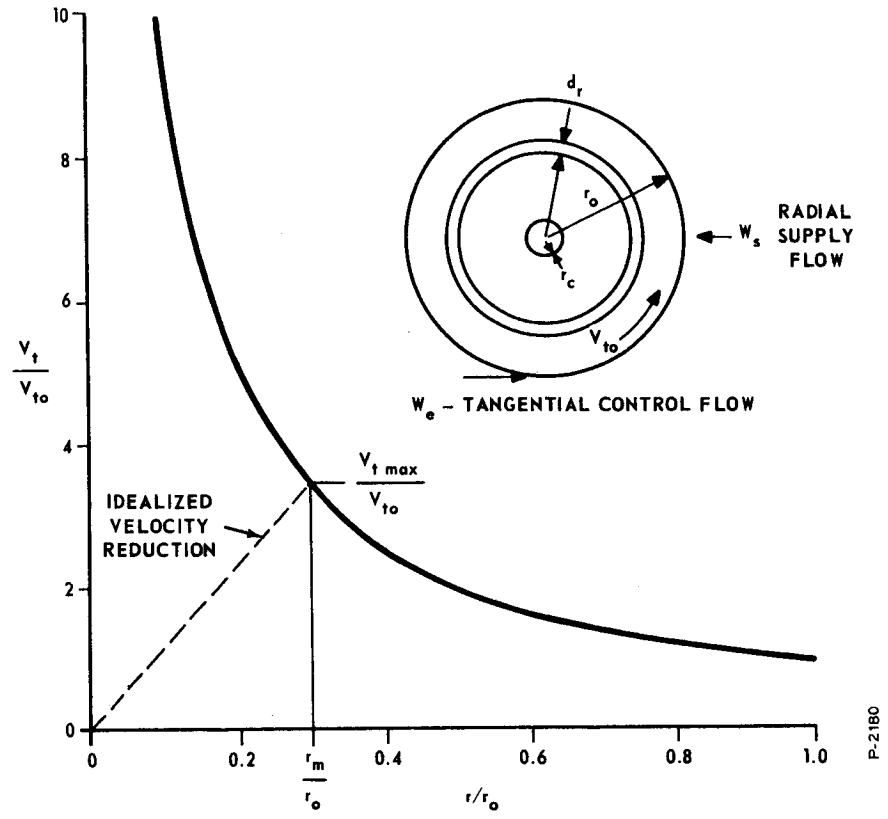

Figure D-1 - Tangential Velocity Distribution and Flow Schematic for Ideal Vortex

where:

$$\frac{r_o}{r_i} = 6$$

$$k = 1.3$$

$$K = \frac{1.3}{2} \times 35$$

$$K = 22.7$$

$$P_i = 415\, e^{-22.7\, M_{to}^2} \qquad \text{(D-4)}$$

$$\frac{\dot{w}_o}{\dot{w}_n} = 2\sqrt{\left(\frac{P_i}{P_e} - 1\right)} \qquad \text{(D-5)}$$

$$\dot{w}_n = \frac{C\, C_d\, A_e\, P_e}{\sqrt{T}} \text{ (Normalized Flow)} \qquad \text{(D-6)}$$

where:

$C = 0.185\sqrt{°R}/\text{sec}$

$C_d = 0.7$

$A_e = 0.379\ \text{in}^2$

$D_e = 0.695\ \text{in}$

$\sqrt{T} = 44.4\sqrt{°R}$

$$\frac{P_e}{P_{o(crit)}} = \left(\frac{2}{k+1}\right)^{\frac{k}{k-1}} \qquad \text{(D-7)}$$

$\dfrac{P_e}{P_{o(crit)}} = 0.547$ (Sonic)

$P_e = 0.547 \times 415 = 227\ \text{psia}$

$$\dot{w}_n = \frac{0.185 \times 0.7 \times 0.379 \times 227}{44.4}$$

$\dot{w}_n = 0.251\ \text{lb/sec}$

$$\dot{w}_o = 0.502\sqrt{\left(\frac{P_i}{227} - 1\right)} \qquad \text{(D-8)}$$

Substitute equation (D-8) into (D-4):

$$\dot{w}_o = 0.502\sqrt{\left[1.828\, e^{-22.7\, M_{to}^2} - 1\right]} \qquad \text{(D-9)}$$

Solving equation (D-9) for M_{to}:

$$M_{to} = \sqrt{-0.044 \ln 0.547 \ (1 + 3.96 \dot{w}_o)^2} \qquad \text{(D-10)}$$

but:

$$M_{to} = \frac{\dot{w}_n \mathcal{S}}{\dot{w}_o} = \frac{0.251 \mathcal{S}}{\dot{w}_o} \qquad \text{(D-11)}$$

where:

$$\mathcal{S} = \frac{2 C_v A_c}{P_e A_e} (P_c - P_o) \text{ (Swirl Factor)} \qquad \text{(D-12)}$$

and:

$A_c = 0.0266 \text{ in}^2$ $D_c = 0.092$ in. (Four Ports)

$$C_v = 2 \left(\frac{2}{k + 1} \right)^{\frac{k + 1}{k - 1}}$$

$C_v = 1.171$

$$\mathcal{S} = \frac{2 \times 1.171 \times 0.0266}{227 \times 0.379} (P_c - 415) \qquad \text{(D-13)}$$

$$\mathcal{S} = 0.000725 (P_c - 415) \qquad \text{(D-14)}$$

Substituting equation (D-14) into (D-11):

$$M_{to} = \frac{0.251}{\dot{w}_o} \times 0.000725 (P_c - 415) \qquad \text{(D-15)}$$

$$M_{to} = \frac{0.000182}{\dot{w}_o} (P_c - 415) \qquad \text{(D-16)}$$

Substituting equation (D-16) into (D-10):

$$\frac{0.000182}{\dot{w}_o}(P_c - 415) = \sqrt{-0.044 \ln 0.547 (1 + 3.96 \dot{w}_o^2)} \quad \text{(D-17)}$$

$$P_c = 415 + 5490 \dot{w}_o - 0.44 \text{ in. } (0.547 + 2.16 \dot{w}_o^2) \quad \text{(D-18)}$$

This equation is plotted as $\dot{w}_o/\dot{w}_{om}$ in Figure D-2.

Free vortex theory is valid under low velocity vortex conditions. As the vortex becomes stronger, actual performance departs from that predicted by free vortex theory. A portion of the negative resistance zone on the free vortex theory is avoided in this theoretical analysis by assuming that there is a vertical transition curve. The ultimate in flow modulation occurs when the supply flow is completely shut off and the total flow is entirely control flow.

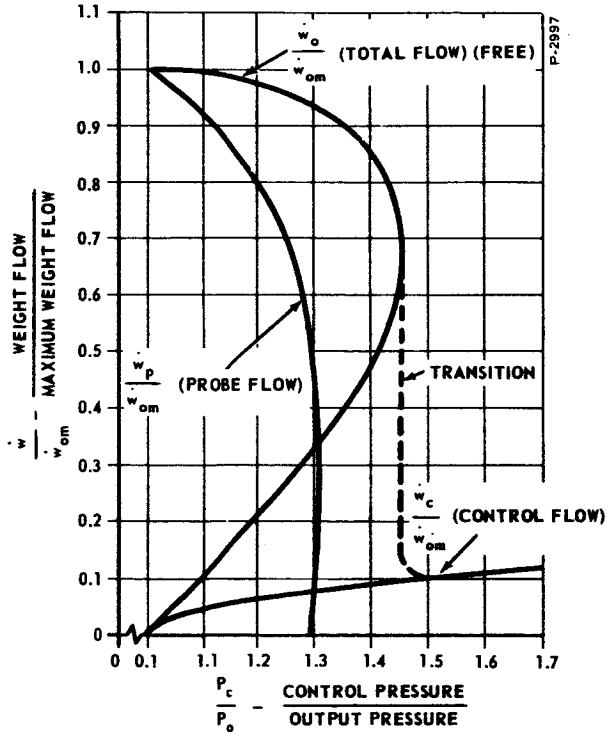

Figure D-2 - Calculated Performance

The control flow curve $\dot{w}_c/\dot{w}_{om}$ was obtained from orifice flow theory. The maximum total flow is:

$$\dot{w}_{o_{max}} = 2\,\dot{w}_n\sqrt{\frac{P_o}{P_e} - 1}$$

$$= 2 \times 0.251\sqrt{\frac{415}{227} - 1}$$

$$\dot{w}_{o_{max}} = 0.456 \text{ lb/sec}$$

$$\dot{w}_c = \frac{2\,C\,C_d\,A_c\,P_o}{\sqrt{T}}\sqrt{\frac{P_c}{P_o} - 1}$$

$D_c = 0.092$ in. (4 holes)

$A_c' = 0.00665 \text{ in}^2$ (1 hole)

$A_c = 0.0266 \text{ in}^2$ (4 holes)

$C = 0.185\ \sqrt{°R}/\text{sec}$

$C_d = 0.7$

$\sqrt{T} = 44.4\ \sqrt{°R}$

$P_o = 415$ psia

$$\dot{w}_c = \frac{2 \times 0.185 \times 0.7 \times 0.0266 \times 415}{44.4}\sqrt{\frac{P_c}{415} - 1}$$

$$= 0.0645\sqrt{\frac{P_c}{415} - 1}$$

This equation is plotted in Figure D-2 as $\frac{\dot{w}_c}{\dot{w}_{om}}$.

Probe Flow Receiver Analysis

The probe flow receiver performance was computed on the basis of unrestricted probe flow. In the assumed case, the probe served as a receiver and collected all of the flow. The task here was to determine the flow divergence cone angle for various control pressures. A model of the probe flow receiver is shown in Figure D-3.

$$V_{ti} = \frac{r_o}{r_i} V_{to} \quad \text{(Free Vortex Theory)} \qquad \text{(D-19)}$$

$$V_{to} = \frac{\dot{w}_c}{\dot{w}_o} V_c \quad \text{(Conservation Momentum)} \qquad \text{(D-20)}$$

$$V_c = 2\,C\,R\sqrt{T}\sqrt{\frac{P_c}{P_o}} \quad \text{(- Orifice Flow)} \qquad \text{(D-21)}$$

$$V_Z = \frac{\dot{w}_o\, R\, T}{C_d\, P_e\, A_o} \quad \text{(Perfect Gas Law)} \qquad \text{(D-22)}$$

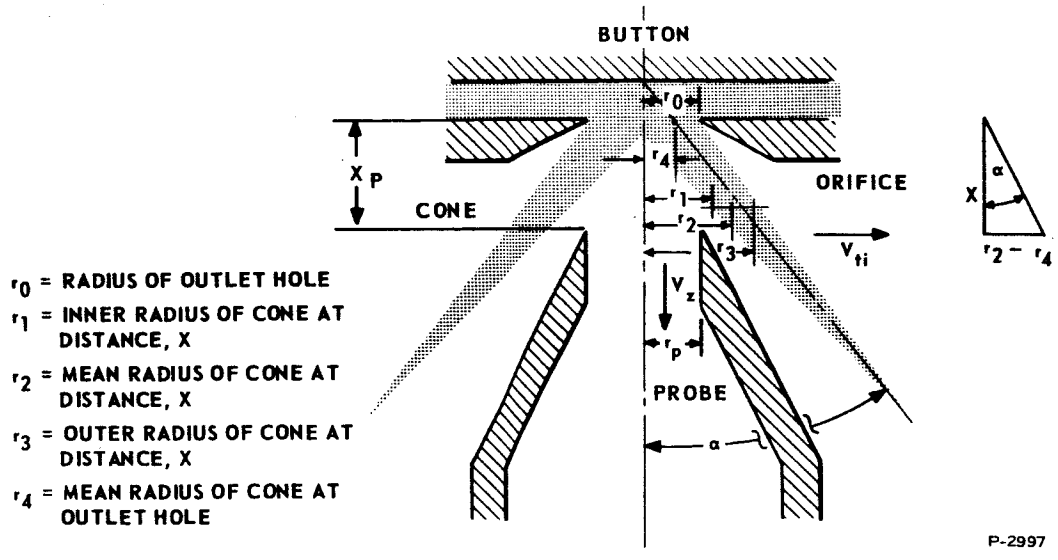

Figure D-3 - Model of Probe Flow Receiver

Refer to Figure D-3:

$$\alpha = \tan^{-1}\left(\frac{V_{ti}}{V_Z}\right) \tag{D-23}$$

Substituting equation (D-20) into (D-19):

$$V_{ti} = \frac{r_o}{r_i}\left(\frac{\dot{w}_c}{\dot{w}_o}\right) V_c \tag{D-24}$$

Substituting equation (D-21) into (D-24):

$$V_{ti} = \frac{r_o}{r_i}\left(\frac{\dot{w}_c}{\dot{w}_o}\right) 2\,C\,R\sqrt{T}\sqrt{\frac{P_c}{P_o} - 1} \tag{D-25}$$

but:

$$\dot{w}_c = 0.0645\sqrt{\frac{P_c}{415} - 1} \tag{D-26}$$

$$\frac{r_o}{r_i} = 6;$$

$$P_o = 415 \text{ psia}$$

$$V_{ti} = 6 \times \frac{0.0645}{\dot{w}_o}\sqrt{\frac{P_c}{415} - 1}\left[2\,C\,R\sqrt{T}\sqrt{\frac{P_c}{415} - 1}\right] \tag{D-27}$$

where:

$$C = C_d C_2$$

$$= 0.148 \sqrt{^\circ R}/\text{sec}$$

$$R = 5190 \frac{\text{in}}{^\circ R} \text{ (Universal Gas Constant)}$$

$$\sqrt{T} = 44.4 \sqrt{^\circ R}$$

$$V_{ti} = 2.64 \times 10^4\left(\frac{P_c}{415} - 1\right)\frac{1}{\dot{w}_o} \text{ (in/sec)} \tag{D-28}$$

$$V_Z = \frac{\dot{w}_o R T}{C_d P_e A_o}$$

$$= 15.72 \times 10^4 \dot{w}_o \qquad \text{(D-29)}$$

The results of equations (D-28) and (D-29) are to be used in equation (D-23).

From Figure D-3 determine mean radii, r_2 and r_4

$$\pi r_4^2 = \pi(r_o^2 - r_4^2)$$

$$r_4 = \sqrt{\frac{r_o^2}{2}}$$

$$\frac{r_2 - \sqrt{\frac{r_o^2}{2}}}{X} = \tan \alpha$$

Let X = 0.200 in.

$$r_2 = \sqrt{\frac{r_o^2}{2}} + 0.200 \tan \alpha \qquad \text{(D-30)}$$

Constant Area Equation:

$$A_o = \pi r_o^2 = \pi(r_3^2 - r_1^2) \qquad \text{(D-31)}$$

$$(r_3^2 - r_2^2) = (r_2^2 - r_1^2) \qquad \text{(D-32)}$$

$$r_3^2 + r_1^2 = 2 r_2^2 \qquad \text{(D-33)}$$

Solving for r_3,

$$r_3 = \sqrt{2 r_2^2 - r_1^2} \qquad \text{(D-34)}$$

Substituting equation (D-34) into (D-31) solving first for r_3,

$$r_3^2 = r_o^2 + r_1^2 \tag{D-35}$$

$$r_3 = \sqrt{r_o^2 + r_1^2} \tag{D-36}$$

$$r_o^2 + r_1^2 = 2 r_o^2 - r_1^2 \tag{D-37}$$

Solving (D-38) for r_2

$$2 r_2^2 = r_o^2 + 2 r_1^2 \tag{D-38}$$

$$r_2 = \sqrt{\frac{r_o^2 + 2 r_1^2}{2}} \tag{D-39}$$

Substituting equation (D-30) into (D-39)

$$\sqrt{\frac{r_o^2}{2}} + 0.200 \tan \alpha = \sqrt{\frac{r_o^2 + 2 r_1^2}{2}} \tag{D-40}$$

$$2 r_1^2 = 2\left(\sqrt{\frac{r_o^2}{2}} + 0.200 \tan \alpha\right)^2 - r_o^2 \tag{D-41}$$

$$r_1 = \sqrt{\left(\sqrt{\frac{r_o^2}{2}} + 0.200 \tan \alpha\right)^2 - \frac{r_o^2}{2}} \tag{D-42}$$

A similar expression is needed for r_3:

$$r_1^2 = 2 r_2^2 - r_3^2 \tag{D-43}$$

$$r_1 = \sqrt{2 r_2^2 - r_3^2} \tag{D-44}$$

Substituting equation (D-44) into (D-31) solving first for r_1

$$r_o^2 = r_3^2 - r_1^2 \tag{D-45}$$

$$r_1^2 = r_3^2 - r_o^2 \tag{D-46}$$

$$r_1 = \sqrt{r_3^2 - r_o^2} \tag{D-47}$$

$$r_3^2 - r_o^2 = 2 r_2^2 - r_3^2 \tag{D-48}$$

Solving equation (D-48) for r_2:

$$2 r_2^2 = 2 r_3^2 - r_o^2 \tag{D-49}$$

$$r_2 = \sqrt{\frac{2 r_3^2 - r_o^2}{2}} \tag{D-50}$$

Substituting (D-30) into (D-50):

$$\sqrt{\frac{r_o^2}{2}} + 0.200 \tan \alpha = \sqrt{\frac{2 r_3^2 - r_o^2}{2}} \tag{D-51}$$

$$r_3 = \sqrt{\left(\sqrt{\frac{r_o^2}{2}} + 0.200 \tan \alpha\right)^2 - \frac{r_o^2}{2}} \tag{D-52}$$

$$r_1 = \sqrt{\left(\sqrt{\frac{r_o^2}{2}} + 0.200 \tan \alpha\right)^2 - \frac{r_o^2}{2}} \tag{D-53}$$

where:

$$r_o = 0.347 \text{ in. } x = 0.200 \text{ in.}$$

$$r_3 = \sqrt{(0.245 + 0.200 \tan \alpha)^2 + 0.060} \tag{D-54}$$

$$r_1 = \sqrt{(0.245 + 0.200 \tan \alpha)^2 - 0.060} \tag{D-55}$$

When $r_1 = r_p$ the flow is zero. Assume an unloaded probe.

$$r_p = 0.347 \text{ in.}$$

$$A_{pf} = \pi(r_p^2 - r_1^2) = \pi(\overline{0.347}^2 - r_1^2) \qquad \text{(D-56)}$$

Here A_{pf} is the total area of the cone within the probe and consequently it is the flow area of the cone. The ratio of this area with the total probe area is the ratio of the total flow that is received by the probe. When the inner radius r_1 of the cone at the probe spacing (0.200 inch) exceeds the probe radius, full flow divergence occurs. The curve obtained is shown plotted as $\dot{w}_p/\dot{w}_{om}$ on Figure D-2.

Notice that the predicted modulation ratio is 10 to 1 and that a P_c/P_o ratio equal to 1.45 is required. Since all physical parameters for the Phase 1 vortex amplifier were used in this analysis, it indicates that a 10 to 1 modulation should theoretically be possible. This conclusion is gross because of the assumptions that were necessary to complete the analysis. They serve as a guide in understanding the actual performance. It is intended to develop this work further and thus increase its usefulness.

APPENDIX E

TEST FACILITY

The test facility used for development of the Phase 1 vortex amplifier is shown in Figure E-1. This was used for both cold and hot gas testing.

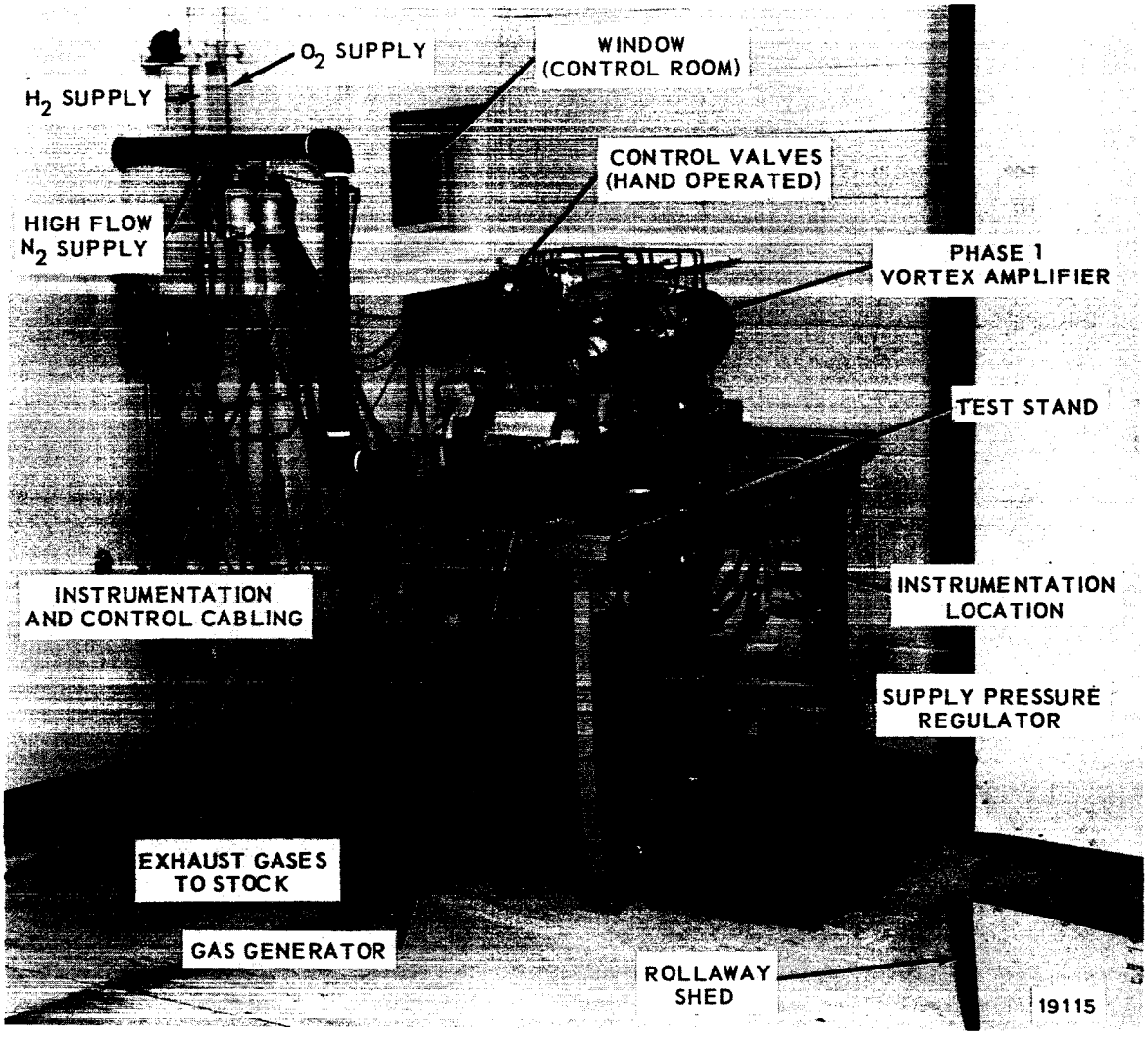

Figure E-1 - General Test Facility (Hot Test Setup)

A schematic diagram of the test installation is shown in Figure E-2. The gas generator is supplied with gaseous hydrogen and oxygen from a trailer tank farm. The generator gas pressure is sensed and regulated using pressure feedback to the pressure regulation system.

Gas generator pressures were maintained at 940 psig. The total flow out of the gas generator was measured with an in-line orifice. Gas temperature was measured at the generator outlet. The gas total flow was split after total flow measurement into supply flow and control flow. The supply flow was reduced in pressure to 400 psig with a Hot Gas Pressure Regulator, a specially designed spring loaded poppet valve. The control flow was controlled by means of special manual valves operated from the control room. Again, in-line orifices were used for flow measurement. Two separate loops were provided for control and bias flow.

The probe flow is restricted by a fixed area load orifice, which essentially simulates a secondary injection application. This orifice is also used to measure probe flow. A differential pressure transducer is not needed, because the downstream or stack pressure is essentially ambient.

All flow-measuring orifices for total, bias, control and probe flow were calibrated with nitrogen gas, using a turbine-type flowmeter at the same pressure levels seen during test. The coefficients of discharge were obtained for various flow levels within the range of operation and averaged to provide a single coefficient of discharge for use in flow calibrations. The orifices were made from an alloy of molybdenum, (99 percent Mo, 0.5 percent Ti), which has excellent high temperature properties. These were inspected periodically for possible erosion. It is estimated that the accuracies of high temperature flow measurements were within 5 percent of actual value.

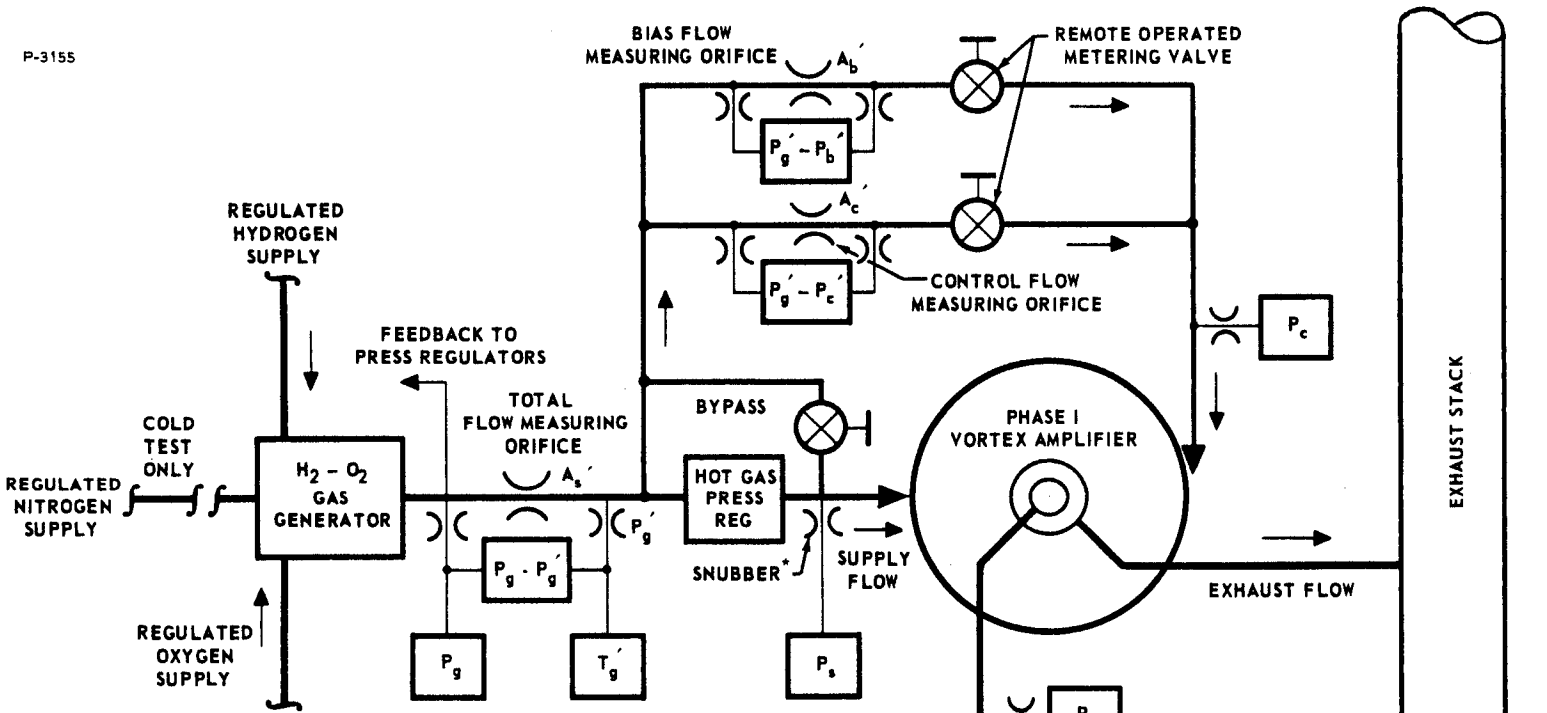

	SYMBOL	VARIABLE MEASURED	CALIBRATION PSIG
1	P_g	GENERATOR PRESSURE	800 – 1000
2	P_s	SUPPLY PRESSURE	0 – 1000
3	T_g'	GAS TEMPERATURE	0 – 2000° F
4	$P_g - P_g'$	TOTAL FLOW ORIFICE PRESS DROP	0 – 50
5	$P_g - P_b'$	BIAS FLOW ORIFICE PRESS DROP	0 – 100
6	$P_g' - P_c'$	CONTROL FLOW ORIFICE PRESS DROP	0 – 100
7	P_c	CONTROL PRESSURE	0 – 1000
8	P_p	PROBE PRESSURE	0 – 100

Figure E-2 - Static Test Schematic

REFERENCES

(1) Blackburn, Reethof and Shearer; Fluid Power Control, John Wiley and Sons, Inc., 1960.

(2) Sievers, G. K., Tomazic, W. A., and Kinney, G. R., "Theoretical Performance of Hydrogen-Oxygen Rocket Thrust Chambers," NASA Technical Report R-111, 1961.

(3) Hall, G. M., and Treirat, E., "Study of Integrated Cryogenic Fueled Power Generating and Environmental Control Systems - Vol. III - Power Generating Equipment Study," ASD Technical Report 61-327, November 1961.

(4) "Properties and Performance of Hydrogen as a Rocket Fuel," Aerojet-General Corporation, Report No. CR-127-360, 1960.

(5) Sutton, G. P., Rocket Propulsion Elements, John Wiley and Sons, Inc., 1956.

(6) Lael B. Taplin, "Phenomenology of Vortex Flow and Its Application to Signal Amplification," RLDP No. 65-14; Bendix Corporation, Research Laboratories Division, Presented at the Summer Engineering Seminars, Pennsylvania State University, July 6-16, 1965.

BIBLIOGRAPHY

Mayer, E. A., and Maker, P., "Control Characteristics of Vortex Valves," Bendix Corporation, Research Laboratories Division, Proceedings of the Second Fluid Amplification Symposium, Harry Diamond Laboratories, Washington, D.C., May 1965.

Emswiler, J. E., Schwartz, F. L., "Thermodynamics," Mc-Graw-Hill Book Company, Inc., New York and London, p. 302, 1943.

GLOSSARY

A - Area, in^2; Amplitude Ratio, db

a - Cold Hydrogen Coefficient

B - Orifice Length, inches

b - Cold Oxygen Coefficient

C_d - Flow Coefficient

C_p - Specific Heat at Constant Pressure, B/lb°F

C_2 - Thermodynamic Gas Constant, $\sqrt{°R}$/sec; (C)

c - Hot Hydrogen Coefficient

D - Diameter, inches

d - Steam Coefficient; differential

e - Base of Natural Logarithms

F - Fuel

f - Frequency cps; O/F Ratio

f_1 - Orifice Flow Function

g - Gravitational Acceleration - in/sec^2

H - Hydrogen

j - $\sqrt{-1}$

K - Gain

k - Ratio of Specific Heats

ℓ - Chamber Length - inches

M - Molecular Weight

N_2 - Nitrogen Gas

O - Oxygen

P - Pressure, psi

Q - Volumetric Flow - in^3/sec

R - Universal Gas Constant, in/°R

s - Laplace Operator, sec^{-1}

$\mathcal{J}$ - Swirl Factor

T - Temperature, °R

V - Volume

v - Velocity

$\dot{w}$ - Weight Flow, lb/sec

x - Probe Spacing - in; mol fraction

π - 3.14

ω - Frequency, radians/sec

ϕ - Phase Shift, deg

α - Cone Angle, deg

ρ - Gas Density

SUBSCRIPTS

a - ambient

ann - annular

b - bias

but - button

c - control, cold

cham - chamber

crit - critical

cyl - cylindrical

d - dynamic

e - exhaust

f - flowmeter

g - generator

h - hot, hydrogen

i - inner

m - molar, maximum

max - maximum

n - nitrogen, normal

o - outlet, oxygen, outer

p - probe

s - supply, steam

t - total, tangential

w - weight

z - axial

PRIME - ASSOCIATED WITH ORIFICES

EXPONENTS

A' - Calibrated Flow Orifice

P' - Pressure Downstream of Orifice

P-3155